Chem Soc Rev

Recent Advances in Bioelectronics Chemistry

SCHOLARONE™
Manuscripts

Recent Advances in Bioelectronics Chemistry

Yin Fang[1][*][#], Lingyuan Meng[2][*], Aleksander Prominski[3][*], Erik Schaumann[3][*], Matthew Seebald[3], Bozhi Tian[1, 3, 4#]

1 The James Franck Institute, University of Chicago, Chicago, IL 60637, USA

2 Pritzker School of Molecular Engineering, University of Chicago, Chicago, IL 60637, USA

3 Department of Chemistry, University of Chicago, Chicago, IL 60637, USA

4 The Institute for Biophysical Dynamics, University of Chicago, Chicago, IL 60637, USA

* These authors contributed equally to this manuscript.

Corresponding author: yinfang@nano-theranostic.com, btian@uchicago.edu

Abstract

Research in bioelectronics is highly interdisciplinary, with many new developments being based on techniques from across the physical and life sciences. Advances in our understanding of the fundamental chemistry underlying the materials used in bioelectronic applications have been a crucial component of many recent discoveries. In this Review, we highlight ways in which a chemistry-oriented perspective may facilitate novel and deep insights into both the fundamental scientific understanding and the design of materials, which can in turn tune the functionality and biocompatibility of bioelectronic devices. We provide an in-depth examination of several developments in the field, organized by the chemical properties of the materials. We conclude by surveying how some of the latest major topics of chemical research may be further integrated with bioelectronics.

Keywords

1. Introduction

Blurring the boundaries between biotic and abiotic systems, bioelectronics is catalyzing profound progress in diagnoses, therapy, prosthetics, as well as facilitating a deeper understanding of physiological processes. New directions and activities are emerging in the bioelectronics community, which signify that this is an active, exciting field with numerous unexplored questions. Some of the recent developments include advanced materials synthesis,[1, 2] closed-loop neural[3, 4] and cardiac[5-8] interfaces, 3D seamless integration of chronic bio-interfaces,[9-12] *in vivo* real-time biosensing,[11-16] therapeutics for restoring lost neural functions and reversing neurodegenerative disorders,[17-21] *etc.*

Generally, the validation and optimization of material and bioelectronics devices are heavily focused on engineering and functional considerations. Electrical circuits of various scales and geometries have been designed and manufactured to interrogate bioelectrical phenomena with high fidelity and sensitivity over a wide range of spatial scales.[22] At the small end, there is the nanoscale subcellular level, where relevant devices include single-channel patch-clamp and nanoscale field effect transistors. Individual cells and colonies exist on the micron to millimetre scale, where electrical monitoring is typically performed with whole-cell patch-clamp or extracellular electrodes. At the mesoscale tissue-level, microelectrode arrays and mesh electrodes are the most widely used tools for monitoring. To obtain tissue monitoring with fine spatial resolution, the integration of hundreds of electrodes in parallel arrays have been developed for simultaneous signal collection. Furthermore, more functionalities, such as drug delivery, optogenetics, MRI or acoustic imaging, and wireless signal transductions, have been factored and assembled into integrated probes intended for more sophisticated investigations of biological activities using integrated fabrication and engineering techniques.[23-26]

While the engineering aspects of bioelectronics are extensively discussed elsewhere,[27-32] the coverage of chemistry-specific developments in the literature has been comparatively sparse. Despite this, they have aided in creating a new functional material toolkit, in tailoring traditional materials to achieve long-lasting functioning, and in improving probe efficacy and functionality. In this review (**Fig. 1**), fundamental synthetic chemistry, surface chemistry, electrochemistry, and biophysical chemistry in bioelectronics are discussed first. Next, we summarize new chemical advances that are essential for bioelectronics performance under each category of material (*i.e.*, inorganic or organic semiconductors or conductors, Table 1). These processes play fundamental and indispensable roles to advance the field as they

produce new material components, optimize cost-efficient production, promote biocompatibility and long-term stability, improve electrochemical and biophysical performance, and help reveal new biophysical mechanisms and functionalities at biointerfaces. At the end of the review, we discuss new chemistry opportunities for future bioelectronics.

2. Fundamentals at biointerfaces

In this section, we want to accustom the reader to the fundamentals of working with junctions between the various materials and biological structures, which are referred to as biointerfaces. First, we discuss the size and time scale of the formation of interfaces and how they affect our choice of materials. We follow with a discussion on the basic biophysical principles behind the transduction of biological signals. Finally, we describe the concepts of mechanical matching between natural and artificial systems and the importance of their biochemical stability.

2.1 Size scales of bioelectronics

Biointerfaces can be formed at different length scales depending on the relevant biological question and application, ranging from large-area non-specific modulation to subcellular sensing (**Fig. 2a**). The following discussion provides not only a description of biointerface design but also a historical perspective on the field of bioelectronics. Relatively large, noninvasive electrodes were developed first and remain widely used today. For recording, those applications are mainly electroencephalography (EEG) for recording brain activity through the scalp, electrocardiography (ECG) for recoding of cardiac activity, and electromyography (EMG) for investigation of skeletal muscles. Similarly, large-area stimulations are routinely used in emergency cardiac arrest defibrillation, in physical therapy for electrical muscle stimulations, and to effectively treat some mental illnesses through electroconvulsive therapy.[33] By definition, large-area techniques have limited resolution and suboptimal efficiency due to making indirect contact and being placed far from the tissue of interest. The bioelectrical effects are averaged over a large area and it is therefore difficult to disentangle the variety of chemical interactions at this scale.

Progress in materials research brought the possibility of the creation of probes with higher resolution placed closer to the active cells, which facilitated the development of smaller and less invasive devices. The first step was the development of direct biointerfaces with a single organ. These efforts brought us artificial pacemakers, cochlear implants, and deep-brain

stimulation probes, which improved survival and quality of life for millions of people. However, the realization of challenging goals such as visual prosthetics or brain-machine communication requires single-cell resolution. Traditional electronics face certain key limitations in such applications. Namely, they possess undesirable mechanical properties, limited biocompatibility, and low interface resolution.

The advent of modern micro- and nanotechnology opened the next frontier in bioelectronics[2, 11, 12, 23, 29, 32, 34-40]. Probes became smaller and more adaptable, improving the biocompatibility of devices. Micron-sized devices allowed for measurement of local electric potentials deep inside tissues and interfacing with small groups of cells, bringing a whole new insight into the study of cell physiology. On this scale, substantial chemical interactions between the materials and the tissues, such as adhesive forces, have to be taken into account. Current state-of-the-art devices are capable of forming exact single-cell extracellular[41] and intracellular[42, 43] interfaces. Hopefully, further development in the field will produce methods for single organelle modulation or even studies on specific cell structures such as microfilaments or ion channels. Such measurements will become highly local and allow the study of heterogeneity[44] and non-equilibrium processes in living cells. On the lowest scale, chemical and mechanical energy terms become approximately equal in magnitude,[45] which will without doubt reveal the presence of new fundamental processes.

With increased spatial resolution comes decreased signal throughput through the biointerface. While large-area recordings give only average readings of electrical activity, such recordings are generally more useful for practical applications. Signals from single cells are usually not representative of the entire tissue and can carry significant noise. Therefore, another challenge that comes with utilizing microscale biointerfaces is achieving high parallelization of modulation and recording. For this purpose, massive amounts of bioelectronic components have to be fabricated or assembled. Recently, significant effort has been put into clinical translation of machine-brain interface technologies by Neuralink. Recent reports demonstrate simultaneous recording from 1020 electrodes.[46] While this number is ten-fold higher than those of classic microelectrode arrays (*e.g.,* Utah or Michigan probes),[47-52] it is still far from that achieved by biological interfaces. For example, human auditory nerves are made of some 30,000 myelinated neuron fibers[53] and optical nerves of more than a million.[54] The number of neuronal connections necessary to establish a high-fidelity computer-brain interface is still a matter of debate. However, with the first devices entering clinical trials,[55, 56] we should expect a better quantitative assessment of these

technologies over the next few decades. It can be envisioned that new materials in a form of massively self-assembled neuro-mimetic fibrils will one day match the parallelization of information transfer observed in nature. A recent report showing bundles of microwires used for neuronal recording represents a promising early step in this direction.[57] It is therefore important to study nanoscale self-assembly processes, dynamic combinatorial libraries and other types of parallel chemistries for the synthesis of future bioelectronic devices.

2.2 Time scales of bioelectronics

The relevant time scales in the bioelectronics can be seen from two orthogonal perspectives. One describes the time scale over which biological signals are generated (**Fig 2b**), and the other is the duration of the biointerface, that is, the time that the device and the biological system spend in contact. (**Fig 2c**). The timing of recording and stimulation with respect to the biological events will be discussed first. For interfacing with highly active cells such as neurons or cardiac muscles, which can fire an action potential on the timescale of milliseconds, a high frequency response is required from the device. For investigations of even more transient biological events such as the action of molecular motors or activity of single ion channels, even higher temporal resolution on the timescale of nano- to microseconds is required. The timing of the target process therefore determines the required kinetics of the recording or stimulation. For example, for studies of transient states, using diffusion-limited processes would be unwise. Conversely, devices meant to sense or stimulate slower physiological processes such as bone regeneration[58] require less temporal resolution but carry with them a different set of considerations. In this case, interfacial chemistry plays an important role as interactions such as adhesion have a significant effect on the stability of an interface as well as any immune response it can elicit. Likewise, devices that can potentially impact mechanotransduction or chemical transduction must consider the time scale of these processes, where signals are delivered and processed with significant delay, on the order of minutes to hours. Understanding the required stimulation or response frequency is thus a critical factor in matching the design of devices with their specific applications.

The other independent time scale is the period over which we expect our biointerface to be active. The interfacing time scale can range from extremely transient experiments to permanent implantation for clinical applications. Biointerfaces used in studies of individual physiological processes can be relatively short-lived. They are used to study single

physiological interactions and disposed of soon after. As such, these types of experiments do not require extensive studies of stability and biocompatibility. Maintaining stable biointerfaces becomes a concern for experiments with tissues or cell cultures. In this case, devices need to maintain their integrity and it becomes important to evaluate additional interactions in the biointerface beyond the designated purpose of the device. If for example, the products of the device decomposition lead to uncontrolled proliferation of cells or increased cytotoxicity, such interactions cannot be ignored. It is therefore critical to take into account the chemical composition of such devices as well as the reactivity of their constituents. For applications requiring implantations of the device into an organism, not only does device stability have to be higher, but additional considerations have to account for the immune system response to the presence of a foreign body. The origin and methods of mitigation of immune response to the biointerface will be discussed in the following section. Excellent stability and biocompatibility are required for a long-term integration of bioelectronics with a host body. An important example of an application that requires long-term integration is the formation of chronic brain interfaces. The delicate nature of brain tissue makes it not only more sensitive to invasive probes, but due to the brain's limited regeneration ability, replacement of used bioelectronics devices with new ones is not a feasible solution. Each removal and insertion of probes causes irreversible trauma that can lead to fatal accumulation of damages. Therefore, clinical applications of the machine-brain interface demand stable, long-term biointerfaces.

For long-term integration of bioelectronics, additional attention has to be paid to all the secondary electronics necessary for their operation. Bench-top controllers, transducers, and power sources can be used in short-term laboratory experiments without concern. The case is significantly different for implantable bioelectronics, where electrodes tethered to extensive external instrumentation limits the mobility of host organisms and makes such a solution impractical. Hence, lightweight and, ideally, remote-controlled recording and modulation devices represent an important design principle that requires significant thought. The essential issue is the integration of bioelectronic devices with proper microscale power supplies. Recent developments point to devices to which power can be delivered remotely, *e.g.*, through magnetic resonant coupling.[59] Another front is led by the freestanding devices that lack traditional electric circuits, but can locally stimulate tissues through magnetothermal,[23, 60] chemomagnetic,[61] photoelectrochemical,[62, 63] photothermal,[64-67] and photoacoustic[38, 68] effects that are initiated with remotely delivered physical stimuli. Future

research in applied bioelectronics will no doubt veer towards the development of integrated, wireless devices for the ultimate goal of seamless, inconvenience-free bionic integration.

2.3 Signal transductions

Biological systems fundamentally differ from standard electronics by their mechanisms of signal generation and transmission. In conventional conductors such as metals, the majority of electric charge is carried directly by electrons. In biological systems, rich in water, ions, and organic matter, electric current is carried mostly by ionic fluxes. These two modes of conduction are, in principle, very dissimilar, which requires a specific interface in which signals can be transduced (**Fig. 3**).

2.3.1 Bioelectricity in cells and tissues

Electrically active cells communicate via spikes of ion fluxes caused by a sudden release of ions, known better as action potentials. The potential difference between insides of cells and their extracellular environment (usually negative) is maintained by active transport and imbalance in the concentration of ions, typically K^+ and Na^+. The resting transmembrane potential existing due to this imbalance is classically described using the Goldman-Hodgkin-Katz (GHK) equation:

$$V_{rest} = \frac{RT}{F}\ln\frac{\Sigma_i^N P_{M_i^+}\left[M_i^+\right]_{out} + \Sigma_j^M P_{A_j^-}\left[A_j^-\right]_{in}}{\Sigma_i^N P_{M_i^+}\left[M_i^+\right]_{in} + \Sigma_j^M P_{A_j^-}\left[A_j^-\right]_{out}} \qquad Equation\ (1)$$

where V_{rest} is the resting membrane potential, R is the ideal gas constant, T is the absolute temperature, and F is the Faraday constant. The sums account for permeabilities P and concentrations [M] of monovalent ions on the inside and outside of the membrane.[69] The resting membrane potential is the mechanism by which cells store energy used for signaling. When stimulation occurs, passive ion channels open and ions freely flow in and out of the membrane. This ion flux generates electric currents which can create a local potential change in the tissue, effectively meaning this cell is interacting with neighboring cells to cause further signal transduction. A potential generated at point (x,y,z) by moving ions can be derived from Ohm's law and, treating the ions as pure monopoles, takes the form of:

$$V(x,y,z) = \sum_{i=1}^{n}\frac{I_i}{4\pi\sigma r_i} \qquad Equation\ (2)$$

where I_i is the current from the ith monopole, σ is the conductivity of the medium, and r_i is the distance from the monopole to the point (x,y,z).[69]

The aforementioned model averages molecular interactions and approximates properties of the media and the surrounding tissues. In reality, the environment of biological fluids is highly crowded, and in dense structures, *e.g.*, brain tissue, electrodiffusion is affected by heterogeneities at a molecular level.[70] Hence deviations from this classic interpretation can be observed on a subcellular length scale. Such heterogeneities can arise from the extracellular environment and interactions with large proteins and charged species, as well as from uneven spatial distribution of ion channels in the membrane. Therefore, it is paramount that the progress in nanodevices' research comes together with the development and validation of new theoretical models.[70]

2.3.2 Electrochemical sensing or modulation processes

The most straightforward electrode-tissue interface utilizes capacitive currents (**Fig. 3**). A chemically inert electrode can only inject current due to building capacitive charge on its surface due to applied potential. Ions with complementary charges will migrate towards the electrode, creating charge currents, and start building up a layer on the electrode surface called an electrical double layer (EDL). Ionic currents will flow only until the electrode is fully charged. The time constant for EDL formation can be described as:

$$\tau_{EDL} = R_e C_e \hspace{4cm} Equation~(3)$$

where R_e and C_e are the leakage resistance and capacitance of the electrode, respectively. This simple relation is an essential operational specification of the electrode. It describes its operational limits as well as its bandwidth – the maximum frequency at which signals can be delivered or received. The electrical interaction between the electrode and the membrane can be estimated with a highly simplified model of an equivalent circuit, in which the cell and electrode are treated as potential sources, an interface is modelled as a parallel capacitor and a resistor, and an additional term is added for internal electrode resistance.[71] Using this equivalent circuit and *Equation 2,* we can derive the relation between cell and electrode potentials:

$$V_e = \frac{1}{4\pi\sigma r}\left[\left(\frac{1}{R_e} + sC_e\right)^{-1} + R_{int}\right]V_{cell} \hspace{3cm} Equation~(4)$$

where V_e is the electrode potential, V_{cell} is the potential at the cell surface, R_{int} is electrode's internal resistance, and s is the complex frequency of interacting waveforms. The above equation can be used to qualitatively describe both stimulation and recording. For stimulation, we choose to control electrode potential V_e and interact with the cell. For recording, the cell is firing its active potential $V_{cell,}$ and we measure readings received on the electrode.

By analyzing *Equation 4*, fundamental qualities of electrode-cell biointerfaces can be derived. First, electrical interaction, as parameterized by the potential, is inversely proportional to the distance r between the electrode and cell membrane. Hence the closer the distance between the electrode and the membrane, the stronger the interaction. Also, for strong interactions, it is recommended to keep leakage resistance (R_e) low and electrode capacitance (C_e) high. Resistance of interconnections plays a role in determining the signal-to-noise ratio (SNR) of the biointerface. For higher currents, R_{int} has to be kept low, but for good SNR, it has to be kept high. For designs in which the electrode is bifunctional and used for recording and stimulation, a compromise has to be made.

Purely capacitive electrodes rely only on EDL and have a limited range of operation. Stimulation with higher potentials can be accomplished using electrodes injecting Faradaic currents (**Fig. 3**). Such an electrode is chemically active and introduces new ions due to electrochemical reduction or oxidation occurring on its surface. It has been shown that highly catalytic electrodes are capable of stimulating with strong potentials.[72] The drawback of using a chemically active electrode is its degradation over time. One possible way to prevent extensive damage to an electrode injecting Faradaic current is the application of principles used for the fabrication of supercapacitors.[73] These principles include the application of nearly completely reversible electrochemical reactions or precise structuring of the electrode on the atomic level, which permit increasing its capacity beyond the limit of traditional materials. Another possible development in this field might be the application of bioelectrocatalysis (**Fig. 3**), which uses electrode-bound enzymes to generate active species *in situ* for selective stimulation or process metabolites present in the system to be used for their detection.[74, 75] Additionally, although redox signaling is paramount in biological systems,[76, 77] it was not thoroughly explored with respect to bioelectronic modulation.

2.3.3 Optoelectronic or photoelectrochemical sensing or modulation processes

Semiconductor-based optoelectronics or photoelectrochemical devices can be used to deliver (*e.g.*, using a light emitting diode [LED] or a photovoltaic device) or read out (*e.g.*, using an *in vivo* photometer) stimulation signals at the biointerface, when matched with electrical circuits or wireless microcontrollers (**Fig. 3**).[78, 79] To perform single cell studies, we can either use semiconductor structures/devices that are microns or nanometres in size, or use highly localized initial stimuli (*e.g.*, a laser spot) over macroscopic structures/devices.

Many of the devices for such studies are based on diode junctions. In particular, for photoelectrochemical stimulation applications, a photovoltaic mechanism is often adopted.[62] A diode device is typically created when hole-rich (p-type) and electron-rich (n-type) semiconductors are placed in contact, causing a shift in their valence and conduction bands near the p-n junction, within a region called the depletion zone. Photoexcitation can promote an electron from the valence to the conduction band, creating an electron-hole pair.[38] The electrons and holes then diffuse away from the depletion zone in accordance with their charge, creating a potential difference on different parts of the device that can be used to stimulate cells and tissues similarly to wired electrodes described above.

Depending on the material, photoexcitation can inject capacitive current, Faradaic current, or a combination thereof into the biointerface (**Fig. 3**). These processes in freestanding structures can be understood within a framework analogous to that of the wired electrode. However, semiconductors are highly sensitive to their environment through the alteration of their surfaces' electronic structure. Photostimulation and other physical behaviors at the interfaces can be predicted both qualitatively and quantitatively using the concept of band bending. Band bending in semiconductor describes the alteration in native electronic structure due to the material environment, surface modification,[80] or the material size and dimensionality.[81] Semiconductor physics and electronic processes underlaying their photoactivity require a more thorough discussion, for which we redirect readers to literature specific to semiconductors.[32, 38]

2.3.4 Photothermal modulation processes

The photothermal effect arises from radiationless energy transfers in photoexcited materials. That is, the emitted energy translates into the kinetic energy of the material or its surroundings, and the temperature increases. In practice, this means that the best candidates for photothermal modulation primary respond to excitation with the generation of phonons or

plasmons. In crystalline materials, nonradiative recombination can produce quantized oscillations in the bulk material, known as phonons, which are responsible for photothermal heating in those structures.[82] For certain metallic nanomaterials, such as noble metal nanoparticles and carbon nanostructures, light absorption results in oscillations of associated free electrons on the material surface. These oscillations are referred to as surface plasmons, and their production can convert almost all incoming light energy to heat.[83, 84] Continuous-wave irradiation of plasmonic materials can therefore create strong temperature gradients (**Fig. 3**).[64]

Transduction of thermal signals is another vital aspect of biophysics, yet it has not been studied as extensively as electrical signals. Cell physiology, especially the catabolic process responsible for energy generation, generates multiple intracellular and extracellular thermal gradients.[85] Such signals can trigger proliferation and affect other cellular metabolic pathways. It can be deduced from the GHK equation (Eq. 1) that temperature affects membrane potential, and its increase will make it more sensitive to stimulations. Additionally, multiple ion channels have been discovered to be especially receptive to temperature gradients such as thermosensitive potassium channel TREK-1.[64] For thermal sensing, purely resistive microelectromechanical devices as well as a range of nanostructures have proven effective. Quantum dots, upconverting nanoparticles, and metal cluster were all applied to create remote luminescent thermometers.[86]

A closely related phenomenon can be observed when instead of steady irradiation, high-power pulsed lasers are used to illuminate plasmonic nanostructures. A sudden release of energy causes evaporation of solvents around the material surface, forming gas nanocavities which, upon collapsing, release ultrasonic waves traveling through the medium. This phenomenon is referred to in the literature as a photoacoustic effect.[65, 68, 87] Although the mechanism of the generation of photoacoustic waves is not fully understood it allowed the development of a variety of imaging and stimulation methods.[88, 89] Recently, the photoacoustic effect was used to facilitate entry of recording electrodes into the cells through the local optoporation mechanism in a similar manner to the classical electroporation (**Fig. 3**), but providing superior process control and cell viability.[90] However, potential applications of the photoacoustic effect in bioelectronics remain largely unexplored.

2.3.5 Transistor-based sensing processes

Transistors are some of the most important elements in nearly all modern electronics and bioelectronics. In particular, field-effect transistors (FETs, **Fig. 3**) are widely used as they have been extensively studied due to their importance in the operation of integrated circuits. In the regular planar configuration, a semiconductor substrate is connected to a source (S), drain (D), and gate (G) electrodes. The gate electrode is separated from the substrate using a dielectric insulator. When a voltage potential is applied between the source and drain electrodes, the current will flow through the semiconductor channel. The current through the semiconductor will be proportional to the potential applied to the gate. Depending on the doping of the semiconductor substrate, a transistor can operate in enhancement or depletion mode. For an ideal transistor in enhancement mode, no current flow will occur at gate potential below the specific threshold and beyond the threshold potential, current will rise linearly until saturation current is reached. The behavior is reversed in a depletion mode transistor. The ratio of current change to the applied potential in a transistor is defined as transconductance g_m and can be a direct measure of its sensitivity.

The external connection to the gate is typically omitted for bioelectronic sensing applications, as the gate potential variation is generated directly by the dynamic processes from charged species or cells. Notably, for FET-based detection of binding of unbinding of charged species (such as protein marker), the sensitivity is limited to the characteristic Debye screening length:

$$\lambda_D = \frac{1}{\sqrt{4\pi l_B \sum_i \rho_i z_i^2}} \qquad\qquad Equation\ (5)$$

Where l_b is the Bjerrum length, $\sum_i$ is the sum of present ion species with concentrations ρ_i and valence z_i. The Debye screening length can be used to approximate sensitivity range and is on the order of <1 nm in concentrated electrolytes.[38] Specificity and sensitivity of FETs in bioelectronic situations can be improved by using surface modifications with biomolecules capable of molecular recognition.[91] The advantage of FET devices over metal-based capacitive and faradaic electrodes is that device current flows in a closed-circuit, so that the potential issues with the electrode impedance, electrode corrosion or biological invasiveness can be minimized. This also allows FET devices to achieve faster response times[92] and lower SNR[93] when compared to single terminal electrodes.

The second type of transistor – electrolyte gated transistor – has gained increased popularity in bioelectronics over the recent years due to its high transconductance,

biocompatibility, and processing versatility. In this configuration, the semiconducting substrate and gate are replaced with porous structures which can be interpenetrated by ions increasing or decreasing current flow through the channel. The most popular materials for gating channels are made of organic conductors and semiconductors forming a class of organic electrochemical transistors (OECTs, **Fig. 3**). Transconductance in OECTs can be described using Bernards model[94, 95] and the equation:

$$g_m = \left(\frac{W}{L}\right) d\mu C^* (V_{th} - V_G) \hspace{4cm} Equation\ (6)$$

which accounts for channel geometry: width W, length L, and thickness d; charge carrier mobility μ; capacitance per unit volume of a channel C^*; gate voltage V_G and specific threshold voltage V_{th}. Capacitance in organic materials can be widely tuned; therefore, characteristic of OECTs is their exceptionally high transconductance.[96] OECTs can be used for ion-selective sensing with the introduction of proper membranes.[97] A closely related topic to OECTs is a class of hydrogel-based devices called organic electronic ion pumps (OEIPs) which can be used for ion delivery[98-100] and as drug delivery platforms.[3, 95, 101] For a detailed discussion on OECTs and OEIPs we direct the readers to recent reviews focusing on these subjects.[102, 103]

2.3.6 Stimulation with molecular and optical signals

Biological systems utilize a range of small molecules and peptides for intracellular or organism-wide signaling. Bioelectronic devices can be used to deliver signaling molecules and pharmaceuticals directly into tissue, increasing their availability and potency.[104] Microfluidic channels present one promising approach to this application. The drawback of this approach is that it requires the integration of secondary elements, such as pressure sources, to function properly. Although some micropumps with low power consumption have been devised,[105, 106] there is still much progress to be made in this area. An alternative approach is to design materials that can dispense drugs from inside their structure on-demand such as the aforementioned OEIPs. However, volumetric materials have limited cargo capacity, and molecules are usually delivered through diffusion and positive pressure, which lowers delivery speed and efficiency.

Apart from some small organisms, most cells and tissues cannot be directly stimulated using light. Two approaches exist to make ordinary cells susceptible to optical signals:

optogenetics and optopharmacology. Optogenetics relies on genetic modification of target cells to display specially engineered optically responsive ion channels,[107] while optopharmacology relies on delivery of photoresponsive drugs which, while inactive in their native form, can be distributed evenly among cells and will become active only upon illumination.[108] Both of these approaches, which are discussed further in section 7.2.2, allow for local optical modulation of cellular activity. Delivery of light to the stimulation location can be accomplished using waveguides or microlight sources such as upconverting materials, or micro-LEDs.[109] Efficiency of light delivery can be calculated using the equation:

$$I = P_S \cdot \eta_{coupling} \cdot \eta_{scattering} \cdot \Phi_{geometry} \qquad\qquad Equation\ (7)$$

where P_s is the output power of the source, η factors are coupling and scattering efficiency, and Φ is the geometric factor of the light interface.[110] The design of materials that can be used as waveguides focuses on maximizing coupling and scattering efficiency. Furthermore, for microlight sources, increasing the light power output without excess resistive heating is a challenge. Additionally, geometric factors can be taken to account, and directional light sources can be devised that focus their emission on the limited angular range and allow for efficient and highly localized stimulation. Because those optical systems require genetic modification or drug delivery for their functioning it is common to integrate them into single optofluidic system.[111]

2.3.7 Transduction of mechanical signals

Nearly all biological systems have been observed to be sensitive to mechanical stimulation. Mechanical stimuli can be transduced through surface receptors and mechanosensitive ion channels or else directly detected by the cytoskeleton.[112] Mechanotransduction is an important mechanism that can be used for bioelectronics since it can greatly influence cell functions and their ultimate fate.[113] For example, mechanical obstacles or stimulation can significantly impair growth and myelination of oligodendrocytes.[114] Historically, studies have focused on the impact of bulk mechanical properties of extracellular matrix, namely its stiffness. More recently, the effects of the presence of static curvature[115] have also drawn interest. Materials with gradients of mechanostatic interactions, tuneable stiffness, and active curvature actuation on the nanoscale are highly sought after.

2.4 Mechanical match and mismatch

Biology sets several constraints on the design of bioelectronics, which makes integrating biological and artificial systems especially challenging. One of the most important considerations is the mechanical matching across the interface. The most widely used metric of stiffness is the Young's modulus, which relates the stress and strain of a linearly elastic material. While cells themselves are in fact viscoelastic, and thus excluded from this definition, the most useful devices for biointerfaces with soft biological tissues have Young's moduli in the range of $0.1 - 50$ kPa, with neural tissue and skeletal muscle targets on the lower and upper end, respectively.[116] In contrast, most of the substrates used in traditional electronic devices have Young's moduli in the range of 100 MPa to 10 GPa. It has been shown that mechanical mismatch can lead to rejection of the interface by causing an inflammatory response in tissues[17, 117] or merely being a nuisance for an organism and limiting its motoric activities.[118] Other reports show that material stiffness affects the complex behavior of surrounding cells such as differentiation and adhesion.[116] As has been discussed in recent specialized reviews on this issue,[17, 22] this knowledge is of critical importance to the realization of neural interfaces for computer-brain communication[119] and deep brain stimulation for the restoration of motor functions.[120] The brain is highly reactive, and even slight insertion trauma caused by stiffness mismatch between the tissue and the probe can cause activation of microglia and macrophages.[17] In effect, this acute inflammation can turn into chronic inflammation, which will cause degradation of the interface or the device itself. Rejection of the implant or loss of its integrity renders the device inoperative and would require extraction, treatment of damages, and reinsertion of new probes, complicating the treatment and significantly increasing side-effects. It is therefore critical to achieve mechanical matching in order to form stable biointerfaces.

Multiple solutions for improving mechanical matching have been devised with the most straightforward solution being reduction of dimensionality of materials and reduction of the size of their constituents to the microscale and nanoscale.[121] This approach allows for a lower bending stiffness and to realize flexible and stretchable biointerfaces with classic electronic materials such as silicon (Si) and gold (Au).[122] While mechanical properties are improved, such materials are still far more rigid than biological tissues and may compromise the stability of a biointerface. The search for materials with intrinsically matching mechanical properties has arrived at organic conductors and semiconductors as suitable candidates, with the highest promise coming from their hydrogel formulations thanks to their high water content, which allows for transfer of ions and dissolved gases. However, significant efforts

are still needed to improve the electronic and optoelectronic functions in these organic materials.

Another critical aspect of mechanical matching is planning for the geometry of the interface. Biological materials generally have rough surfaces which leave a gap when put against flat materials, such as thin inorganic layers. Intrinsically rough materials such as nanostructures and carbon-based materials tend to perform better in this area.[123] When possible, biocompatible adhesives could be employed to fill the gap.[124]

An alternative approach is to use hard-soft composites, which may ultimately solve the compromise between the electronic/optoelectronic functions and the mechanical properties needed for future biointerfaces. The hard-soft composites contain hard materials, which bear some useful functionality, and soft matrix materials that can act both to improve the mechanical match and to potentially offer some biological functionality themselves. This allows for a wide variety of hard materials, which include materials such as Si and noble metals that are already ubiquitous in electronics, to be incorporated into biological tissues while attenuating the immune response. By carefully tailoring soft carrier materials to desired applications, hard-soft composites can be employed to *in vitro* cultures, on the skin of test subjects, or even implanted into organisms.

2.5 Reactivity of the materials

Biointerfaces are formed in environments that inherently can be volatile and difficult to design and control for. Cells and tissues present on the materials possess a wide range of pH values, varying concentration of ions, and a spectrum of molecules and biomolecules – most of them chemically active. For achieving chemically stable and electrically functional devices over a desired time frame, it is important to keep in mind the chemical processes that it undergoes during its operation. Depending on the application, this can be undesired or desired. Careful investigation of chemical properties of the material allows for proper tuning of its stability.

2.5.1 Reactivity of the components

Bioelectronic components might be either unintentionally or intentionally reactive. Unintentional reactivity leads mostly to deterioration of the materials causing it to lose performance over time due to mechanical damage, chemical disintegration, or loss of electrical or electrochemical properties. Constituents released into the environment might

also in turn react with biological structures. Unintentional reactivity can be minimized with the use of materials that are inert to their environment or chemical passivation of their surfaces. Some materials, such as faradaic electrodes, require chemical reactions to perform their functions. Such materials will unavoidably interact chemically with the environment. This must be taken into account when designing the system. In this case, utilizing reversible redox reactions can substantially increase the lifetime of the interface. Other intentionally reactive materials are ones that undergo controlled disintegration and can be used for the applications in transient electronics – devices which do not require extraction as they safely decompose in biological conditions. Finally, reactive materials can be used to adapt to their environment or have self-healing properties. Achieving these properties requires careful study of chemistries present in the environment and the device alike.

2.5.2 Consequences of reactivity

Reactive components will inevitably interact with their environment. Almost all devices undergo some deterioration and releases in a small number of their constituents, but for some transient applications in modulation or sensing, *e.g.,* intermediate heart pacing or drug delivery, long term stability might be undesired. An ideal device could be implanted and, after fulfilling its duty, decompose and be safely metabolized by an organism.[125] This approach would make a follow-up surgical extraction of the device unnecessary. For both cases it is important to ensure that the release of the material or its constituents into the system will not impair the development of cells and tissues or alter the cellular process in a harmful way.[126, 127]

Important classes of reactive materials are those capable of self-repair and self-healing. Inspired by biological systems, these materials are able to self-regenerate from mechanical and chemical damages and regain their original properties.[115] Self-healing properties arise from the insightful engineering of the chemical interactions present in the structure of materials. They can be realized using either reversible reactions or through the implementation of mechanisms or catalysts that can be activated by damages to help the material recover its integrity.[39] In turn, these can be engineered using independent chemistries or processes working in concert with the biological environment. Self-healing properties are essential for conductive materials, which require constant electrical continuity

for their uninterrupted operation. It is expected that the long-term integration of bioelectronics will require some type of regeneration ability in such materials.

3. Inorganic semiconductor-based bioelectronics

3.1 Si-based bioelectronics

Inorganic semiconductors are widely utilized in electronic and photonic bio-interface research. They are essential for the design of high performance devices with desirable applications such as electronic sensing, signal amplification and transduction.[22, 38] In particular, semiconducting Si has attracted researchers' interest due to its biocompatibility and well-developed microfabrication methods.[38] Si exhibits high charge carrier mobilities (electron mobility ~1300 $cm^2 \cdot V^{-1} \cdot s^{-1}$; holes mobility ~400 $cm^2 \cdot V^{-1} \cdot s^{-1}$ at 300K), leading to rapid responses and good sensitivity for the device performances. This property enables accurate probing of complex biological dynamics[128] with bioelectronic devices. The well-established and precisely-controlled synthesis of Si makes it easy to fabricate various architectures from nano- to macroscopic scale. Such multiscale material control matches well with the multi-scale application for different biological components and enables integration with various biological systems.[38] More specifically, one-dimensional (1D) Si nanostructures, exhibiting improved mechanical flexibility and increased carrier transportation capacity, can be delivered into neural cultures or tissues in a drug-like manner with high spatial resolution.[22, 129, 130] In this section, we review and discuss several chemistry aspects of Si-based biointegrated systems, including the synthetic chemistry of Si nanostructures, chemical and biochemical sensing by Si-based transistors, photoelectrochemistry and electrochemistry of Si materials, surface chemistry for biocompatibility and specific targeting, and chemical etching and degradation.

3.1.1 Overview of synthesis methods for Si-based structures

Chemical vapour deposition (CVD) is a commonly used strategy to produce Si-based materials.[131] In a CVD system, Si nanowires (SiNWs) are typically synthesized through the vapor–liquid–solid (VLS) growth mechanism.[38] Metal catalysts, *e.g.*, Au, Pt or copper (Cu), act as energetically preferential sites for the absorption and decomposition of gas-phase Si precursors (*e.g.*, silane (SiH_4), disilane (Si_2H_6), or silicon tetrachloride ($SiCl_4$)), when operated above the eutectic temperatures. The continuously fed gas reactants establish supersaturated metal/Si alloy droplets, followed by the nucleation and precipitation of SiNWs.

Besides producing nanowires, CVD is also useful in the scaleable synthesis of a variety of other nanostructures, such as 0D nanoparticles, 2D multilayered membranes,[38] and 3D mesoporous structures.[67] In particular, the Si mesoporous structures were synthesized from a nano-casting method by using mesoporous silica (*e.g.,* SBA-15) as a template, in which SiH_4 was decomposed inside the mesopores in a CVD system. Precision Si synthesis in a CVD system is important since the doping profile, morphology, and crystal structure can determine their physical properties and the corresponding bioelectronic applications.[38]

Besides the conventional vacuum processes and vapour-phase deposition method, Si structures can also be synthesized by solution processes.[132] For example, hydrogenated polysilanes are feasible liquid Si precursors, as they show excellent solubility in organic solvents.[132] In a nitrogen atmosphere, through a photo-polymerization process under UV light and a heat treatment, polycrystalline Si can be obtained from the polysilane precursor. As scaleable fabrication methods such as spin-coating or ink-jetting can be used, poly-Si films with large area and high electron mobilities (*e.g.,* 108 $cm^2 \cdot V^{-1} \cdot s^{-1}$) have been produced.[132] Crystallized Si can also be obtained at high temperature (>745 ^oC) in a molten salt system. For example, SiO_2 nanoparticles were used as the precursor to produce Si in a $CaCl_2$ molten salt (850 ^oC) system.[133]

Chemical etching methods are also commonly used for the synthesis of Si-based materials.[134, 135] In a hydrofluoric acid/hydrogen peroxide (HF/H_2O_2) solution, Si can be selectively removed by a metal-assisted chemical etching (MACE) process, where noble metals serve as catalytic sites for directional etching.[135] MACE has produced various morphologies, such as nano- or microwires,[136] needles,[137, 138] thin films,[139, 140] and other structures.[141, 142] In a recent example, it was found that even atomic Au can trigger the MACE process, producing SiNWs with massively parallel 3D grooves on their sidewalls. The groove spacing can be as small as ~5 nm, and the starting atomic Au patterns were likely generated by a 'stick-slip'-like droplet instability during the VLS growth (**Fig. 4a**).[143]

Many other chemical etching methods, such as KOH etching or defect selective etching using solutions such as $K_2Cr_2O_7/HF$ or CrO_3/HF, are also efficient routes for the fabrication of Si nanostructures.[144-150] For example, anisotropic SiNW spicules were synthesized by wet chemical etching of p-doped SiNWs in KOH solutions (**Fig. 4b**), using atomic Au diffusion–induced patterns as the etch mask.[144] An ENGRAVE (Encoded Nanowire Growth and Appearance through VLS and Etching) strategy was also developed to control the etching

rate of Si in KOH using variable dopant concentrations.[145-147] Specialized features ranging between 10 nm to 700 nm in length have been successfully encoded along the SiNWs.[145-147]

Finally, electrochemical etching allows for the synthesis of nanoporous Si films and particles from single-crystal Si substrates.[139] The loose porous structures in electrochemically etched Si substantially reduced the Young's modulus,[67, 137] which is beneficial for establishing minimally invasive biointerfaces.

3.1.2 Degradation of Si-based structures

The physical and chemical properties of Si-based electronics are known to be very stable at dry states. But for bioelectronic applications, the degradation of Si at biointerfaces needs to be carefully considered in wet environments.[151] Si reacts with water via hydrolysis to form silicic acid $Si(OH)_4$: $Si + 4H_2O \rightarrow Si(OH)_4 + 2H_2$, where the $Si(OH)_4$ departs the Si surface through diffusion. Silicon dioxide (SiO_2) may also form as an intermediate.[134] Several parameters play important roles in the degradation, including surface chemistry, dopants, pH, ion concentration and temperature.[128, 152-155] Understanding the chemical processes of Si degradation has already opened a new way toward safer biomedical applications, *e.g.*, *in vivo* implants based on transient electronics.[125, 134, 156-159]

Ultrathin single crystalline Si nanomembranes (SiNMs) are the main constituent in several well-performing, transient electronic systems. For example, Hwang *et al.* developed a transient integrated circuit by using degradable materials such as magnesium (Mg), MgO/SiO_2, Si, and silk for parts like inductors, capacitors, and transistors (**Fig. 5a**).[134] Si nanomembranes of 70 nm thickness were dissolved via hydrolysis with speeds of 4.5 nm/day and 2 nm/day under physiological temperatures (37°C) and room temperature (25°C), respectively. Magnesium coils, Si Joule heating elements, and silk substrates and packages conferred transient thermal protection against infection, as increased local temperature suppressed bacterial growth as well as eased pain. Similarly, Bai *et al.* developed injectable bioresorbable devices that can be naturally resorbed or undergo clearance from the body after an operational lifetime (**Fig. 5b**).[160] This bioresorbable device can be successfully used for continuous checking of the cerebral microenvironment (*i.e.,* temperature changes, oxygenation and neural activity) in freely moving mice. More recently, Shin *et al.* developed SiNM-based bioresorbable optical pressure sensors that depend on pressure-induced deflections of SiNM diaphragms (**Fig. 5c**).[157] The potential of using this material, which is

also compatible with magnetic resonance imaging (MRI), for clinical applications is very promising based on *in vitro* studies, histopathological evaluations, and acute measurements of intracranial pressure (ICP) and temperature (ICT).

For long-term applications of Si-based bioelectronics,[161, 162] degradation needs to be minimized. One technique for accomplishing this employs a thermal oxide thin layer directly grown on the surface, which can prevent biodegradation in phosphate-buffered saline solution.[163] Several efficient passivation coating materials also work well to inhibit Si degradations, including stable Al_2O_3,[162] TiO_2,[164] and $SrTiO_3$.[165] As demonstrated by Hu *et al.*, atomic layer deposition (ALD) of TiO_2 layer (4 to 143 nm thick) significantly improves the stability of Si photoanodes under basic water oxidation conditions.[161] More generally, TiO_2 stabilizes many semiconductors during oxidative photochemical processes by engineering the band structures and the defect states.

3.1.3 Chemistry for optical functionalities at the Si biointerfaces

Among the many useful functions of Si semiconductors, their ability to convert light into electric current is one of the most important uses. After Si semiconductors absorb light, the photonic energy can be transferred into electronic energy. When Si-based materials are used in cell cultures or as implants, they are usually surrounded by biological fluids, forming semiconductor/saline interfaces. With light, this can yield transient, photocapacitive modulation of cells or tissues (**Fig. 3**), or longer-lasting photofaradic reactions (**Fig. 3**) where the electrons and holes participate in cathodic and anodic reactions, respectively.

Palanker *et al.* developed a series of photovoltaic retinal implants, where the high-pixel-density devices provide local modulation of rat retinal neurons for potential restoration of vision.[166-168] In order to enhance photostimulation by nano-bioelectronic devices, the photovoltaic or photoelectrochemical effect must be maximized. Parameswaran *et al.* found that dopant modulation and surface chemistry of the Si nanostructures could enhance their performance as neuromodulators (**Fig. 6a**).[129] They used coaxial p-type/intrinsic/n-type (p-i-n) SiNWs, each consisting of a p-doped core nanowire, an interlayer of intrinsic Si, and a n-doped shell, to modulate primary rat dorsal root ganglion (DRG) neurons through photoelectrochemical processes. Experiments also showed that diffused atomic Au on the SiNW sidewalls could significantly enhance the generation of photoelectrochemical currents, and thus the neuromodulation efficacy (**Fig. 6b**).[129] A similar conclusion was found in

another study conducted by Jiang *et al.,* which studied 2D p-i-n Si membranes with noble metal nanoparticles (*e.g.,* Au, Ag and Pt) decorated on their surfaces by means of an electroless deposition method.[38] They found that metal-decorated p-i-n membranes enhanced photoelectrochemical current generation by at least an order of magnitude. This successfully yielded photo stimulation of the brain cortex and behavior control (**Fig. 6c**).[38] Si photovoltaic devices can also play a key role in ultrasensitive detection of biometric signals. Yokota *et al.* recently reported the fabrication of a conformable imager derived from low-temperature polycrystalline Si (LTPS) thin-film transistor (TFT), which can read out small photocurrents of less than 10 pA with low noise.[169] The TFT readout circuits are designed by Si oxide film (SiO), Si nitride film (SiN), and amorphous Si film (a-Si) that was transferred from polycrystalline Si through excimer laser annealing. Combined with sensitive organic detectors, the imager can detect and calibrate the displacement of the device electronically on the basis of fingerprint or vein feature points.

Electric energy generated from light radiation on Si can also be converted into heat, in a process known as the photothermal effect as described in section 2.3.4 (**Fig. 3**). The local temperature increase induced by light can be exploited to activate biological responses. This is a promising avenue for Si-based photostimulation. Researchers have developed strategies to enhance this Si photothermal effect. Jiang *et al,* developed mesoporous Si microparticles with a nano-casting method (**Fig. 6d**).[67] The replica Si from hexagonal mesoporous silica SBA-15 display open-framework and porosity. The microparticles have an improved photothermal effect, as the porosity reduces the thermal conductivity and heat capacity but enhanced the light absorption. This mesoporous Si can modulate action potential (AP) firing and deterministic neuronal responses up to ~15 Hz through an optocapacitance mechanism.[67]

3.1.4 Chemistry for electrical functionalities at the Si biointerfaces

One of the most common applications for semiconductor-based bioelectronics is sensing bioelectrical signals. While patch-clamp electrodes have been developed enough that they can sense localized electrical signals from single ion channels, the electrodes are invasive and the biointerface is brief. With a smaller dimensionality, SiNW-based nano-bioelectronics[43, 170-172] have been developed for intracellular recordings.[43] The chemical designs of the SiNWs play a key role in facilitating the intracellular entrance. For example, the first nanoscale FETs (nanoFETs) used for intracellular electrical recording involved the CVD synthesis of kinked

nanowires with dopant modulation. The kinked SiNWs with two cis-linked kinks of an overall ~60° angle of the bent junction were achieved by repeated pressure modulations (**Fig. 7a-c**).[43] The nano-sized FET region was established by inserting a lightly doped region (~200 nm) in heavily doped n-type nanowire backbone (**Fig. 7a**). Such doping control enables a localized FET region for sensitive intracellular recording. [43]

Atomically sharp nickel silicide interfaces derived from solid-state reactions on Si nanowires yielded short-channel nanoFET devices.[173] Using this method, Zhao *et al.* realized a scaleable fabrication of highly sensitive nano-bioelectronics (**Fig. 7d** and **e**) through deterministic shape-controlled nanowire assembly.[174, 175] These devices were able to record the full amplitude APs from primary neurons and other electrogenic cells in a multiplexed layout.

Additionally, the Rogers group has developed a series of works about the thermal growth of SiO_2 layers over Si nanomembranes. This oxide design not only enabled the electrical coupling of devices to tissues, but also served as an encapsulating material against the penetration of biofluids. These bioelectronic devices showed safe and long-term applicability, including epicardial mapping of *ex vivo* hearts and electrical stimulation.[176-178]

Lastly, molecular functionalization of silicon surfaces has been widely applied to improve the electrical performance of silicon substrates in biosensing applications and memory devices.[179] H-terminated silicon surface can be directly or indirectly coupled with electrically active moieties via oxide-free functionalization. Such moieties include but are not limited to ferrocene,[180-182] quinones,[183] metal-complexed porphyrins,[184] tetrathiafulvalene (TTF),[185, 186] and fullerene (C60).[187, 188] Additionally, Bunimovich et al. reported FET-based biosensors with oxide-free Si–C layers that showed exceptional sensitivity ($< 0.1 \times 10^{-9}$ M) in DNA detection,[189] where single-stranded DNA was electrostatically adsorbed. Changes of molecular length, packing density, and coverage in surface terminating groups can largely influence insulating properties and capacitance performance.[180, 190-192]

3.1.5 Chemistry for tight integration at Si biointerfaces

Overall, molecules with a variety of terminal groups can be anchored directly onto silicon surfaces via covalent bonds, e.g., silicon-carbon, silicon-nitrogen, and silicon-oxygen bonds. The resultant properties strongly depend on the surface molecular layer formation processes, which include carbonization, oxidation, hydrolytic condensation, thermal dehydrocoupling, and ring-opening click chemistry.[193, 194] The functionalized surface monolayer further serves

to provide linkages that are useful for attachment of native bioderivatives (*e.g.,* peptide motifs[195, 196] and proteins[197-200]) and synthetic nanomaterials.[201] When immobilized on the silicon surfaces, these species can effectively improve cell-silicon interactions or biosensing abilities.[89, 202]

Si surface chemistry plays an important role in the interaction between Si-based materials and biological targets. For example, surface modifications of Si substrates with polylysine can be used for deterministic patterning of Si/neurite interfaces.[203] Surface modification can also enable controlled cellular internalization of SiNWs. Zhang *et al.* reported strong interactions between SiNWs modified with folate and CHO-β cells, and uptake of the modified SiNWs by the cells.[204] Surface coating of SiNWs has also facilitated intracellular recording. The Lieber group has reported several cases which showed that surface modification of SiNW-based nanoFET probes with a phospholipid bilayer can promote intracellular entrance for the device through a possible membrane fusion process.[42, 43, 175]

Surface geometry modification can also help establish close biological integration. For example, through Au diffusion in SiNW growth and subsequent wet-chemical etching, Luo *et al.* reported the synthesis of anisotropic Si spicules (**Fig. 4b**). With a spiky sidewall, the spicules established very strong mechanical interactions with extracellular matrix materials, such as a collagen hydrogel[144]. Similar structural features may be adopted for future implantable material design and implementation.

3.2 Other inorganic semiconductor-based materials

Besides Si, inorganic semiconductors such as ZnS nanoparticles, TiO_2 nanotubes, MoS_2 nanosheets, and many other metal oxides and metal sulfides have also been widely used in bioelectronics or bioelectrical studies. Their stability, diverse band gaps, and broad range of nanostructures make them good candidates for chemical and biological sensing, *in vitro* or *in vivo* labeling, and energy transduction at biointerfaces.[205-208]

3.2.1 General synthesis methods

Here we discuss a number of methods for synthesizing semiconductors that are tailored to fit the eventual biological question or application for the materials. The four processes we focus on are gas phase, solution phase colloidal, electrodeposition/molten salt-enabled, and bioinspired mineralization syntheses. These techniques allow for a vast array of possible compositions and device geometries, depending on the specific needs of the biointerface with

respect to parameters such as band gap, size, and toxicity. For instance, interfaces intended to be used with photoelectrochemical modulation work best with bandgaps in the visible light range.

a) Gas phase synthesis

Conventional epitaxial growth methods of semiconductor thin films include molecular beam epitaxy (MBE), pulsed laser deposition (PLD), and CVD.[209] The MBE method could precisely control the growth process at the atomic level. However, ultrahigh-vacuum ($<10^{-10}$ torr) conditions are required. PLD requires a low-pressure system in the presence of precursor gases such as O_2, N_2 and H_2 and is good at creating artificially layered oxides for fabrication of oxide electronic and magnetic materials. CVD and metal-organic chemical vapour deposition (MOCVD) are most commonly used methods for semiconductor thin film epitaxial growth. Various kinds of semiconductor thin films, such as MoS_2,[210] WS_2,[211] WSe_2,[212] $SiGe$,[213] $GaAs$,[214] $InGaP$,[215] and GaN[216] have been synthesized from the CVD or MOCVD methods.[123, 205, 217] Semiconductor thin films with single-atom thickness and unique electronic band structures provide key advantages in developing novel electronic and photonic devices.[218] Compared with other synthesis methods, the precise control over chemical composition, the high-quality crystalline nature, and the low defect level of semiconductor thin films ensure excellent electrical and optical properties across the entire materials.[208] Additionally, CVD and MOCVD syntheses can produce bulky chips and circuits for future large-scale bioelectronic applications.

b) Solution phase colloidal synthesis

There are a variety of solution-based methods available, including sol–gel process, co-precipitation, thermal decomposition, and hydrothermal method. The sol–gel process, i.e., hydrolysis and polycondensation of metal alkoxide (or halide)-based precursors, has been applied to synthesize nanocrystalline or amorphous semiconductors. For making nanocrystals with a narrow size distribution, co-precipitation is widely used, as its lack of extra calcination and post-annealing steps make it more convenient. Polyvinylpyrrolidone (PVP), polyethylenimine (PEI), and other capping molecules have been used for tailoring the particle nucleation and growth kinetics and for stabilizing nanocrystals. Solution-phase methods provide a variety of synthetic combinations for different structural and compositional features. Furthermore, dopants enable tuneable electronic and photonic properties to meet desired specific requirements at biointerfaces.[219]

c) Electrodeposition/molten salt method

GaAs, GaP, InP, and GaInP$_2$, can also be synthesized using electrodeposition in plating solutions.[220] For example, GaAs can be co-deposited by Ga(III) and As(III) oxides (*e.g.*, H$_3$AsO$_3$, HAsO$_3$$^{2-}$) through high temperature reduction and sequential room temperature aqueous solution deposition. Because the as-deposited semiconductors are usually amorphous or poorly crystallized, further annealing processes are frequently required. Electrodeposition of GaP or InP is usually completed by melting eutectics, *e.g.*, NaF/NaPO$_3$/Ga$_2$O$_3$ or In$_2$O$_3$/NaPO$_3$/KPO$_3$/NaF/KF salts at about 600-900 °C. Alternately, a two-step method involving cathodic electrodeposition of In, followed by post-deposition phosphorization with red phosphorus also resulted in the synthesis of InP.

d) Bioinspired mineralization processes

Ion exchange methods developed by Holtus *et al.* have demonstrated the successful transformation of carbonate minerals into perovskite semiconductors.[221] This method can be used to produce 3D structures with tuneable bandgaps, without significant changes to the overall morphology of the material. This raises the possibility of combinatorial investigations into biointerface formation, where the material structure remains consistent, but the electrical parameters of the material vary.

3.2.2 Quantum dots-based bioelectrical studies

The photoluminescence of semiconductor materials, especially for quantum dots, has been widely used for cell and tissue imaging.[154, 222] They are used to track organelle or cell dynamics upon electrical modulation or for correlative bioelectronic sensing and imaging. Quantum dots have been demonstrated to be nanosized tools which can efficiently record subthreshold and suprathreshold events. In particular, detecting bioelectrical events in the space between two lipid layers of the cell membrane (**Fig. 3**) has been proposed and demonstrated preliminarily,[223-225] which is challenging for electrode recording methods. By coupling quantum dots with other molecular systems, bioelectrical sensing in neural membranes can also be conducted. For example, Nag *et al.* reported using CdSe/CdS/ZnS QD for electric field-sensitive charge transfer and for mapping membrane potential in living cells (**Fig. 8**).[225] They designed a QD (electron donor) – peptide/fullerene (electron acceptor) bioconjugated system, where hydrophilic QDs were localized at exofacial leaflets of the plasma membrane while multiple copies of hydrophobic peptide−C$_{60}$ fullerenes self-

assembled within the lipid bilayer.[225] Upon membrane depolarization, electrons transfer with enhanced basal rate from the photoexcited QD donor to the fullerene acceptor, giving rise to further quenching of QD/PL. The fluorescence response of this integrated bioelectrical probe exhibits comparable temporal responsiveness, but with 20- to 40-fold greater normalized change in fluorescence values than those reported for voltage-sensitive dyes.

Moreover, the nanoscale sizes of QDs have enabled light-triggered redox reactivity in the cytosolic space from the subcellular biointerfaces. This has produced light-harvesting bacteria and yeast cells for energy-efficient biofuel or fine chemical production, a new approach in synthetic biology and biomanufacturing.[226-230]

Finally, the emission from QDs can be used for optogenetics stimulation. A notable example is a recent demonstration of using ZnS-based mechanoluminescent QDs for ultrasound-triggered optogenetics[231]. The photoexcited QDs were injected into the blood circulation and can be recharged by 400 nm light at the superficial vessel location. The QDs emit light on-demand by applying a focused ultrasound through intact scalp and skull. This demonstration opens up a new avenue for future *in vivo* bioelectrical studies with QDs.

3.2.3 2D-semiconductors bioelectronics

2D semiconductors such as MoS_2[226-229], just a few nanometres in thickness, are good candidates for soft bioelectronics.[232] The band gap of monolayer MoS_2 is 1.8 eV and 1.2 eV for the bulk.[233] MoS_2-based FET devices have a high on/off ratio,[205, 234] together with high surface-to-volume ratio, which makes them highly suitable for bioelectronic sensing.[123, 213] Sarkar *et al.* reported a MoS_2-based FET sensor that can detect streptavidin at ultralow concentrations, about 100 fM.[232] Additionally, the flexibility and the piezoresistivity of MoS_2[235] have enable the fabrication of a skin-like tactile sensor array, as reported by Park *et al.*[236] This MoS_2-based conformal tactile sensor can be placed over uncommon surfaces such as leather and a human fingertip. The device showed sensitive and robust behaviors and linear responses even after 10,000 loading cycles.

2D semiconductors also possess advantages for optoelectronic applications due to their excellent absorption in the visible range and the capability to generate photocurrent. For example, Choi *et al.* reported the design of a human eye-inspired, hemispheric image sensor with high array density, which was fabricated from a MoS_2-graphene heterostructure.[237] These soft implantable bioelectronics act as retinal prosthetics and can successfully stimulate

optic neuronal cells of a rat under external optical irradiation. Furthermore, MoS_2 demonstrates high rates of electron-hole pair generation in response to illumination. Liu *et al.* reported that the reactive oxygen species (ROS) generated from the photocatalysis effect of few-layered vertically aligned MoS_2 achieved *E. coli* disinfection with >99.999% inactivation.[236] Photoexcited electron−hole pairs in other semiconductor composites,[238, 239] such as C_3N_4/rGO heterojunctions,[240] may also enable the photocatalytic effect in cells and tissue. Zhang *et al.* reported a modulation neuronal interface between C_3N_4 and PC12 cells, where neuronal differentiation can be achieved upon photostimulation.[240] Moreover, the photocatalytic effect has enabled g-C_3N_4 mediated conversion of NADH into NAD^+, a process which can be utilized for the catalytic synthesis of L-lactate from L-lactate dehydrogenase.[241-243]

The shape, dimensions, chemical composition, and surface properties of 2D semiconductors are all related to their biocompatibility. While 2D MoS_2 has been demonstrated to show low cytotoxicity,[244, 245] biocompatibility *in vitro* and *in vivo* remains a concern for other 2D materials, especially for those transition metal dichalcogenides containing Se, Te, or As.[246-248]

3.2.4 Metal oxide-based bioelectronics

Many metal oxide semiconductors can be configured as FET devices. For example, Nakatsuka *et al.* used thin-film In_2O_3 FETs for biomolecular sensing under physiological condition. They modified their FETs with DNA aptamers whose conformation changes upon binding to various molecules such as serotonin, dopamine, glucose and sphingosine-1-phosphate. Notably, the detected molecular concentration ranges from 10^{-14} to 10^{-9} M in PBS solution, overcoming the limitations of Debye screening .[249]

Metal oxide semiconductors are also frequently applied as photocatalysts and solar-to-chemical energy conversion materials because of their inherent ability to generate electron and holes upon photoexcitation, good charge carrier mobility, excellent stability, and tuneable structures. TiO_2 is one of the most frequently used materials for *in vitro* and *in vivo* bioelectronic applications. Demonstrated by Tang *et al.*, a vertically oriented Au-decorated TiO_2 nanowire array of artificial photoreceptors successfully restored functional and behavioral light sensitivity in blind mice.[250] This nanowire array resembles the architecture and function of photoreceptors in retinas. Unlike other engineered bioelectrical implants for

sight restoration, TiO_2 arrays require no trans-ocular cables or power supplies and are expected to offer optimized spatial resolution. With Au nanoparticle decoration, surface roughness guarantees enhanced interfacing between innate retinal circuits and TiO_2. Design of future retinal implants or bioinspired devices would need materials with broadband photo-responsivity from the UV region to the near-infrared region, for which oxide composites or doped oxides may meet the requirement (*e.g.*, Au-WO$_3$-TiO$_2$,[251] CuO/Ta$_2$O$_5$,[252] or In-doped TiO$_2$[253]). Other example in this category includes niobium oxide (Nb$_2$O$_5$)-based photoelectrochemical sensing.[254]

Many metal oxides, such as tantalum pentoxide (Ta_2O_5), ruthenium oxide (RuO_2), nickel oxide (NiO), manganese dioxide (MnO_2), and cobalt oxide (Co_3O_4) are widely applied as electrode materials in lithium-ion batteries, supercapacitors, and solar cells;[255,256] the device configurations and operational mechanisms can be tailored for bioelectronics more broadly. Most of these metal oxides can be obtained through hydrothermal synthesis to yield controllable shapes and electrochemical or optical properties.

4. Organic semiconductor-based bioelectronics

Organic semiconductors have become excellent candidates for flexible and stretchable bioelectronic applications, because of their low temperature solution-phase processability, good mechanical deformability, and applicable charge transport properties.[39, 257] When in contact with skin or implanted into tissues, mechanically compliant organic bioelectronics can minimize discomfort and adverse effects due to the mechanical mismatch.[39, 257-260] Moreover, some organic semiconductors are self-healable and biodegradable, which is ideal for wearable and injectable bioelectronics.[261, 262] However, several factors, including the balance between mechanical deformability and device mobility, long-term stability under physiological conditions, stretching and bending durability, need to be considered during the development of the next generation of organic bioelectronics. In this section, we discuss the molecular design of semiconductor polymers, chemical and biochemical sensing from organic transistors, surface chemistry for targeting, photoelectrochemistry and photochemistry of organic semiconductors, and energy conversions of organic semiconductors used in bioelectronics.

4.1 Chemical designs for mechanical deformability

Rational design of semiconductor polymers can help improve the mechanical properties without negative changes to the electrical transport behaviors.[263-266] Increasing the size or number of amorphous regions by lowering regioregularity could prevent crystallization in semiconductor polymers. This would lead to an increase of stretchability, however, it also impacts the electrical performance.[267] Side chain engineering of semiconductor polymers is another efficient route for modulating stretchability.[267] For example, the linear alkyl side chain modification of poly(3-alkylthiophene) (P3AT) developed by Savagatrup et al.[268] and poly(butyl acrylate) (PBA) side chain modification of isoindigo-based polymers PII2T developed by Wen et al.[269] showed that the tensile moduli of such polymers can be reduced by softening the side chains.

Recently, the introduction of conjugation breaking spacers (CBs) into the backbone was demonstrated to be an efficient strategy to endow stretchability to the semiconductor polymer.[270-272] Oh et al. reported the creation of 2,6-pyridine dicarboxamide (PDCA) conjugation units that integrated with 3,6-di(thiophen-2-yl)-2,5-dihydropyrrolo[3,4-c]pyrrole-1,4-dione (DPP) semiconductor polymers (**Fig. 9**).[273] PDCA moieties introduce hydrogen bonding units into the polymer backbone. While the semiconducting crystalline parts allow remarkable charge transport, amorphous polymer chains crosslinked by hydrogen bonds – which can reversibly undergo dynamic breakage and reformation – offer the polymers excellent flexibility and tolerance to stretching. Organic thin-film field effect transistors (OTFTs) fabricated using this intrinsically stretchable semiconductor can be stretched without significantly compromising the semiconducting behavior, with only a slow decline in field effect mobility when stretched up to 100%. When mounted on human limbs, this OTFT device can tolerate various human movements such as arm folding, hand twisting, and elbow stretching, while retaining an average mobility bigger than 0.1 $cm^2 \cdot V^{-1} \cdot s^{-1}$.

4.2 Chemical designs for degradation and stability

Organic semiconductor-based bioelectronic devices are typically not as stable as their inorganic counterparts. Depending on the intended purpose of the device, specifically the duration of the interface, this can be either a positive or negative aspect.

There are two major routes for the degradation of semiconductor polymers: hydrolytic degradation and oxidative degradation.[274] Hydrolytic degradation is determined by the microstructure and composition of the polymer, as well as the temperature and pH of the

surroundings. For hydrolytic degradation, several kinds of sites on the polymer backbone can initiate chemical and enzymatic degradation, including ester/thioester, carbonate, anhydride, urea, urethane, and imide/amide groups, *etc.*[274] An increase of crystallinity and cross-linking density would typically lead to a decrease of degradation rate. Oxidative degradation is a chemically and enzymatically relevant oxidative cleavage procedure of polymers. Common sites for oxidative degradation in polymers are shown in reference.[274]

For long-term bioelectronic devices, stable performance is required (*e.g.,* organic photovoltaic components used as a retinal prosthesis). Encapsulation of the device to prevent water and oxygen transmission is an efficient strategy. For example, in organic LED (OLED) synthesis, the semiconductor polymer can be protected by a ~1 μm thick multilayer encapsulation.[275] The encapsulation contains three layers of Al_2O_3 and two layers of crosslinked acrylic polymer, complying with the standards for typical encapsulation of OLED microdisplays. This multilayer structure encapsulating effect is $10^{-5} - 10^{-6}\ g \cdot m^{-2} \cdot d^{-1}$, which is comparable with low water vapor transmission rates. Rational design of the polymer structure is another efficient strategy to improve stability.[276] For example, Giovannitti *et al.* reported that 3,3′-dimethoxy-2,2′-bithiophene comonomers in alkoxy-Benzo[1,2-b:4,5-b']dithiophene (BDT) copolymers improved the material stability.[277] Specifically, they found that alkoxybithiophene units stabilize positive charges on the polymer backbone, playing a vital role in the long-term operation of OECT.

In some biomedical applications, transient bioelectronics are useful for *in vivo* healing or regeneration,[153, 261] as was discussed in section 2. Nondegradable implants may create a risk of causing a chronic inflammation, necessitating extra surgeries to take them out which risks infection. Thus, molecular designs that make organic semiconductor-based devices degradable at physiological conditions are desirable. For example, Lei *et al.* utilized imine-linked DPP and p-phenylenediamine to synthesize degradable organic materials in acidic (pH = 4.6) environments.[278] By coupling this material with iron electrodes, they fabricated ultra-lightweight disintegrable pseudo-CMOS logic circuits and polymer transient electronics. Their biodegradable organic semiconductor electronics have the potential use for biointegrated applications.

4.3 Chemical designs for electronic functionalities

Organic semiconductors have been developed for numerous bioelectronic applications, notably the skin-inspired electronics.[279, 280] For example, transistor-matrix based organic electronics with thousands of flexible sensory units can potentially replicate skin sensation.[270] Wang *et al.* developed a large-scale high yield uniform transistor array with an intrinsic stretchability up to 100% strain while keeping a ~1 cm^2·V^{-1}·s^{-1} charge-carrier mobility.[259] Kim *et al.* configured organic transistors into artificial synaptic junctions,[279] where the active channels in an ion gel can be gated by multiple inputs. A hybrid monosynaptic reflex arc was demonstrated by connecting this artificial synaptic transistor to nerves of a discoid cockroach.

4.3.1 Chemical designs for charge carrier mobility control

Rational design of semiconductor polymers is the efficient route for improving carrier mobility while keeping good mechanical properties.[263, 265, 266] The crystalline domains in semiconductor polymers, which arise from intermolecular π-π stacking, are favourable for charge carrier mobility.[271] Thus, molecular weight plays an important role in charge carrier mobility.[281] Zen *et al.* reported that in the case of poly(3-hexylthiophene), abbreviated as P3HT, high molecular weight P3HT has higher mobility in organic field-effect transistors,[282] which rely on tie chains with connection function and effective charge transportation between crystalline regions. However, high molecular-weight P3HT showed a lower elastic modulus. More recently, new molecular design routes have been developed for less crystalline polymers to achieve both the high charge mobility and stretchability. For example, Xu *et al.* used a nanoconfinement method to increase polymer chain dynamics and suppress crystallization, while maintaining the mechanical properties of high-mobility polymers.[270, 271] When introducing nanofibrils into a soft deformable elastomer, semiconducting films can be stretched to 100% strain without influencing mobility.

4.3.2 Surface chemistry in organic transistors

Two kinds of transistors, including organic electrochemical transistors[95, 283-285] (OECTs, based on electrochemically doping/de-doping upon ionic species injection into the active materials) and electrolyte-gated organic field effect transistors[286-288](EGOFETs, based on gate voltage-modulated channel currents via a capacitive field effect mechanism at the channel/electrolyte interface) are commonly used in bioelectronic sensing. For detailed information regarding the working principles of these devices, we refer the interested reader to a number of excellent reviews on the subject.[26, 95, 289]

Surface modifications with functional chemical moieties, peptides, proteins, and nucleic acids enable specific chemical and biological detection with high sensitivity.[290-292] For example, the Inal and Owens groups have conducted extensive research on surface biofunctionalization of OECT devices.[290, 293-295] Several enzymes, including glucose oxidase (GO$_x$), lactate oxidase (LO$_x$), and cholesterol oxidase (ChO$_x$), were covalently immobilized onto the PEDOT:PSS gate electrodes to enhance the sensing selectivity.[290] For instance, the PEDOT:PSS can be blended with polyvinyl alcohol (PVA) to introduce hydroxyl functional groups, and then linked with heterobifunctional silanes, i.e., 3 - glycidoxypropyltrimethoxysilane or GPTMS, via a condensation reaction prior to the protein attachments. Containing an epoxy ring, this silane can form chemical bonds with amides from target proteins. The OECT device is based on the n-type copolymer P-90 with lactate oxidase grafting. Working as a resistor, the LOx-functionalized micro-channel amplified the signal of the transistor circuit with its current changing near the noise level with lactate.

Biorecognition can also be realized by surface functionalization (**Fig. 10a** and **b**).[294] Mulla *et al.* employed monomeric porcine odorant binding proteins (pOBPs) as ligands and assembled them on the metal gate of a capacitive coupled p-type organic FET (polymer, PBTTT-C14) device.[291] This device can be used for the selective detection of chiral differential interaction in OBPs in the picomolar concentration range (**Fig. 10c** and **d**). Subtle capacitance changes that associated with the ligand-protein complex formation allow sensitive determination of the free-energy balances from conformational events, *i.e.,* the interaction of chiral (S)-(+)- and (R)-(−)-carvone enantiomers with OBPs. While pOBPs are negatively charged in pure water, the chiral molecules bear a dipole moment and physically bind to pOBPs.

Different to chemical conjugation, physical adsorption process depends on binding kinetics and equilibrium and can be driven by surface energy, intermolecular forces, polarity, charges, and morphology.[296-298] The desire to understand how these factors impact protein adsorption and to predict and control the adsorption process have been main motivating forces for the research in this field, which can help optimize engineering techniques performance in biomedical or physiological applications.[299]

4.3.3 Photoelectrochemistry of organic semiconductor-based biointerfaces

Organic semiconductors can also be utilized in light-triggered electron injection or stimulation. Capacitive processes from double layers and Faradaic process from

reduction/oxidation of a solution species, as discussed in section 2.3.2, are the two main processes that occur at liquid/solid interfaces. Applying photostimulation strategies on the biointerface, such as optical neuronal modulation,[300] presents a potential future direction for biomedical implants as brain disease therapeutics or retinal prostheses.[301-304] Due to the mechanical deformability properties of polymers, organic semiconductors are ideal for injectable and implantable bioelectronics.[305-307] Meanwhile, organic semiconductors may also produce electron-hole pairs upon exposure to sufficiently energetic light. This capability for photostimulation may be further enhanced by the good charge carrier mobility available in organic semiconductors.[98, 305, 308-315]

Ghezzi *et al.* reported that by employing semiconductor polymer regioregular poly(3-hexylthiophene-2,5-diyl) with phenyl-C61-butyric-acid-methyl ester (rr-P3HT:PCBM) as a photosensitive layer, and ITO as a reference electrode, hippocampal neurons cells could be photostimulated through a photovoltaic mode.[309] Maya-Vetencourt *et al.* developed an organic implant for restorative retinal prostheses using a similar method.[308] They utilized P3HT as an active semiconductor layer, poly(3,4-ethylenedioxythiophene): polystyrene sulfonate (PEDOT:PSS) as intermediate conductive layer, and 30 μm thick silk fibroin layer as a passive substrate (**Fig. 11a**).[308] After implantation, this biocompatible and photosensitive organic prosthetic can rescue light sensitivity and spatial acuity *in vivo* for nearly a year. Additionally, a P3HT-based optoelectronic epiretinal interface was reported by Gautam *et al.* to provide visual cues that could stimulate blind retina.

Jakešová *et al.* demonstrated that organic electrolytic photocapacitors (OEPCs)[316] could be used to generate photocapacitive current for X. laevis oocyte stimulation.[317] Photoexcitation of the H_2Pc (P-layer, donor) and PTCDI (N-layer, acceptor) junction accumulated electronic charges, forming the opposite electrolytic double layer at the front and back plane of semiconductor electrodes (**Fig. 11b**).[317] Furthermore, organic photovoltaic photosensors of (2,4-bis[4-(N,N-diisobutylamino)-2,6-dihydroxyphenyl] squaraine, (SQIB) blended with a fullerene acceptor (phenyl-C61-butyric acid methyl ester, PCBM) were utilized by Abdullaeva *et al.*, to examine how activation of voltage-gated ion channels works in single neuroblastoma (N2A) cells by utilizing patch-clamp recording.[318]

4.3.4 Other organic semiconductors devices relevant for biointerfaces

Organic semiconductors may serve as energy transducers, converting solar energy to electrical energy (organic photovoltaics, OPVs). Thus, organic semiconductor-based devices

can be employed as a power and light source in various kinds of biomedical applications.[319-321] Park *et al.* created a self-powered organic electrochemical transistor (OECT) based sensor with high signal to-noise ratios (SNR) for on-skin and on-tissue cardiac signal detection.[322] In this case, the organic conductor PEDOT:PSS served as an active channel of the OECT, which was powered by integrated OPVs. The potential variance between the gel electrode on the chest and the OECT channel on the fingertip acted as the gate bias, affecting the channel conductance and producing the sensing signals. Jinno *et al.* reported environmentally and mechanically stable ultraflexible OPVs generated from a mixture film containing a donor–acceptor polymer with quaterthiophene and with naphtho[1,2-c:5,6-c′]bis[1,2,5]thiadiazole (NTz) (PNTz4T) and [6,6]-phenyl C71-butyric acid methyl ester (PC71BM) used as a stable active layer.[323] This device exhibited a stable photoconversion efficiency (PCE) up to 7.9% under ambient air conditions. The PCE of the double-side-coated OPVs remains stable after 20 compressions and with 100 minutes of water exposure, implying it may be used as a stable power source for wearable electronics.[322] Similar designs from the same group were utilized in a self-powered compliant electronic device, which may be used to realize precise and sensitive biological signal acquisition.

Organic semiconductors also serve as important active materials in OLEDs, which are commonly used as light sources in biomedical application.[324] For example, OLEDs are desirable for making epidermal pulse oximeters owing to the processability and fabrication of flexible devices.[325, 326] Khan et al. reported the fabrication of a reflectance oximeter array (ROA), realized by printing and integrating organic optoelectronic arrays and conventional Si circuits.[326] ROAs contain four red OLEDs, four NIR OLEDs, and eight organic photodiodes (OPDs), which are blade coated and screen printed on flexible polyethylene naphthalate substrates. Significantly different molar absorptivities of HbO2 and Hb endow the device with the capacity for *in vivo* 2D mapping of oxygenation of forearms under pressure-cuff-induced ischemia. By taking advantage of design freedom for organic devices, Lee *et al.* reported organic pulse oximeters (OPOs) with low power consumption, which are good candidates for stand-alone wearable devices ready for continuous monitoring.[325]

OLEDs also represent a candidate for illumination in optogenetic experiments,[320, 327, 328] because of their high array density at sub-cellular length scales and easily-tuneable emission properties by chemical synthesis. Steude *et al.* reported the fabrication of a blue-emitting fluorescent p-i-n OLED stack that contains more than 200,000 pixels across a ~20 mm² area with small pitch size of 6 × 9 μm². Using OLED arrays, they controlled multiple *C.*

rheinhardtii behaviors such as moving speed and swimming direction, by light stimulation. The same group also found significantly altered membrane current upon illumination.

5. Inorganic conductors for bioelectronics

Metal- and carbon-based materials are the two major groups of conductive inorganic materials that are exploited in many bioelectronics devices. New developments in chemistry to adjust the conductivity, biocompatibility, chemical stability, and workability in terms of fabrication and patterning of these materials is crucial for the performance of next-generation bioelectronics. The general characteristics of common inorganic conductor materials were summarized in Table 2.

5.1 Metal-based materials

Many bioelectronics devices for biosensing and modulation involve the usage of metal-based materials, which include pure metals, metal oxides, metallic alloys, and their composites with carbon or organic materials. Typically, many metals are used directly as electrodes for recoding electrical signals or inputting stimulation current, with classic options including Pt, Au, and Pt-iridium alloys (Pt-Ir). These metallic materials are chemically stable and have minimal cytotoxicity. As an alternative to conventional electrodes, intrinsically soft, low melting temperature liquid metals, such as gallium-based liquid metal (*e.g.* EGaIn), are promising for the further convergence of biology and epidermal electronics.[329, 330] Chemical engineering methods have been advancing these metals or metallic alloys towards better functionality, stability and biocompatibility by increasing charge injection capacity (CIC),[331] electrochemical stability,[332] inertness or resistance to corrosion,[333] ductility,[334] and surface softening.[335]

5.1.1 Pt

Pt, a ductile transition metal with good chemical stability and biocompatibility, can be fabricated into a variety of geometries for bioelectronic applications.

a) PtNPs. PtNPs are widely used as decoration on other materials to offer active reactive sites and enhanced material properties. For instance, PtNPs show high affinity with liquid metals, resulting in the uniform dispersion of liquid metal on Pt-decorated carbon nanotubes (**Fig. 12a**).[336] With both mechanical and electrical properties superior to pristine liquid metal, the Pt/CNTs/liquid metal composite can be printed into high-resolution 3D structures (**Fig.**

12a), enabling the construction of future 3D wearable bioelectronics. In this study, the PtNPs were decorated by reducing $Pt(NH_3)_4(NO_3)_2$, on carboxylated nanotubes in an H_2 atmosphere.

PtNP-decorated silicone composites have a high surface area and can produce a cathodal charge storage capacity of ~50 mC·cm^{-2}, comparable to highly doped organic electrode coatings.[337] PtNPs also improve the current density and detection sensitivity of a graphene-based glutamate sensor[338] and glucose sensor,[339] owing to their superior catalytic behavior over hydrogen peroxide (H_2O_2). When combined with natural reducing agents, such as tannic acid (TA) polyphenols,[340] the catalysis of H_2O_2 is accelerated via synergistic effects.

b) 1D Pt structures. Pt wires or fibers have also been widely utilized as electrodes, especially for measuring extracellular activity *in vivo*. Alloyed with Ir, electrodes are strengthened while retaining the chemical stability and biocompatibility. Pt-Ir shows low conductor resistance (impedance of ~400 MΩ·μm^2 at 1 kHz) but with a limited CIC below 200 μC·cm^{-2},[341] which limits its usage in liquid solutions due to possible toxic products generated from Faradic interfacial charge transfers. Further improvements can come from synergistic effects with carbon. For example, a coaxial graphene/Pt fiber-like electrodes showed an increased CIC of ~ 10 mC·cm^{-2} (**Fig. 12b**).[342]

c) 2D Pt structures. Planar Pt materials are attractive as recording sites in bioelectronic devices. With nanofabrication and photolithography, Pt of a few nanometres thickness is patterned with spatial precision on Au interconnection networks, as shown in many state-of-the-art electrophysiology probes, such as the flexible 3D mesh electronics,[10, 40, 343] and neuron-like electronics[344]. Encapsulated by flexible polymers, these probes seamlessly integrate with biological tissues (for example, brain), which helps the signal transduction for electrophysical recording or stimulation and elicits minimal cell losses at the interface.

d) 3D Pt structures. 3D nanostructured Pt electrode arrays are widely applied as 3D metamaterials in different interfacing scenarios. For example, vertically aligned Pt nanopillars have been utilized in measuring both intracellular and extracellular activities from individual cells.[345-347] Pt pillar arrays can be constructed via focused ion beam (FIB) milling and FIB-assisted Pt deposition.[345] This technique, however, is incompatible on flexible substrates like parylene C. While electrochemical deposition[348, 349] and dealloying Pt-based compounds[350, 351] can result in 1D Pt nanostructures, noxious byproducts, such as electrochemical surfactants and Pt black, limit its usage.

3D porous Pt constructed by selective chemical etching addresses the above-mentioned challenges. Ganji *et al*. synthesized porous Pt nanorods (PtNRs) on parylene C substrates by dissolving Ag from a co-sputtered PtAg alloy (**Fig. 12c**).[352] These Pt nanorods display good stability, biocompatibility, and electrochemical parameters. With similar chemical etching, nanoporous Pt meta-electrodes fabricated by Dipalo *et al*. were characterized with great nanoscale surface roughness, a near-infrared (NIR) light absorption, and an intimate biointerface with cardiac cells.[90] These Pt meta-electrodes function like 3D antennas, and when paired with plasmonic optoacoustic poration, can record intracellularly. Overall, porous Pt meta-electrodes have several merits compared to 3D arrays with high aspect ratio Pt nanostructures, including easier fabrication, simple electronic circuitry design, and cost-efficient large scale production.

5.1.2 Au

Au is another good candidate for forming bioelectrical interfaces because of its excellent electrical conductivity, ductility, biocompatibility, chemical stability, and various fabrication and surface modification methods. Besides, Au has plasmonic properties, which can be used to generate localized heating in the vicinity upon light irradiation. Thus, Au has been widely used in many bioelectronic systems, as interconnections and leads for sensing, by enhancing tissue engineering as a good conductor, and to modulate and sense biological behaviors via plasmonic responses.

a) Au for electrical sensing. Au nanostructures perform well in sensing intracellular action potentials in excitable cells, like neurons and cardiomyocytes. Au nanopillar with a mushroom-shaped cap can also record subthreshold synaptic activity and action potentials *in vitro* with minimal invasiveness for days,[353] longer than the conventional patch-clamp methods. As was demonstrated by Fendyur *et al.,* mushroom-shaped Au microelectrodes improved membrane engulfment substantially (**Fig. 13a**),[353] which is desirable for their application due to the formation of high resistance seals between interfaced cell and the electrodes. Recently developed OpticSELINE microelectrodes[354], flexible on-skin electronics,[355] and aforementioned mesh electronics[10] are also examples of Au-based electronics.

For intracellular recordings of single-unit electrical activities of networks of neurons and refined modulation of subthreshold events, Au nanopillars[345, 356] and monocrystalline Au

nanowires (AuNWs) of ~100 nm in diameter[357] are valid. The AuNWs were grown on sapphire substrates via CVD and later mounted on a tungsten (W) tip that was coated with nail varnish solution for passivation. AuNWs are also widely applied in flexible electronics that are wearable and implantable. For example, Au-coated Ag nanocomposites (**Fig. 13b**) in an elastomeric block-copolymer matrix exhibit an excellent conductivity of up to ~73,000 S·cm^{-1}, and a stretchability up to more than 800%.[358] This Au-Ag nanocomposite conformed to human skin and swine heart, and performed electrophysiological recording and electrical/thermal modulation. The inert Au coating prevented silver oxidation and ensured biocompatibility.

b) Tissue engineering. Cardiac patches made of 3D porous biomaterial scaffolds with seeded cardiac cells can be used to treat damaged heart tissues after a heart attack.[359-361] While the porosity of polymer substrates offers environmental cues for healthy cell growth and functioning, it is expected that integration of electrically conductive materials can not only enable electrical sensing,[362] but also increase synchronized contraction of cardiac cells and therefore improve the therapeutic value of the cardiac patch.[363, 364] For example, ultrasoft polymer nanomeshes with 100 nm of Au deposition have been demonstrated by Lee *et al.* to map electrophysiological dynamics during cardiomyocyte beating (**Fig. 13c**).[362] Besides, Au-decorated alginate cardiac patches designed by Dvir *et al.* enhanced electrical communication between adjacent cardiac cells and thereby improve synchronization of cell contractions.[364]

An on-off on-demand drug release functionality can be integrated by depositing drug-loaded electroactive polymers within Au-decorated cardiac patches. For example, negatively charged chondroitin 4-sulphate hydrogels can load positively charged growth factors and cytokines, such as insulin-like growth factor 1 (IGF-1), vascular endothelial growth factor (VEGF), and stromal cell-derived factor-1 (SDF-1), while positive polypyrrole (PPy) films can load dexamethasone (DEX). These biochemical cues control cardiac function and improve therapeutic effects of the patches through different regulation pathways.[6]

c) Plasmon-enabled bioelectrical sensing and modulation. Beyond Au nanoparticle (AuNP)-based photothermal cancer therapy, plasmonic effects are also widely used for bioelectronic sensing and modulation through neural photostimulation. For example, Dipalo *et al.* fabricated 3D plasmonic Au nanoelectrodes for intra- and extracellular recording of spontaneous neural APs. Photo-triggered plasmonic optoporation allowed AuNWs intracellular access without perturbing ongoing electrical activity.[356] Au nanorods (AuNRs), generating surface plasmons in response to near-infrared light, can facilitate neuromodulation

through the optocapacitive effect.[65, 66] In contrast to this, the ability to photothermally inhibit single-neural activity *in vitro* with NIR-sensitive nano-Au has also been reported by Yoo *et al.*[64, 365, 366]

d) Fabrication and surface modification. A variety of approaches have been reported to fabricate nano- and microscale Au, for example the reduction of $HAuCl_4$ into Au nanorods by citrate or borohydride[367] in water solution (bottom-up method), photolithography, and electron beam lithography (top-down method). Reported by Lu *et al.*, welding under relatively low pressures and near room temperature produced crystalline AuNW network with diameters smaller than 10 nm.[368] The atomic diffusion and surface relaxation enabled cold welding within seconds merely via mechanical contact. This nanoscale welding is expected to advance bottom-up assembly of 1D metallic nanowires in future bioelectronics with improved mechanical durability and electrical properties.

Surface functionalization of Au can promote desirable functions, such as physisorption of biological cargo loading and cell adhesion, and create favourable electrostatic or ligand-receptor interactions by replicating naturally occurring binding sites. For example, ligands like Ts1 promote AuNPs binding to neuronal membrane with washout resistance.[66] Arginylglycylaspartic acid (RGD), the most common motif responsible for cell adhesion to the extracellular matrix (ECM), can promote membrane/Au contact and cause the phagocytosis-like cell engulfment of the Au-mushrooms nanoelectrodes.[369] Electrostatically charged polymers, such as polylysines[370] and polyornithines,[371] have also been widely applied to enhance cell adhesion to Au nanoelectrodes. Additionally, Au nanoelectrodes coated with Pt, iridium oxide (IrOx), and titanium nitride (TiN), offer excellent electrical coupling, surface area, and cell adhesion characteristics without influencing the plasmonic performance. Au-nanostructured microelectrodes were also used as a component in a system to process to detect cancer in unprocessed serum, in conjunction with a gene-responsive peptide nucleic acid coating and $Ru(NH3)_6^{3+}/Fe(CN)_6^{3-}$ electrocatalytic redox pair[372]

Overall, different surface coating materials, ranging from binding motif-mimicking synthetic coatings to natural extracellular matrix gels, such as fibronectin, laminin, and collagen, and to inorganic materials, interplay with biological systems through differing mechanisms and can induce various biological responses and downstream regulations.[373-375]

5.1.3 Liquid Metal

Taking advantage of the extreme deformability and excellent metallic conductivity, liquid metals are widely used in many flexible bioelectronic devices or e-skins, such as Ga-based neural probes,[376], all-soft matter circuits,[377] and conformal and reconfigurable electronics that can undergo extreme strains.[329, 378] While the most well-known liquid metal, mercury (Hg), is lethally toxic, gallium (Ga) and several Ga-based alloys, commonly gallium indium (EGaIn) and Galinstan, are considered to be biologically safe.[379]

In air, the surface of Ga quickly forms a thin oxide layer, which prevents surface tension-driven droplet formation and thereby allows the patterning of Ga into designed geometries and structures. The electrochemistry of native surface oxides of Galinstan in electrolyte solution is highly dependent on the electrolyte concentration. Ga oxide can be removed via etching with acidic (pH<3) or basic (pH>10) solutions or *via* electrochemical reactions under a reducing bias.[380, 381] For example, NaOH solution dissolves Ga(III) oxide and produces $NaGa(OH)_4$, which forms hydrophilic interfaces and results in low interfacial tension between the electrolyte and liquid metal.[382]

Along with an increasing number of studies focused on the liquid metal-based bioeletronics, several patterning methods have been developed to fabricate liquid metal traces, for example, microfluidic injection, additive and subtractive process, and lithography methods.[383] Recently, liquid metal patterning technologies to match cellular dimensions have been developed. To achieve single cell spatial resolution, all-soft EGaIn-based devices with submicron feature sizes down to 180 nm were created.[384] Fabricated using both electron-beam lithography and soft lithography, this device generated the current highest resolution of liquid metal patterning. Additionally, sonication has been used to produce liquid metal droplets for printable devices. The morphology of liquid metal particles can be stabilized by positively charged molecular or macromolecular surfactants, such as cetrimonium bromide (CTAB) and lysozyme.[385] Embedded in polymers, liquid metal-based soft electronic devices are not only stretchable, but also self-healing. For example, abundant hydrogen bonds in PVA recovered the mechanical and electrical properties of patterned liquid metal circuits after cutting without any addition of any agents or solvents.[386] Liquid metal-suspended soft elastomers also have self-healing abilities without requiring manual repair or external heat.[387] When impaired, the metal droplets break to generate new connections with nearby metal droplets, rerouting the transportation of electrical signals without disruption. For more information about the chemistry, physical properties, patterning, and device fabrications of liquid-metal-based materials, readers may refer to available literature.[329, 388]

5.1.4 Other Metals

Nano-silver structures, *e.g.,* Ag nanowires (AgNWs), and 2D Ag flakes, have received extensive attention as conductive fillers for stretchable bioelectronics or rubbery transistors. Ag is highly conductive and mechanically durable, and AgNW-based meshes or arrays can have high conductivity due to contacts between long nanowires. Besides previously mentioned Au-Ag nanocomposites,[358] other Ag nanostructures have also been embedded in stretchable polymers, such as polyurethane (PU) and polydimethylsiloxane (PDMS), to make devices that can endure ultrahigh stretching. Yang *et al.* seeded high density AgNWs into PU using intense pulsed light, which heated local PU so that it melted and softened to allow AgNWs to be embedded.[389] Light-induced melting of PU enables tight contact without breaking the substrate, while simultaneously improving junction conductivity between each nanowire. Similarly, Kim *et al.* embedded AgNWs in P3HT-percolated PDMS to construct stretchable transistors,[390] where AuNPs were also coated onto the AgNWs for reducing the energy barrier between the source and the drain. Recently, 2D Ag flake-based conductive networks in a fluorine rubber were studied by Matsuhisa *et al.* As 2D nanostructures have a larger junction area, which in turn allows for reduced contact resistance, 2D Ag flake-based conductive rubber presented a high conductivity of more than 700 S·cm^{-1} at 0% strain.[391] With in situ formed AgNPs, a reinforcement effect led to a conductivity ten times higher than Ag flakes alone (about 6000 S·cm^{-1} at unstretched stage).[392]

Stainless steels (SS) possess good stability, resistance to corrosion, and are characterized with good electrochemical properties, for example, capacitive interfacial charge transfer. A study by Schwarz *et al.* using SS probes 30-50 μm in diameter successfully recorded brain activities in unrestrained, naturally moving rhesus monkeys for close to five continuous years.[393] The scalability of SS also enables large-scale monitoring with volumetric probes with thousand-channel capacity. However, most stainless steels are not compatible with magnetic resonance imaging (MRI) because of their iron-rich chemical composition, which induces severe magnetic field distortions.[394] Therefore, stainless steel induces undesirable artifacts and is potentially unsafe for patients under MRI testing as high frequency magnetic fields may cause high magnetic dislocation forces and torque.

Comparatively, Cu is considered MRI safe with minimal imaging artifacts within a magnetic field less than 40 T·m^{-1}.[395] Although Cu is acceptable to use in MRIs due to its low

magnetic susceptibility, close to that of water and tissues, the potential cytotoxicity of Cu impedes its direct implantation for *in vivo* applications.[396, 397] Zhao *et al.* overcame this limitation by encapsulating the Cu microelectrodes with graphene via a low-pressure CVD process. Remarkably, graphene-coated Cu (G-Cu) electrodes generate negligible magnetic field distortion and MRI artifacts, presenting great opportunities for simultaneous brain activity mapping and electrophysiological recording. Cu, a cheaper alternative to Au, is also widely used as interconnecting wires in flexible electronics in serpentine or waveform patterns that can survive extreme strains.[398, 399]

5.2 Carbon

Graphene and carbon nanotubes (CNTs) are favoured in bioelectronics for their outstanding chemical stability, biocompatibility, high mechanical flexibility, large surface area, a wide electrochemical window for doping and modification, and a variety of fabrication methods.[400] Many flexible monolithic devices and fiber-like probes are fabricated with nanocarbon for bioelectrical sensing,[401, 402] energy storage,[403] and electrochemical measurements[404]. Furthermore, carbon microelectrodes with nanoscale tips (**Fig. 14a**) are ideal for high resolution measurement of synaptic activities and vesicles (**Fig. 14b**).[405] With a carbon fiber in a cell or at close proximity to a cell, oxidation currents elicited by known redox reactions (**Fig. 14c**) can be electrochemically detected.[405-409]

5.2.1 Graphene

Graphene, a 2D structure of hexagonally arranged carbon that is one atom in thickness, has been widely used in bioelectronics. It has extraordinary mobility of charge carriers near 10,000 $cm^2 \cdot V^{-1} \cdot s^{-1}$ at room temperature[410] and a high surface-to-volume ratio (theoretically, a specific surface area of ~2600 $m^2 \cdot g^{-1}$). Coating carbon allotropes on top of metal microelectrodes and vice versa can lead to a synergistic effect between carbon and metal constituents, forming a structure with better electrochemical performance than either individual material, for example, lower electrode impedance, improved charge injection capacity (CIC), and higher surface area. A thin-Pt-coated graphene fiber shows an unrivalled CIC of more than 10 $mC \cdot cm^{-2}$ and an extremely low impedance at 1kHz of ~3 $M\Omega \cdot \mu m^2$, which is two-magnitudes lower than its Pt counterpart (~ 400 $M\Omega \cdot \mu m^2$) and smaller compared to the graphene comparisons (~ 9 to 28 $M\Omega \cdot \mu m^2$).[342] In a wearable patch for diabetes monitoring and therapy (**Fig. 15a**), a serpentine bilayer of Au mesh and Au-doped

graphene together showed improved electrochemical activity compared to bare graphene, owing to the formation of efficient interfaces for stable charge transfer.[404] The hybrid patch, consisting of several sensors and drug delivery microneedles, stably operated under various mechanical deformations (**Fig. 15b**).

Graphene films are also attractive candidates for fabricating sensitive field effect transistors (FETs). Because the formation of unstable potentials at the tissue/metal interfaces causes large direct current (DC) offsets and drift, ultraslow neural activities are always distorted, making it challenging for metal electrodes to record ultraslow signals. Masvidal-Codina and co-workers reported graphene-based solution-gated FETs (or gSGFETs), in the form of 2D flexible epicortical and intracortical arrays which can serve as an alternative to metal electrodes for mapping ultraslow (below ~0.1 Hz) cortical brain activity that occurs in neurologic diseases..[401]

High-quality graphene can support primary neuron growth without other biomaterials.[411] Graphene substrates were reported to enhance differentiation of neural stem cells and promote mouse hippocampal neurite sprouting and extension.[412, 413] Graphene is also widely applied as an advanced coating biomaterial by exfoliation-and-transfer or direct CVD growth onto bioprobes.[414, 415] Graphene-coated probes demonstrated excellent biocompatibility, and generally exhibit intimate and robust graphene/cell interfaces, which help cell maintain a viability of more than 90%.[416] A scattered distribution of microglia and astrocytes was observed around the graphene-coated electrode.[402, 417] The biocompatibility can be further improved by appropriate material treatments.[418] For example, hydrophilization treatment using steam plasma[419] and layer-by-layer deposition with poly-L-lysine[420] improve the proximate contacts between graphene and cells.

3D graphene structures provide cells with spatial microenvironments and synergistic cell guidance cues. For example, 3D graphene foams synthesized by Ni-foam-templated CVD formed 3D interfaces with neurons, which increased the proliferation and growth of neural stem cells (NSC) and enhanced NSC differentiation towards neurons, compared to planar graphene films.[421] These 3D graphene foams can also serve as a conductive scaffold for electrical cell stimulations, where an increased intracellular Ca^{2+} signal in neurons upon electrical stimulation was observed. Similarly, high density microelectrode arrays of 3D porous graphene, fabricated by direct laser pyrolysis, offer a minimally invasive but efficient cortical neuromodulation and sensing.[422] As was demonstrated by Lu *et al.*, the porous

graphene can be doped with 70% nitric acid to decrease electrode impedance and increase the charge injection capacity.[423]

Graphene has broadband optical transparency of more than 90%, which can benefit simultaneous optical imaging, optogenetic stimulation, and electrophysiology.[424-427] For example, contact lenses fabricated from graphene on soft Parylene C film (**Fig. 15c**) enabled simultaneous *in situ* infrared fundus visualization during multi-electrode electroretinography (ERG) recording (**Fig. 15d**).[427] Transparent graphene contact lenses have also been applied for electromagnetic interference shielding,[428] glucose level measurement,[429] and intraocular pressure sensing.[430] Besides, Kuzum *et al.* have demonstrated transparent flexible 2D graphene neural electrodes that provide simultaneous neural calcium and electrical visualization with high spatiotemporal resolution.[424] However, a few layers of graphene generate photoelectrochemical currents during light illumination, which may interfere with the neural electrophysiological signals and produce artifacts.[431]

Graphene is magnetically insusceptible, and therefore ensures a negligible artifact during magnetic resonance imaging (MRI). Zhao *et al.* fabricated a graphene-covered copper (G-Cu) microwire that is compatible with 7.0 T MRI scans as well as being biocompatible and nontoxic.[402] A thin layer of graphene prevents Cu-induced acute tissue toxicity and fast corrosion of Cu. However, over chronic implantation, the rigidity of the G-Cu microelectrodes may elicit neuroinflammation, such as activation of microglia and astrocytes and glial scar formation.

5.2.2 Carbon nanotubes (CNTs)

Similar to graphene, CNTs show a capability to reinforce cell adhesion and growth.[432-434] The large surface area of CNTs promotes neuron adhesion and the formation of tight junctions between CNTs and neural cell membranes, facilitating sensitive recording or efficient electrical stimulation. Excellent biocompatibility of carbon-based nanomaterials can be achieved by adjusting the dosage, surface chemistry, and structure patterning into various architectures that are ideal for biointerfaces.

CNTs display electrical conductivity ranging from metallic to semiconductors, depending on the orientation in which the carbon is wrapped. The specific impedance of CNT fibers is ~20 m$\Omega\cdot\mu$m^2, which is only one-twentieth of Pt/Ir (~400 m$\Omega\cdot\mu$m^2), while the charge injection limit of CNT fibers is ~6 mC$\cdot$cm^{-2}, sixtyfold larger than Pt/Ir (~100 μC$\cdot$cm^{-2}) with

the same geometrical area.[435] The low impedance and the large CIC enable a remarkably high SNR and charge injection across the bioelectronics/cell interfaces.

The flexibility of CNTs allows for conformal integration on human body and within dynamic tissue environments, and CNTs have been broadly examined in many intrinsically stretchable transistor-based bioelectronics[436, 437], self-healable electronic skins,[438, 439] and implantable microfibers.[16, 440] By varying the size and hierarchical structures of CNT, tissue-comparable bending stiffness of $\sim 10^{-8}$ nN·m^2 can be reached in a case of carbon helical fiber bundles (**Fig. 16a** and **b**),[16] which is much lower than those of Si wires and Au wires (~ 0.1 nN·m^2). This flexibility allows for conformal integration within dynamic tissue environments and helps to reduce inflammatory responses (**Fig. 16c**). Similarly, a soft ultra-small MRI compatible implant based on CNTs formed a scar-free neural interface, allowing for stable recording of single-unit action potentials for several months. With magnetic insusceptibility, MRI global mapping of brain activity can be performed during electrical recording.[440]

5.3 Oxides, nitrides and carbides

The use of graphene oxide nanosheets (s-GO) to selectively downregulate the glutamatergic synaptic activity of hippocampal neurons *in vitro* and *in vivo* was reported by Rauti *et al.*, who exploited the use of carbon for trimming down specific synaptic activity and target joint diagnostic/therapeutic applications.[441] Reduced graphene oxide (r-GO) has also been reported with enhanced charge injection capacity that is preferable for electrical neural stimulation.[442] These graphene oxides can be reliably prepared via modified Hummers methods, where potassium permanganate is added into a solution of graphite, sodium nitrate, and sulfuric acid.[443, 444]

Metal oxides with nanostructured surfaces, such as iridium oxide (IrOx) nanotubes, can interrogate cultured cells. For example, Cui *et al.* have demonstrated the usage of IrOx nanotube electrodes for intracellular action potential detection.[445] This platform was used to evaluate the effect of ion-channel blocking drugs on the electrophysiology of cardiomyocytes with significantly improved SNR. These hollow nanotube arrays would be more valuable than solid nanowires when there is a need for intracellular sampling or intracellular delivery of materials such as drugs.

Oxides and nitrides, such as ZnO nanowires, titanium nitride (TiN), and IrOx have also been used as coating materials to improve the electrode performance. Coated with TiN, Pt-Ir

electrodes can be largely improved to reach a 5-fold increase in CIC, due to the large effective surface area TiN provides. The roughness of TiN surfaces also promotes cell adhesion in many cases, for example, the TiN-coated Au cardiac patch.[6] When coated with IrOx, Pt-Ir reaches a higher charge capacity of around ~5 mC·cm^{-2} because of the charges transferring in a reversible faradaic reaction between Ir^{3+} and Ir^{4+} oxide states.

MXenes, which are a class of 2D transition metal carbides, nitrides, or carbonitrides, have been used mostly for energy storage applications. They have tuneable surface terminations, high conductivity, and remarkably high volumetric capacitance.[446] Recently, Driscoll *et al.* used 2D Ti$_3$C$_2$ MXene as high-resolution neural electrodes.[447] Distinct among carbon-based nanomaterials, Ti$_3$C$_2$ is processable in aqueous dispersions. Possessing high effective surface area, this MXene-based neural interfaces displayed low impedance, good sensitivity for neural signals, and high spatiotemporal resolution. Besides serving as biocompatible electrodes, the MXene family of materials may also yield high power density energy storage systems for bioelectronics.

6. Organic conductor-based bioelectronics

The synthesis of conducting materials that are highly flexible while maintaining mechanical integrity remains one of the most challenging aspects facing bioelectronics to date. Organic conducting materials, including conjugated polymers and hydrogels, can be more biocompatible and easier to fabricate compared to most inorganic materials.[448] For hydrogels, in particular, their Young's moduli and water content are much closer to those of biological tissues, allowing them to form more compliant biointerfaces while at the same time, providing satisfactory electrical performance via ionic conduction.[71, 449] While many conductive polymers have been identified for applications in flexible electronics,[450] only a few have been used for bioelectronics. Current research focuses almost entirely on three in particular: Poly(3,4-ethylenedioxythiophene):poly(styrene sulfonate) (PEDOT:PSS), polypyrrole (PPy), and polyaniline (PANI).[289, 451] The characteristics of these polymers are summarized in Table 3.

6.1 PEDOT:PSS

Poly(3,4-ethylenedioxythiophene):poly(styrene sulfonate), or PEDOT:PSS, is a polymer mixture formed of two ionomers that has proven to be one of the most promising conductive polymers for bioelectronics. PEDOT synthesized through oxidative polymerization is

conductive but insoluble in water. A counterion, PSS, is added to increase its dispersion and stability *via* Coulomb interactions therefore making it suitable for the synthesis of hydrogels.[452] PSS is an insulator, and the conductivity of the overall composite is determined by the PEDOT crystallinity. This combination offers numerous advantages in terms of processability and biocompatibility. Whereas conventional hydrogels are generally poorly conductive, PEDOT:PSS hydrogels possess a highly tuneable electron and ion conductivity using a variety of dopants, which either add or remove π-electrons from the polymer matrix.[453, 454]

6.1.1 Chemistry-enabled conductivity, stretchability, and adhesion

One of the challenges in PEDOT:PSS chemistry is managing the strong π-π interactions that are necessary to achieve conductivity. Most PEDOT:PSS materials are prepared as composites, with additives such as poly(vinyl alcohol),[455] acrylamide,[456] and polyacrylic acid[457] allowing for the formation of hydrophobic fibers to minimize unfavourable interactions in their structure. Yeon *et al.* found that blending dodecyl sulfate to PEDOT:PSS aqueous solution enhances the conductivity by selectively removing insulating PSS, increasing interconnectivity between conductive PEDOT cores.[458] This technique allowed them to achieve high conductance materials that can be blended with fabrics and used as Joule heaters for thermal stimulation. However, such additives could potentially compromise the electrical properties of the polymer, so an alternative approach is to fabricate PEDOT:PSS as a thin film and then transfer and fix it onto other elastic substrates, *e.g.,* PDMS. This preserves the high conductivity of native PDMS, while also providing the additional mechanical stability offered by the presence of the substrate. Numerous transfer printing methods have recently been reported that could enable high-throughput synthesis of such devices.[459-462]

An important merit of organic bioelectronic devices is their ability to withstand mechanical stress and maintain their useful properties under deformation. While PEDOT:PSS can only sustain near 2% stretching, modification using dopants and copolymerization permits high composite flexibility. For example, Cuttaz *et al.* demonstrated that the combination of PU and PEDOT:PSS formed a conductive elastomer that integrated the flexibility of PU and the conductive properties of PEDOT:PSS.[463] It was shown that these materials could be directly laser micromachined into devices with comparable performance to Pt arrays in *in vitro* experiments. Additionally, the conductive properties of PEDOT:PSS can stimulate and promote tissue regeneration. In recent work, Iandolo *et al.* demonstrated 3D

printed scaffold made of conductive polymer-based composites that support bone regeneration and showed the proof of concept using human fetal mesenchymal stem cells.[464]

Most dopants are capable of improving either mechanical or electrical properties, but not both. To resolve this issue, Wang *et al.* proposed the application of additives called stretchability and electrical conductivity (STEC) enhancers, taking inspiration from a styrene-ethylene-butylene-styrene block copolymer elastomer structure.[465] The authors suggested that properly chosen STEC enhancers can weaken the PSS interaction with PEDOT, softening PSS domains while promoting high conductivity and crystallinity in the PEDOT network (**Fig. 17a**). This architecture yields a stretchable and conductive PEDOT:PSS-based material. They identified numerous potential STEC enhancers such as sodium dodecyl benzenesulfonate, dioctyl sulfosuccinate sodium salt, and bis(trifluoromethane) sulfonamide lithium salt. The PEDOT:PSS films thus obtained achieve conductivities up to 4100 S·cm^{-1} under 100% strain. They validated the utility of the material by fabricating interconnects for electrical devices that preserve the conductivity under mechanical stretch and large deformations (**Fig. 17b**). In another example, D-sorbitol was used as both a secondary dopant and plasticizer to improve biocompatibility and to permit conductivities higher than 1000 S·cm^{-1} under strains greater than 60%.[466] D-sorbitol can form hydrogen bonds with the hydroxyl groups of polymers such as PEDOT:PSS, promoting phase segregation and increasing the overall stretchability of the material, as well as inducing conformational changes for the formation of conductive PEDOT chains. Overall, research focusing on the stretchability of PEDOT:PSS has focused on partially reducing connections within the PEDOT:PSS matrix while either maintaining maximum PEDOT core interaction or substituting ionic additives to make up for reduced intrinsic PEDOT conductivity.

Since additives can impair material homogeneity and invite possible cytotoxicity, synthetic strategies to increase the purity of PEDOT:PSS are desirable. Synthesis of pure PEDOT:PSS hydrogels under regular conditions is challenging due to the collapse of the fibrillar structure, which decreases the conductivity (**Fig. 18a**). Lu *et al.* have developed a method to synthesize pure PEDOT:PSS while retaining its stability, elasticity, and conductivity.[467] They were able to form interconnected and pure PEDOT:PSS nanofibrils by the addition of DMSO to aqueous PEDOT:PSS, dry annealing, and rehydrating. During this process, drying the solution concentrated the PEDOT:PSS and annealing at high temperatures induced recrystallization and chain rearrangement (**Fig. 18b**). This results in a dry, phase-separated system that, when maintained in a well-spaced network, remains interconnected

once the hydrophilic PSS domains are rehydrated. The mechanical properties of these gels can be tuned by varying the amount of DMSO and method of dry annealing (**Fig 18c**). Importantly, this technique is compatible with inkjet printing and allows for fast pattern fabrication (**Fig. 18d**).

Finally, to enable adhesive properties, a mussel-inspired PEDOT:PSS composite was recently synthesized by Gan *et al.* by using PEDOT:PSS and polydopamine-reduced sulfonated graphene oxide (PSGO). The material was highly elastic, redox-active, and strongly adhesive due to the abundance of catechol groups that can effectively interact with a range of substrates. Its utilities in bioelectronic applications was demonstrated by recording a range of bioelectrical signals using both epidermal and implantable electrodes.[468]

6.1.2 Chemistry-enabled functionalities in electrochemical transistors

Ion-gated organic electrochemical transistors (IGTs) are promising in bioelectronics, however most IGTs operate only in depletion mode (are conductive under zero bias) and are not suitable for sensitive recordings. Fabrication of enhancement mode IGTs (e-IGTs) requires nontrivial chemical modifications, which often make the device hydrophobic, unstable or cytotoxic, therefore compromising its biocompatibility. To address these challenges, Cea *et al.* devised a composite of PEDOT:PSS with polyethylenimine (PEI) to realize a biocompatible e-IGT.[469] Main components of the active channel in the new e-IGT are PEDOT:PSS, PEI and D-sorbitol. D-sorbitol was used as a biocompatible stabilizer to increase hydration and mobility of ions, but novel electrical properties come from the interaction between PEDOT:PSS and PEI (**Fig. 19a**). PEI causes electron transfer and reduction of PEDOT through formation of PEI:PSS complexes and causes de-doping in PEDOT which loses its conductivity. Upon application of gate bias, PEI gets protonated and releases PSS, which upon binding with PEDOT, restores conductivity in the channel. The resulting material is highly stable and the redox reaction ideally reversible.

The obtained materials can be easily fabricated using a standard lithographic approach to form thin and flexible membranes (**Fig. 19b**). The applicability of e-IGTs was validated by recording a number of different bioelectronic signals (**Fig. 19c**). To demonstrate long-time *in vivo* biocompatibility, soft circuits made of depletion and enhancement IGTs were used for nonlinear signal amplification of high-fidelity detection of epileptic discharges (**Fig. 19d**). Such local nonlinear amplifiers showed both a high response rate as well as improved

detection quality over classic thresholding methods (**Fig. 19e**). The devices were stable for over two weeks after implantation and provided high quality recording from freely moving animals. This study is an excellent example of how chemical principles can be applied to realize new functionalities while at the same time preserving the stability and biocompatibility of the device.

6.2 PPy

Polypyrroles (PPy) offer similar advantages as PEDOT:PSS for conductive, organic bioelectronics. When oxidized, PPy becomes conductive because of delocalized π-electrons in a conjugated double bond network along the polymeric nanofibrils**.** Furthermore, they are highly biocompatible and environmentally stable. Ease of synthesis, thermal stability, and biocompatibility make this material uniquely useful for bioelectronic applications. PPy is typically synthesized as monolithic sheets that are highly conductive and accrue significant actuation strain after the application of an electric current. Therefore, PPy can also be used for electrochemically induced strains in the fabrication of artificial muscles or mechanomodulation.[470] Additionally, PPy can be synthesized through photopolymerization, and free-standing structures can be fabricated using methods of 3D additive manufacturing[471] and two-photon polymerization.[472] One of the drawbacks is the high sensitivity of PPy to the pH of the environment and the strong correlation between protonation level and conductivity. In order to address these difficulties, different PPy microstructures were evaluated, and it was found that conductivities of nanotubular structures were up to ten times stronger than for globular PPy, even in body pH levels.[473, 474]

6.2.1 Chemistry-enabled adhesion

PPy films are intrinsically stretchable but do not easily adhere to cells and tissues. Texidó *et al.* found that doping PPy with hyaluronic acid strengthens the composite's adhesion to stretchable materials such as PDMS, offering an alternative means to create stretchable PPy-based conductive devices.[475] Another report shows strong dependence of hyaluronic acid molecular weight on its adhesive properties with higher molecular weight providing improved adhesion, higher electrochemical activity and lower impendence of the bioelectrodes.[476] A dopant-free solution for achieving strong adhesion is direct PPy polymerization on a porous PDMS surface that has been pre-activated using UV/ozone oxidation. With this technique, Tsao *et al.* built stretchable devices on three-dimensional

PDMS substrates that have high stretchability and stable conductivity, and which can be used for measuring stretching forces.[477]

One issue that consistently arises is that conductive polymers generally become hydrophobic once optimized for their conductive, optical, and elastic capabilities. For bioelectronics, it is important that a material be self-adhesive and interface well with a biological tissue. Recent research has focused on the synthesis of PPy composites, incorporating additives to improve its hydrophilicity. Han *et al.* found that incorporating polydopamine (PDA) via in situ formation of PDA-PPy nanofibrils (**Fig. 20a**) within a polyacrylamide matrix increases its overall hydrophilicity while retaining transparency and its electronic properties.[478] They found that functional groups on PDA bond with water molecules while its catechol groups form a complex with PPy, creating an electrically functional (**Fig 20b**), hydrophilic composite device capable of transmitting 70% of the visible spectrum (**Fig. 20c** and **d**). The material can withstand strains exceeding 2000% and adheres with ease to the human skin tissue, which was demonstrated by the fabrication of electrodes for MCG and ECG. Beyond copolymerization, deposition of adhesive biomolecules has shown promise for increasing PPy adhesion. Jang *et al.* demonstrated a method to immobilize Arg-Gly-Asp peptide on the electrode surface using electrodeposition.[479] By varying electrodeposition time, they achieved high control over peptide surface density without significantly affecting the electrical impedance of the electrode. Material adhesion properties were quantified using *in vitro* biointerfaces with human mesenchymal stem cells.

To accurately sense or stimulate a desired target molecule or cell, the device must be able to integrate with that target specifically. This issue led to the development of methods for targeted adhesion. One method for obtaining targeted adhesion can be the integration of antibodies or biomolecules with the materials. Golabi *et al.* used 4-*N*-Pentylphenoboronic acid as a functional dopant with PPy to specifically increase its affinity towards diols.[480] Boronic acid interacts with *cis*-diol to form cyclic esters and interfaces well with PPy, thus making it an ideal candidate to create PPy devices that selectively interact with organisms with sugar-rich membranes like bacteria. Golabi *et al.* further researched PPy bacterial differentiation using a variety of ion dopants. They found that adhesion of specific bacterial strains can be modulated by changing the dopant type.[481] This material allowed the creation of a new method of label-free bacterial differentiation. Further studies will focus on electrical modulation or stimulation for bacterial adhesion, which might prove useful for monitoring of

bacterial population in mixed culture. This, in turn, could be used in a clinical setting, *e.g.*, for monitoring the gut biome.

6.2.2 Chemistry-enabled dynamic substrates

Electroactive properties of PPy were recently used to study mechanotransduction at the nano-biointerface in mesenchymal stem cells. The Jiang group used template-free electropolymerization to obtain PPy nanotubes array on a titanium substrate (**Fig. 21a**). [482] In this material, during the electrochemical reduction/oxidation cycle, the morphology of the interface switches between nanotubes and nanotips (**Fig. 21b**). [482] This morphological change allowed them to cycle the interface between the highly adhesive hydrophobic surface and poorly adhesive hydrophilic surface, providing attachment and detachment stimuli to MSCs. The stimulation effectively changed the distribution of actin filaments (**Fig. 21c**), cell surface area (**Fig. 21d**), and caused nuclear translocation (**Fig. 21e**). Such geometric stimulation may be used in the future for smart materials promoting tissue regeneration.

Electrostimulation with PPy-based conductive hydrogels was also recently used to treat spinal cord injury. Zhou *et al.* were able to cross-link PPy with tannic acid (TA), a plant-derived polyphenol commonly used in many medical products due to its antioxidant, antibacterial, and anti-inflammatory properties.[483] Optimization of TA content allowed the authors to obtain a hydrogel with low Young's modulus and conductivity matching that of the native spinal cord. *In vitro* studies showed that the hydrogel stimulates differentiation of neural stem cells, while at the same time suppressing the development of astrocytes. *In vivo* studies in mice models of spinal cord injury showed that hydrogel implantation promotes tissue regeneration and leads to significant recovery of neural connectivity. PPy films were also successfully used for controlled drug delivery. PPy films were successfully loaded with dexamethasone[484] and salicylate[485] and used for electrically controlled delivery. In an interesting study, Antensteiner *et al.* developed a method of fabricating PPy conductive microcups through PLGA microsphere templating.[486] These cups possess a unique morphology and could possibly be used for electrical stimulation, drug release, and mechanomodulation.

6.3 PANI

Polyaniline (PANI) is another conductive polymer that has been extensively studied for its applications to bioelectronics. PANI is a low-cost, easily synthesized alternative to other conductive polymers with comparable mechanical stability and electrical properties. Early reports indicated poor biocompatibility with PANI but further investigation shown that this arose from the presence of residual monomers and acid catalysts.[487] Studies using optimized synthetic protocols have shown that pristine aniline, especially in a base form, is biocompatible and free of embryotoxicity.[488] Similar to other conductive polymers, PANI can be produced as a freestanding film, or as composites doped with secondary materials.

6.3.1 Chemistry for material processing

Compared with other conductive polymers, PANI has some limitations towards its use in bioelectronics, namely low solubility in many solvents and reduced conductivity in higher pH environments. Crystalline nanocellulose (CNC) can be used for PANI stabilization as its surface is rich in the hydroxyl groups, which stabilize the polymer structure. Razalli *et al.* showed that a polyaniline-crystalline nanocellulose (PANI-CNC) composite protonates in neutral environments, which allows it to be conductive in nearly neutral pH environments typically found in biological systems.[489] CNC is also an appealing material for biointerfaces due to its natural availability, biodegradability and biocompatibility, which are discussed further in Section 7.5.[490] Another example of a biocompatible dopant is gelatin methacrylate. It is especially attractive for developing transient biointerfaces as it maintains a stable structure for about 4 weeks and completely degrades in about 6-8 weeks in cell culture media.[491] Recently gelatin-PANI nanofibers co-doped with camphorosulfonic acid were fabricated by electrospinning and used to stimulate and direct the growth of C2C12 myoblast cells. A combination of electrical and mechanical cues for directing cell growth might prove useful for applications in tissue regeneration.

6.3.2 Chemical stabilization

Maintaining the electric integrity of conductive polymers over time is critical for the use in implant fabrication. In cell cultures, PANI has a tendency to lose dopants in a process called de-doping. Furthermore, if composites are washed off and polymer exposed to body fluids, the pH is sufficient to deprotonate amine groups of PANI, which will significantly impair its conductive properties. Preventing this unwanted alteration has been the focus of recent research. For example, Mawad *et al.* created degradation resistant PANI by immobilizing

phytic acid, the dopant, using a prefabricated chitosan film.[492] Phytic acid is anionic and interacts with the positively charged amine groups of both chitosan and PANI and thus is immobilized via coulombic interaction. This material was used to create a suture-less conductive patch that survived *in vivo* for two weeks. This phytic acid doped PANI/chitosan material was later utilized to develop a bioelectronic patch which can couple with a damaged cardiac tissue. The patch alters heart electrophysiology, enhancing conduction velocity across damaged cardiac walls with minimal invasiveness and only mild inflammation. [493]

6.3.3 Genetically assisted chemical assembly

Presently, even cutting-edge chemical tools do not allow for the fabrication of structures that can match the structural complexity of biological systems, and there is no implantation strategy that can lead to precise placement and integration of bioelectronics. To address these challenges, new routes to self-assembled bioelectronics have to be devised. Recently, Liu *et al.* developed a method of selective *in situ* modification of cell membranes with conductive polymers guided by the expression of a catalytic enzyme.[494] Classically, PANI is synthesized under oxidative and strongly acidic conditions. To create biocompatible reaction conditions, target cells were transduced with humanized ascorbate peroxidase Apex2 using adeno-associated virus vectors (**Fig. 22a**). Additionally, to further lower polymerization potential a mixture of monomer and dimer of aniline in 1:1 molar ratio was used as a substrate for directed polymerization (**Fig. 22b**). It was shown that this strategy allows for selective and efficient modification of neuronal membranes *in vitro*. Besides, subsequent doping of PANI with *p*-toluenesulfonic acid can significantly increase the conductivity of polymer structures. Also, the enzymatic system allows for synthesis of other polymers such as conductive PEDOT and insulating poly(1,1'-diaminobenzidine) (PDAB).

Patch clamp experiments have allowed for a thorough characterization of electrophysiology during polymer modification. It was shown that modification of neurons with conductive PANI increased their membrane capacitance and decreased spike number (**Fig. 22c**), while modification with insulating PDAB had the opposite effect (**Fig. 22d**). This method was proven successful when applied to cultured brain-slices and freely moving animals. In the former case, either excitatory or inhibitory motor neurons of *Caenorhabditis elegans* were genetically modified with Apex2 protein and PANI was selectively deposited. This procedure resulted in alteration of motor functions of an animal consistent with previous

studies using optogenetics.[495] Although the present work leaves the open questions of cytotoxicity of monomers and side products of radical oxidation reactions, it represents an important direction in the field of organic conductors. The presented methodology is especially important as similar *in situ* synthesis and directed self-assembly methods are likely to be developed for the inorganic materials.

7. Outlook – New Chemistry Aspects in Bioelectronics

The study of bioelectronics is, by its nature, highly interdisciplinary in that it draws from most areas of the physical and life sciences. In this section, we provide a small sample of new developments in chemistry that are of interest to bioelectronics. While each of these topics is a large and active area of research in its own right, we have selected a number of key topics that are particularly relevant.

7.1 Mechano-biochemistry

A major component of how an organism biologically adapts to its environment comes from the mechanical interactions between the two.[496-498] As such, the field of mechanobiology shares some overlap with bioelectrical investigation, as both fields require an understanding of how physical stimuli can be translated into biochemical signals and vice versa. While the explicit study of coupling between bioelectricity, biomechanics, and biochemistry remains relatively uncommon,[499] a number of highly relevant questions arise from considering the intersection of these fields. Here, we will examine the salient cell level processes where bioelectronics may be employed. This includes both mechanosensing as well as the processes by which cells generate and distribute mechanical forces (**Fig. 23**).

Cells employ a variety of methods for sensing the mechanical characteristics of their physical environments. This allows them to perform such functions as sensing the stiffness of their substrate,[500] responding to stretching[501] and shear flow,[502, 503] and detecting local topography,[115, 504] among others. Cells are also out of thermodynamic equilibrium by definition, and they actively move, change shape, and transmit forces to their local environments. A vast array of interlinked biochemical pathways function to transduce mechanical stimuli to chemical signals and back again to mechanical outputs. Within this set of pathways, we can construct a minimal mechanical model of a cell using a number of candidates that emerge as ideal targets for integration with bioelectronics.

We begin with the calcium ion, Ca^{2+}, for a number of reasons. First, Ca^{2+} is a ubiquitous and well-studied secondary messenger, *i.e.*, calcium signaling is integrated into a vast array of biological functions. This is true of mechanical functions where, depending on cell type, calcium can induce cell contractions, modulate membrane waves,[505] and coordinate cell migration during development.[506, 507] Second, biocompatible Ca^{2+} sensitive dyes are readily commercially available, so that monitoring of intracellular Ca^{2+} concentration is fairly easy. Finally, it is an appealing target for bioelectronic devices, as many excitable and non-excitable cell types possess voltage-gated calcium channels, such that devices may alter calcium signaling directly, through membrane potential modulation, or through alternate means, such as the optocapacitive mechanism.[65]

The actomyosin cytoskeleton constitutes the unifying machinery for cell mechanics. The globular protein actin assembles into long filaments (F-actin) that provide the basic structural integrity of the cell (**Fig. 23**). Forces are generated both from the ATP-driven polymerization and depolymerization of F-actin[508] and by myosin, a molecular motor protein that forms contractile units with F-actin. Recent work has tracked the diffusivity of single charged particles, and from those results highlighted an aspect of the cytoskeleton in producing heterogeneities of intracellular mechanical and electrical characteristics.[44] These results also point to the possibility of perturbing cytoskeletal architecture using electric fields alone. This may be achieved by manipulating actin[509, 510] or other cytoskeletal filaments.[511, 512] Another possibility is to alter molecular motor transport through bioelectronic means. To do so, we must consider where pathways involved in bioelectrical signal transduction intersect with mechanotransduction pathways.

Two of the best-studied regulators of cell mechanics are RhoA and YAP/TAZ (**Fig. 23**). RhoA, a small GTPase, regulates cell contractility by acting on the rho kinases ROCK1 and ROCK2, which phosphorylate myosin light chains and thereby induce contractions. Stresses are transmitted from the cytoskeleton to the substrate at focal adhesion complexes, where RhoA and ROCK activity is enriched.[513, 514] Yes-associated protein (YAP) and transcriptional coactivator with PDZ-binding motif (TAZ) respond to mechanical cues – high cell density,[515] low cytoskeletal stress,[516] or substrate stiffness[516] – by translocating from the nucleus to the cytoplasm. YAP/TAZ are effectors of the Hippo signaling pathway,[517] and when present in the nucleus they encourage cell spreading and proliferation.[518] The Linker of Nucleoskeleton and Cytoskeleton (LINC) complex couples the cytoskeleton to the nucleus and thus enables mechanotransduction.[519, 520] These core regulators of cell mechanics intersect with

bioelectronics through calcium. Like RhoA, Ca^{2+} is upstream of myosin light chain kinase[521] and other regulators of contractility,[522] and calcium is necessary to stabilize cell-cell adherens junctions, so Ca^{2+} dynamics can influence how cells sense their environments. There also exists a wide variety of other pathways that putatively transduce electric fields into a number of mechanical and morphological outputs, including wound healing,[523] angiogenesis,[524] and cell motion directionality.[525]

The Piezo channels are of particular relevance to bioelectronic and biomechanical applications. Piezo proteins function as stretch-activated pores of ion channels, allowing ion flux when their associated bilayer is under tension.[526, 527] They are evolutionarily conserved[528] and broadly important to physiology: they are necessary components in vascular development in mice,[529] stem cell differentiation,[530] and mechanotransduction in light touch sensing.[531] Interestingly, Piezo channels also display a voltage-sensitive functionality that is also well-conserved.[528] Positive applied voltages increase the probability of a channel being open, and they also allow the channel to retain sensitivity after several mechanical impulses.[528] As such, Piezo channels are appealing targets in bioelectronics, both as potential targets for modulation, and as major components of electromechanically coupled machinery in cells.

Nano-biointerfaces can perturb the mechano-biochemistry just described through a number of ways. One potential route to modulation is the material properties of the bioelectronic devices, such as stiffness[532-534] or topography.[115, 504, 535] Exogenous impulses are also viable candidates. Recently, electric fields were shown to induce alignment in the traction stress field of epithelial monolayers,[536] and Si nanowires with photoelectrochemical functionality have been applied to control beating in cardiomyocytes.[62, 130] Furthermore, electrically conductive cell coatings have been explored in the specific instance of graphene sheaths around cells.[537] Mechanical changes, for instance, cell shrinking, induce wrinkles in the coating that alter the conductivity, allowing shape deformations to be tracked in a manner somewhat reminiscent of traction force microscopy.[538] We anticipate further investigations to explore coupling in the opposite direction, that is, using electrically active substrates or coatings to induce cell mechanical effects.[38]

7.2 Bioelectrical responses to acoustic, optical, and magnetic stimuli

To overcome the activation energy barrier, chemical reactions require energy inputs as a vital ingredient. This most often takes the form of thermal inputs, *i.e.*, heating the reaction vessel, but it is not necessary to rely on thermal energy to enable reactions to proceed. Optical, acoustic, and magnetic inputs present other techniques for promoting reactions, with many methods offering good spatiotemporal control over these processes. Such precise control is a key feature of the latest developments in bioelectronics, and as such, these methods all provide unique opportunities for integration with bioelectronic devices.[539]

7.2.1 Acoustic processes in bioelectrical chemistry

Sonochemistry, the field of study surrounding the interaction of acoustic vibrations and chemistry, came to prominence with the 1895 discovery of cavitation-induced damage to warship propellers.[540] Ultrasonic – above 20 kHz – vibrations in fluids are capable of producing cavities on the scale of hundreds of microns. The collapse of these cavities, which have lifetimes of microseconds, induces local hot spots with temperatures of greater than 5000K and pressures exceeding 1000 atm.[541, 542] These extreme conditions facilitate a number of chemical reactions, frequently including the lysis of the solvent into radicals, *e.g.,* the formation of hydrogen and hydroxyl radicals in water. While cavitation and collapse are not typically accompanied by bulk increases in temperature,[543] the production of radicals is usually undesirable in biological settings. As such, sonochemical applications in bioelectronics tend to deviate from the "usual" picture of sonolytic reactions, and instead integrate other methods that use ultrasound as a trigger, or else consider lower-frequency vibrations.[544]

Ultrasound imaging is probably the most widespread use of ultrasound in medical technology.[545-547] In its most basic form, the technique relies only on the reflection of ultrasonic waves from biological tissue.[548] However, recent developments have incorporated the use of ultrasound-responsive contrast agents (UCAs). The basic design of UCAs consists of a thin shell, typically composed of phospholipids, albumin, or other surfactants, enclosing a gas bubble, which can consist of air, sulfur hexafluoride, or various perfluorocarbons.[546] The difference in impedance between gas and tissue can be up to 3000-fold, such that sound waves reflecting off of UCAs are considerably stronger than those reflecting off of tissue boundaries.[546] Another interesting recent development in ultrasound-based imaging is the use of acoustoelectric imaging,[549] which relies on changes in local resistivity introduced by pressure waves in any conductive medium.[550, 551] Recently, this principle was employed to image across the skull and observe changes in current density enacted by deep brain

stimulation therapy.[552, 553] This raises the exciting possibility of electric field or electrochemical mapping of systems using noninvasive, surface-mounted bioelectronics.

Ultrasound has also been employed as a means to target drug delivery. A common means to achieving this comes from infusing certain types of UCAs, namely ones containing perfluorocarbon droplets, with a given drug.[546] Perfluorocarbon droplets undergo a rapid expansion upon ultrasound exposure, from a droplet to bubble phase. This expansion is posited to aid in drug delivery by varying mechanisms, depending on the composition of the droplet shell. Lipid shell droplets are posited to fuse with cell membranes after expansion, which aids in the transfer of drugs from droplet to cell.[554] Droplets based on block copolymers show similar phase-transition functions, but the mechanism of drug delivery is different in that the volume expansion results in the shell thinning rapidly. Drugs embedded in the shell, then, become more accessible upon ultrasound exposure.[554, 555]

Similar principles to those used in drug delivery have been employed to varying therapeutic ends, ranging from sonodynamic therapies[556] to transient poration of various biological barriers for drug delivery.[556, 557] Neural activity stimulated by focused ultrasound[558] is an especially exciting prospect, one that is further developed in recent reports of acoustogenetics, that is, systems that genes that encode responses to ultrasound for visualization[559] or modulation[557] purposes. As mentioned earlier in Section 3.2.2, focused ultrasound has also enabled light emission from mechanoluminescent QDs for local and *in vivo* optogenetics.[231] A common theme throughout these techniques is the ability to deliver energy with good spatiotemporal localization and little energy loss through tissues. This makes them attractive candidates for integration with bioelectronic methods, which can be engineered to be orthogonal when interaction is not desired, and synergistic when it is useful.

7.2.2 Optical processes in bioelectrical chemistry

We have discussed extensively photochemistry in the context of electrical responses to light from organic and inorganic semiconductors and conductors in previous sections. Here, we consider several other areas of photochemical research that show promise for integration with bioelectronics.

a) Photoswitch. Phototriggers are caged compounds that release their contents upon light exposure. Photon-driven uncaging for biological applications was first demonstrated using *o*-nitrobenzyl esters of cAMP[560] and ATP.[561] Since then, the field has seen the development of

many different photolabile cages, which have been applied to selectively control the release of Ca^{2+}, neurotransmitters, secondary messengers, DNAs, and RNAs, among others.[562, 563] Recent attention has also been cast on photoswitching mechanisms, in which the uncaging is reversible.[563] Most applications of photoswitching compounds include azobenzene groups (**Fig. 24**), which can undergo a reversible *cis-trans* isomerization under UV illumination.[564-566] Recently, a membrane-targeted photoswitch was developed, where photoisomerization elicited action potentials *in vitro* and *in vivo* (**Fig. 24a**).[564] Molecular dynamics simulations and electrophysiology recording revealed a transient hyperpolarization followed by a delayed depolarization, a novel mechanism for neuromodulation (**Fig. 24a**).[564] Azobenzene-based materials also enabled photo-controllable adhesions (**Fig. 24b**).[509] Other photoswitch candidates include norboradienes,[567] spiropyrans,[568] and systems of ketone electrophiles with amine/hydrazide nucleophiles.[569]

b) Optogenetics. Optogenetics refers to a suite of techniques involving the genetic engineering of organisms to display light-responsive properties. It has seen a massive amount of interest since the early 2000s, when the phototransducer rhodopsin was employed to activate neurons,[570] and the light-gated ion channel channelrhodopsin-2 was used to depolarize cells.[571] Subsequent developments took advantage of ligand-gated channels and photocaged ligands, e.g., DMNB-capsaicin and DMNTE-ATP, to optically control the relevant channels.[572] Since then, optogenetic methods have also been extended to the light-oxygen-voltage (LOV) sensing domain of *Avena sativa* phototropin 1 (**Fig. 25**).[573] In this method, light activation uncages a domain that interacts with PDZ domains; in effect, allowing optical control over protein recruitment. This method, dubbed tuneable light-interacting protein tags (TULIPs), has been employed to great effect in studying cell mechanics by modulating actin severing by the protein cofilin,[574] microtubule gliding assays,[575] cell adhesion via switchable extracellular matrix,[576] as well as force generation enacted via RhoA signaling.[577, 578]

Because of optogenetics and other light-activated techniques in bioelectronics, the development of small, biocompatible light sources is of great interest. Micron-scale LEDs, for instance, have shown promise due to their small size and integrability,[579] and they have been applied to neural modulation using optogenetics.[580] They also function credibly as components of closed-loop systems,[581] and have recently been validated for that purpose.[4] Such devices should also prove feasible for use in photoswitching and photouncaging applications, such as controlled neurotransmitter release.

c) Upconversion. Upconversion is the process wherein two photons of low frequency are absorbed by a structure and a single photon of higher frequency is emitted. Upconverting nanoparticles (UCNPs) are typically formed through heavy doping of trivalent lanthanides, especially Yb^{3+} and Tm^{3+}.[582] UCNPs with these dopants are particularly useful in biology, as they can absorb from within the so-called NIR-I window at 700-950 nm, where light has the greatest tissue penetration depth.[583] The emission wavelengths can then be tuned to various desirable wavelengths in the visible range.[584] This property has been used to enable NIR vision in mice, by complexing UCNPs with rods and cones.[535] UCNPs have also been applied in conjunction with optogenetics, to overcome the depth limit imposed by the allowable wavelengths for optogenetic functionalization.[585]

These applications do not specifically involve bioelectronics, but they present a general template that will undoubtedly prove useful in the future: NIR light is used to access deep tissues and is upconverted to higher frequency light by UCNPs acting as intermediaries in the relevant tissues. These higher frequency photons can then be used to trigger bioelectrical signal generation and transmission, increasing their versatility and reducing the invasiveness of the overall therapy.

7.2.3 Magnetic processes in bioelectrical chemistry

Historically, the influence of magnetic fields on chemical reactions has been assumed to be nonexistent for most practical purposes.[586] With a few notable examples, namely the radical pair mechanism,[587-589] there is a paucity of proposed means by which external magnetic fields may inject enough energy into a system to induce an appreciable change in reaction outcomes or kinetics, particularly in the context of biochemical reactions.[590] When measurable impacts of sub-Tesla magnetic fields have been observed, most notably in the case of enzymatic ATP synthesis rates,[591] reproduction of these results has been elusive.[592] The development of magnetic nanoparticles, however, has revitalized the possibility of magnetic stimuli to biology, with a few recent advances deserving particular attention.

Magnetic nanoparticles can be synthesized using a variety of metals and metal oxides, with iron, nickel, and cobalt being common choices.[593] At room temperature, the magnetic moments of ferromagnetic particles below a material-dependent size threshold become small enough that they can be flipped by thermal fluctuations. They then have a net zero magnetic moment, but very high magnetic susceptibility (superparamagnetism).[594] When a sample of

particles are exposed to an alternating magnetic field (AMF), typically at radio frequencies, the induced oscillations have a heating effect that has been employed to kill cancer cells (magnetodynamic therapy),[595] as well as activate transient receptor potential (TRP) channels.[596] This TRP activation has been further applied to stimulate neurons both *in vitro*[60, 596] and *in vivo*.[60, 597] Recently, an elegant design was demonstrated for the remotely-controlled chemomagnetic modulation of neurons, where thermally-responsive liposomes (phase transition temperature, 43 °C) released chemical payloads (*e.g.*, hM3D(Gq) ligand clozapine N-oxide, endogenous dopamine receptor D1 agonist) upon AMF application (**Fig. 26a**).[61] This has allowed for magnetically-triggered motivated behaviors and sociability in mouse models (**Fig. 26b**). Magnetic nanoparticles with other shapes, such as hollow ones have been engineered for magnetically controlled drug release.[593, 598] These examples highlight the recurring theme of novel forms of energy input to spatiotemporally control drug release.

7.3 Biomimetic Chemistry

Biomimetic materials comprise a large and active area of interest, focused on materials that aim to replicate some facet of biology. Some biomimetic materials are designed to only match a specific property, for example, soft substrates that approximate *in vivo* extracellular matrix more closely than glass[599] but are otherwise quite chemically different from their biological counterparts. On the other hand, there exist biomimetics that are nearly identical to biological substances but for certain key differences, such as peptoids, which contain similar backbone structures to polypeptides but whose chemistry is entirely altered by having side chains substituted on backbone nitrogen atoms instead of alpha carbon atoms.[600, 601]

A key advantage offered by biomimetic materials is that, by their definition, they are based on designs that have been well-validated over the entire history of evolution. For bioelectronic applications, there is the additional benefit of their being more likely – although not guaranteed – to integrate nondestructively with biological targets. Despite this promise of reduced invasiveness, they may also be more resistant to biological degradation and able to operate in environments not accessible to strictly natural substances. For instance, certain biomimetics may operate in extreme temperature or pH conditions. Finally, many biomimetics are adaptable in two senses of the term. In one sense, the modular nature of biomimetic polymers enables large and versatile design spaces. In the other sense, they can

also yield devices that automatically adjust themselves to suit their environments. This latter possibility was recently demonstrated with an artificial heart valve that adjusts its shape to maintain functionality with pediatric patients as they grow (**Fig. 27a** and **b**).[602]

Considering the fascination Michael Faraday had with electric eels,[603] it is perhaps fitting that researchers have recently turned to electric eels (**Fig. 27c**) as inspiration for next-generation power sources.[604, 605] Briefly, *Electrophorus electricus* supports the production of potential differences up to 600 V and short-circuit currents near 1 A,[606] with stacks of electrocytes – electrically active cells. The functionality of electrocytes comes from their ability to selectively modulate Na^+ and K^+ ion channel activity at the anterior and posterior ends. During activation, K^+ efflux is reduced at the posterior end only, while Na^+ influx is increased at the same region. This alters the total transcellular potential, that is, the potential across both the posterior and anterior areas, to about 150 mV. To recapitulate this behavior, the authors of a recent report designed a sequence of four hydrogels that contain alternating high concentration NaCl and low concentration NaCl, interdigitated by cation selective and anion selective gels that act as semipermeable membranes. When the full sequence of gels is placed in contact with each other, Na^+ flows through the cation selective gel and Cl^- flows through the anion selective gel, so that the resulting potential across the entire series was observed as high as 185 mV. While the total size of these biomimetic hydrogel stacks is not yet competitive with the size of the electrocytes that inspired them, these results are encouraging.

In the case of electronic plants, the "biomimetic template" is literal, rather than aspirational – plant structures are used as part of the fabrication process. This allows for the complex interlocking designs of plant structures to be replicated comparably easily. One example of this is seen in the production of conductive xylem wires and logic gates, made by immersing a cut rose in PEDOT-S:H solution.[607] Such designs have also been employed to create plant tissue/conductive xylem supercapacitors.[608] As the field of biomimetic and bio-inspired materials continues to grow, there are certain to be similar keen analogies drawn between what biology already does and what can be incorporated into bioelectronics design.

7.4 Bioelectrocatalysis

The field of bioelectrocatalysis is drawing growing interest, as it promises to yield renewable energy materials that are also environmentally sustainable in their manufacture.

Much of the focus of this field has centered on systems that function like either biomass fuel cells or solar energy.[74, 609] Both approaches rely on similar components, namely, an electrocatalytic site, a means of charge transport to the electrode, and the electrode itself. Redox proteins and cofactors use a wide variety of both organic and metal centers in electrocatalysis, enabling the use of H_2, glucose, or light as energy sources.

Electron transfer – from redox site to electrode – is the key process in bioelectrocatalysis (**Fig. 28a**). Under certain circumstances, namely that the distance from redox site to electrode is less than 2 nm,[75] electrons can transfer directly from one to the other. This mechanism is called direct electron transfer (DET). While DET systems thus require less components than other strategies, the distance requirement places major restrictions on the design of the electrocatalytic site and the electrode, and the overall throughput is limited to what can be achieved with a single layer of sites.[74, 75] This restriction can be partially lifted by direct wiring of redox sites and electrodes, which has recently been demonstrated using metalloprotein-prion domain protein chimera nanowires (**Fig. 28b**).[610] Such methods, however, come with the caveat that such wiring schemes entail additional complexity for the system. Mediated electron transfer (MET) uses redox mediators to shuttle electrons from electrocatalytic site to electrode. This opens up the list of viable redox proteins, as mediators can access cryptic redox sites,[74] and allows for more redox sites per electrode area. Designs using MET also frequently make use of inert polymer media, which can improve the stability of the overall device.[74]

Finally, the electrode selection can also have an impact on electrocatalytic performance. Surface chemistry, for example surface wettability (**Fig. 28c**), and topography each play important roles in ensuring good contact between the electrocatalyst and electrode.[75, 611, 612] Additionally, the bioelectrochemical reaction may only take place on certain substrates, e.g., with microbes that harvest energy through iron oxidation or sulfate reduction.[613]

7.5 Biologically derived materials for bioelectronic systems

Recent years have seen a growing interest in materials that can be derived directly from biological sources, including plant biomass and animal sources. This owes itself to several factors. First, the raw materials are readily available: the primary components in plant biomass, cellulose and lignin, are among the most abundant biopolymers on the planet. Chitin, which is obtained from fungal, arthropod, and other sources, is also ubiquitous. As such, they

are inexpensive and easy to procure. Additionally, they are derived from renewable sources, and the raw materials are biodegradable, making the manufacture of biomass-based materials potentially more environmentally friendly than fossil or mineral materials.

Cellulose is composed of β-1,4 linked D-glucose subunits (**Fig. 29a**). In many plant cell walls, cellulose is synthesized into nanofibers, which can vary in organization from species to species.[614] Processing of these plant materials can yield additional nanostructures, with a great deal of recent attention focusing on cellulose nanocrystals. On its own, cellulose and its derivatives are good insulators, however, the high concentration of surface hydroxyl groups allows for a number of functionalization techniques that can endow such materials with capabilities relevant to bioelectronics. Nanocellulose materials integrated with carbon nanomaterials (nanotubes and graphene) have yielded flexible supercapacitors with high capacitance retention, even after being subjected to large deformations.[615-617] Likewise, nanocellulose has been combined with conductive polymers PPy (**Fig 29b**), PANI, and PEDOT to yield supercapacitor devices.[618-621] Such supercapacitors are immensely useful in bioelectronics, primarily as energy storage devices.[622] To that end, they have been used in wearable technologies, integrated into clothing, and implanted.[623]

The structure of lignin is considerably more variable than that of cellulose: whereas the latter is well-defined as a polymer of glucose, the structure and molecular composition of lignin is highly heterogeneous (**Fig. 29c** and **d**). Nevertheless, its abundance and structural properties make it an attractive target for bioelectronic devices. As a photocatalyst, lignin hybrids with ZnO, TiO_2, CeO_2, and CuO have been found to improve photocatalytic depollution.[624] Furthermore, lignin integrates well with conductive polymers for photovoltaic applications. The high content of aromatic structures in lignin and derivatives aid in hole transport, a fact that has been exploited to improve performance in PEDOT-based photovoltaics.[625, 626] Like nanocellulose, lignin nanofibers have also served as a structural basis for supercapacitor devices.[627, 628] Although we are not aware of any biological applications of lignin-based photocatalysts or photoelectrochemical stimuli in the existing literature, these materials show promise as low-cost devices that may enhance biological integration compared to artificially derived substrates.

Other biologically derived materials for electronics include chitosan, as well as reflectins and eumelanins obtained from cephalopods.[629] Chitosan is a derivative of the polysaccharide chitin, which is among the most widely available biopolymers and is therefore a cost-effective and biocompatible material for bioelectronics.[630] In the bioelectronic context,

chitosan is frequently derivatized further into maleic chitosan and proline chitosan.[631] Chitosan conductivity arises from proton mobility, so chitosans fall within the bioprotonics class of ionotronics.[632, 633] As evidence of this, chitosan-based FET devices have been fabricated on SiO_2 with palladium hydride contacts used to measure the protonic current.[634]

Biopolymers derived from cephalopods have attracted considerable interest on account of the wide variety of intriguing material behaviors squid skin can demonstrate, including sophisticated thermal regulation[635] and colour changing.[636] Reflectins, which constitute a family of proteins that are only found in cephalopods, are the primary component responsible for colour changing.[637] In addition to their applicability to adaptive colour and camouflage, reflectins have been coaxed into self-assembly to form nanoparticles and films.[638, 639] Studies of reflectin conductivity have found them to be bioprotonics,[640] and they have been employed to form bioprotonic transistors.[641, 642] Eumelanins comprise another protein family that can be found in cephalopod ink and also possess interesting electrical properties. In particular, hydrated thin films of eumelanins demonstrate conductivity that has been attributed to protonic conductivity as well as electrochemical reactions,[643] that is, they are simultaneously bioprotonics and electrochemically active. The relative contributions of the protonic and electrochemical currents remain unclear, however, and it has been suggested that melanins behave as nearly purely protonic devices.[644] Together with chitosan and reflectin, these three materials, which are all relevant to cephalopod physiology, compose a promising class of bioprotonics, and are likely to be incorporated into novel devices and materials with unique responsiveness.

7.6 Computational approaches to bioelectronics

Computational approaches have a long record of success in chemical and materials discovery. Large combinatorial libraries and high-throughput discovery techniques, for instance, take advantage of chemical information processing (cheminformatics) for both data handling and candidate identification.[645-648] Similarly, *in silico* modeling of structures can rapidly narrow down a field of promising candidates, without requiring experimental validation for every possibility – a prospect that quickly becomes untenable as the size of the library grows.[649] A functional example of this has been displayed with photoswitchable molecules, as discussed in section 7.2.2. In order to ensure that further experiments would be worthwhile, DiFrancesco *et al.* conducted molecular dynamics experiments to verify that

their target molecule, Ziapin2, would integrate with cell membranes and still undergo *cis-trans* photoisomerization.[564]

The incredible success of computational methods for electronic structure have enabled a more precise understanding and characterization of new developments in organic electronics, including organic semiconductors and photovoltaic.[156, 650] The principles of "molecular design," in which functional improvements arise from fine tuning of the relevant molecules, rely in part on our ability to efficiently compute the effects of modifications to various moieties of those molecules. Of particular interest to bioelectronic applications are the frontier orbital energies, solubility characteristics, and morphological stability of organic electronics.

Machines that are capable of learning have been actively studied since the 1950's.[651] However, a series of high-profile achievements in the early 2010's, coupled with the advent of practical implementations of deep learning,[439, 652] have led machine learning (ML) to the forefront of academic interest in recent years. Proposed and actual applications of machine learning techniques have proliferated in most areas of the physical and life sciences, from particle physics beyond the Standard Model[653] to pathology diagnosis from medical images.[654, 655]

As an illustrative example, we may consider neural decoding. Neural decoding is the process of converting records of brain activity into an understanding of both normal and pathological brain functions. As such, it relies heavily on signal processing, clustering, and other tasks ideally suited to machine learning.[656] In principle, the information decoded by machine learning provides insights into the representational content of those signals. While this assertion is epistemologically suspect,[657] such methods have produced functional results. For example, comprehensible machine-generated speech was recently derived from neural patterns,[658] and the means to both control[659] and receive[660] sensory feedback from bionic arms have been reported. To further understand the architecture of the brain, we will require better means to measure neural signaling, therefore the future of neuronal decoding is intertwined with the development of bioelectronic sensors.

With the goal of more precisely tuneable bioelectronics – both in terms of design and effect – in mind, machine learning has shown great promise in this field. Recently, ML has been combined with molecular dynamics simulations to obtain structural and material properties of amorphous Si at low computational cost compared to *ab initio* methods.[661]

Similarly, ML has been employed to devise an interatomic potential for Si that improves on empirically derived force fields in describing a number of observable properties, *e.g.,* phase changes by different mechanisms.[662] ML has also been used to predict sets of structures that will be similar and stable under given thermodynamic constraints.[653, 663]

7.7 Living bioelectronics

Continued progress in bioelectronics and related areas of research has led to developments in a nascent field that combines biological cells with electronic systems in a genuinely synergistic fashion. This field of "living bioelectronics," also referred as "biohybrid robots" in the literature,[664, 665] promises to combine the strengths of artificial robots – information density, reliability, and processing speed – with the strengths of biology – error-tolerance, energy-efficiency, and dynamic responses.[666] Currently, there is a good deal of attention on the development of reliable and scaleable actuators for living bioelectronics. There are a number of proposed paths towards this goal, ranging from biomimetic composites of synthetic parts[548] to self-assembling "tissues" of engineered cells.[664, 665]

The artificial approach makes extensive use of piezoelectric motors,[667] shape memory alloys,[209] and dielectric elastomers.[668] There have been notable recent successes for piezoelectric[669] and shape memory alloy-based[209, 670] actuators in soft robotics,[671] as well as a striking biomorphic design of artificial wings using dielectric elastomers.[672] For applications in living bioelectronics, however, engineered tissues have drawn a great deal of attention.[665] This is due to many factors, including the multiple functionality of cells[665] and the potential for implants where the interactions with the biological environment are features that are designed, rather than minimized or tolerated.[504, 673] To that end, systems that incorporate cell-based actuators into their design include artificial muscles,[664] light[674] and electricity-responsive[536] coordinated undulations in a synthetic ray, and motors powered by the optically-controlled swimming of bacteria.[675]

As fundamentally robotic systems, living bioelectronics would be autonomous biological systems controlled by computer hardware, a premise that carries with its major implications for biomedical ethics[676-678] as well as computer/information ethics.[679, 680] It is not sufficient to call for ethical clarity at some unspecified point in the future. Given the potential global impact of living bioelectronics and the cost mistakes in this field may incur,[681, 682] it is vital that all developments are firmly based on an ethical foundation.

8. Concluding remarks

Chemistry offers numerous opportunities for improving bioelectronics into devices with excellent biocompatibility, biomechanical properties and electronic/optoelectronic performance. This goal requires considerable cross-disciplinary efforts; when done successfully, it blends materials science, bioengineering, and electronic device/system fabrication, along with new developments in chemistry. The chemistry aspects accelerate important advances in how we think about bioelectronics. As we have seen, devices may include components that are organic or inorganic, and which function as conductors or semiconductors. The characteristics of each type of material allow for bioelectronics that acts on length scales from the molecular to the organismal, with durations from nanoseconds to months or even years.

In the near future, we expect that chemical considerations will be employed to great success in formulating synergistic combinations of some of the recent discoveries highlighted here. This may happen in two main ways. In one approach, materials with similar chemistries but varying functionalities can be used in tandem to create devices that expand the range of capabilities beyond either material. The other approach entails combining materials with much more differing chemical properties, to either attenuate the weaknesses of each other, or to bestow the eventual device with multiple distinct functionalities. It is likely that both approaches will yield highly significant insights. Hard-soft composites offer a mechanical example of this principle, in which the combination of stiff and compliant materials can both mitigate the impacts of mechanical mismatch between device and tissue, as well as offering new routes of sensing or stimulation.

Furthermore, developments in disciplines that are adjacent to bioelectronics offer a wealth of possible applications to bioelectronics. For instance, a common theme is the use of energy input methods with good spatiotemporal resolution – acoustic, optical, and magnetic impulses – to dramatically improve the localization of various therapies. There is enormous potential for bioelectronic discoveries based on perspectives from multiple disciplines. This is as valid for bioelectronics collaborations within the natural sciences as it is for collaborations between scientists and other areas of inquiry, such as ethics or sociology. In all cases, advances in chemistry will enable many of the most critical insights.

Conflicts of interest: The authors declare no conflicts of interest.
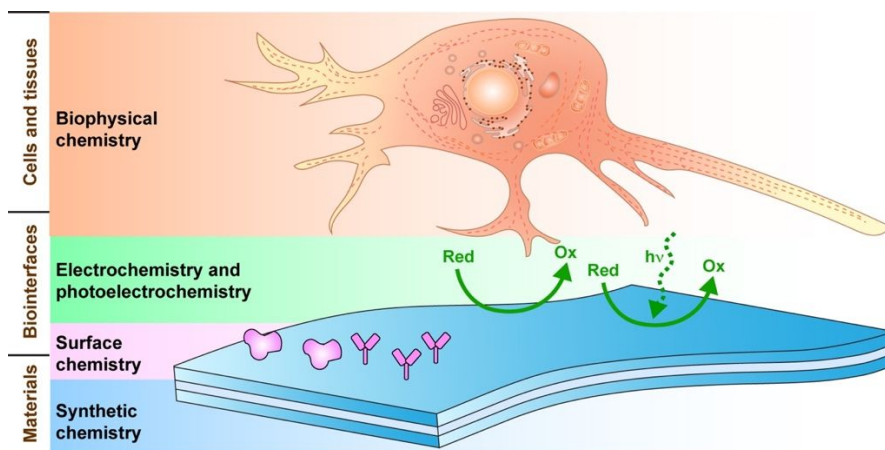
Figure 1. Chemistry aspects of bioelectronics.

(a) Biointerface Length Scale

nanometer | micrometer | millimeter | meter

Nanowire probe | 'Cyborg' organoid | Heart patch | Epidermal electronics

(b) Biological Activity Time Scale

microsecond | millisecond | second | 10^3 second

Ion channel | Neural signals | Cardiac signals | Animal behavior

(c) Biointerface Time Scale

second | hour | day | month | year

Patch clamp | Protein sensor | Transient electronics | Neural-like electronics

Figure 2. Bioelectronics and bioelectrical studies span a range of length and time scales. Awareness of chemistry and physics at all applicable levels is necessary to devise appropriate synthetic and analytical methods for the study of biointerfaces.
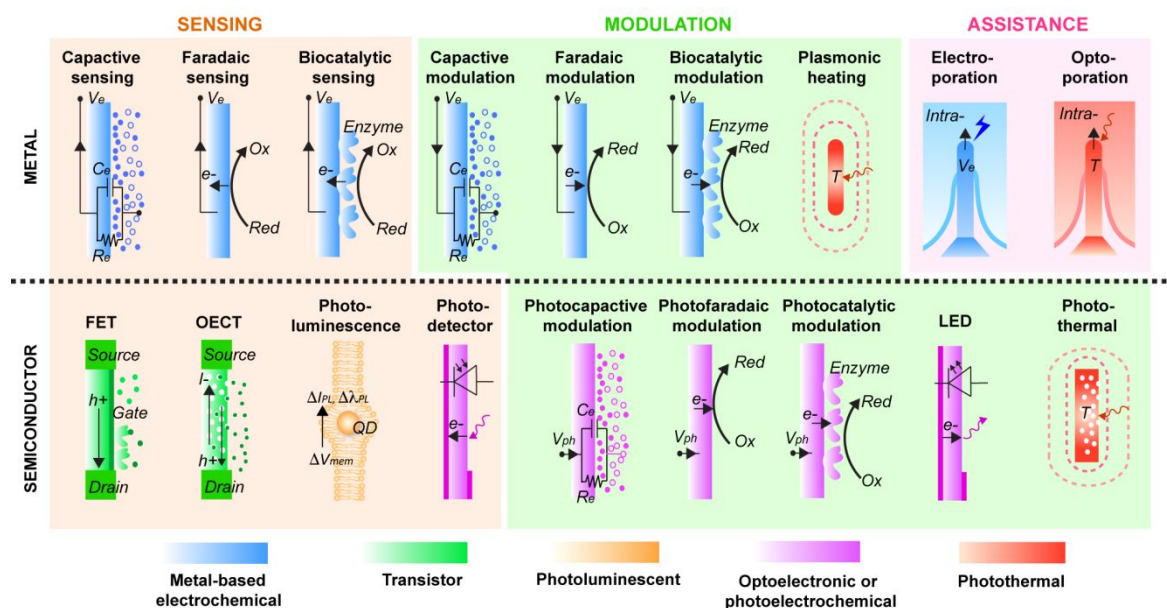
Figure 3. Signal transduction mechanisms in bioelectrical interfaces can vary depending on the material design and chemistry. Top: Metal-based electrodes can be used for recording or injection of capacitive, faradaic, and biocatalytic currents. Free-standing metallic nanostructures allow used for plasmonic heating. Additionally, metallic structures can be used to facilitate interface interrogation penetrating cellular membranes using electroporation and optoporation. Bottom: Highly sensitive recording of bioelectric signals using field-effect transistor (FET) and organic electrochemical transistors (OECT). Readout of optical signals using photoluminescent materials and photodetectors. Free-standing nanoscale semiconductors allow for wireless injection of currents through photocapacitive, photofaradaic and photocatalytic effects. Micro light-emitting diodes (LED) can be used to deliver optical signals. Semiconductors without electric and radiative energy decay pathways can generate photothermal heating.
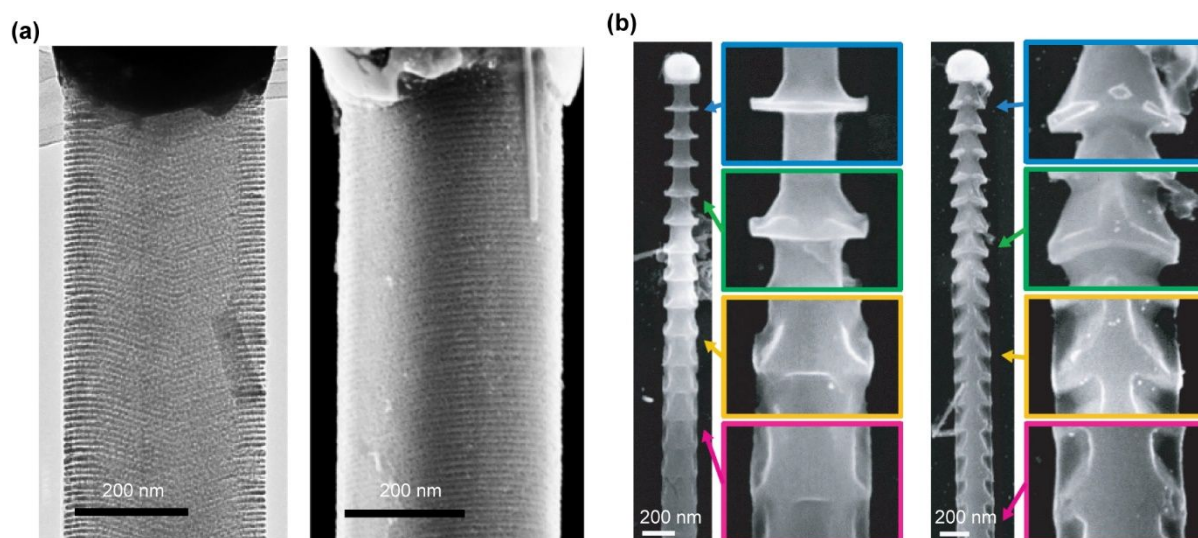
Figure 4. Si nanowires with various structures and morphologies can be produced from metal-assisted chemical etching methods. (a) SiNWs with ordered grooves, etched from a mixture of hydrofluoric acid/hydrogen peroxide. Reproduced from ref.143 under the terms of the Creative Commons Attribution License from Springer Nature, copyright 2017. (b) SiNWs spicules formed by wet chemical etching in KOH solutions. Reproduced from ref.144 with permission from the American Association for the Advancement of Science, copyright 2015.
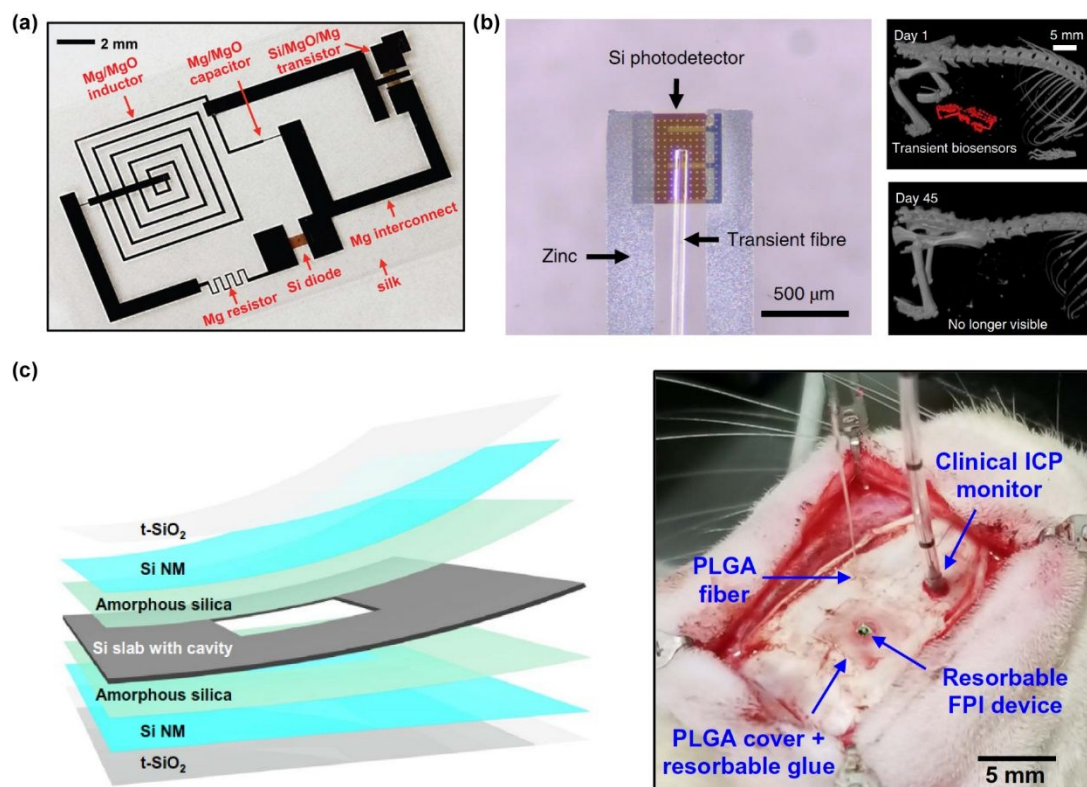
Figure 5. Transient and bioresorbable electronics derived from the degradation of Si and other transient materials. (a) Optical image of circuit design and components of a transient device. Reproduced from ref.134 with permission from the American Association for the Advancement of Science, copyright 2012. (b) Left: photograph of a SiNM-based bioresorbable spectrometer. Right: implanted device can be naturally resorbed after 45 days. Reproduced from ref.160 with permission from Springer Nature, copyright 2019. (c) Left: a schematic diagram of a SiNM-based bioresorbable sensor designed for the measurements of intracranial pressure (ICP) and temperature (ICT). Right: photograph of the bioresorbable sensor implanted in the intracranial space of a rat. Reproduced from ref.157 with permission from the American Association for the Advancement of Science, copyright 2019.
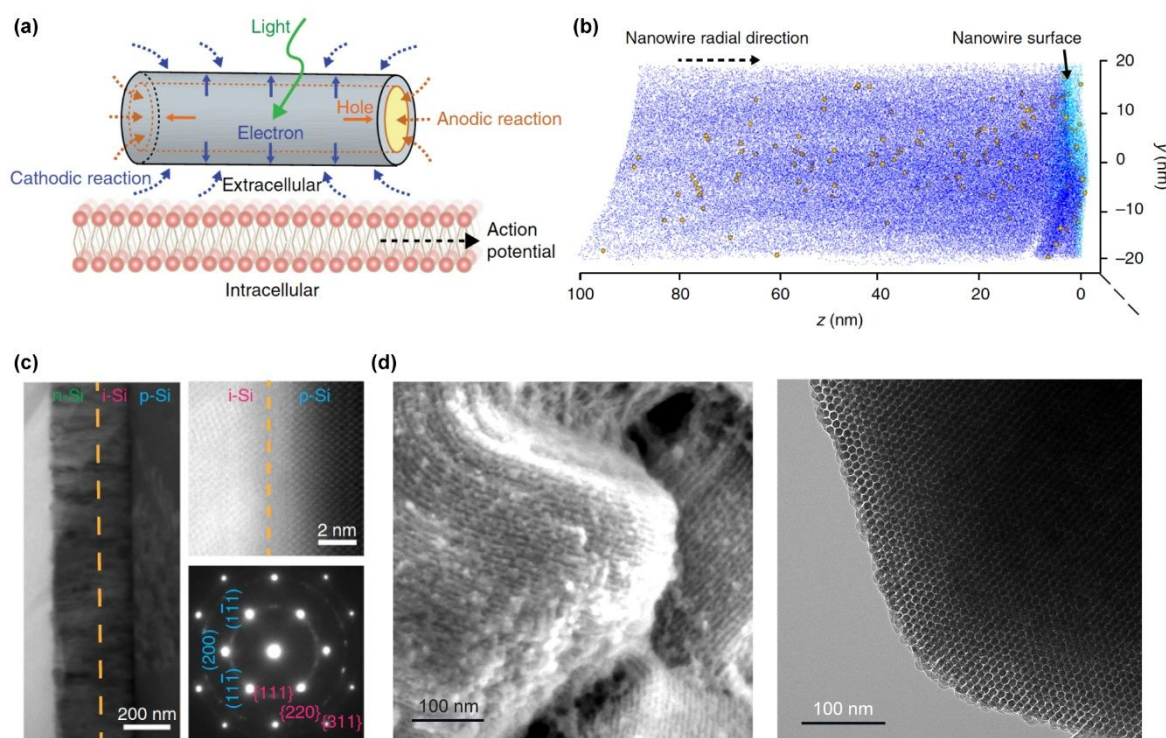
Figure 6. Si nanostructures used in the photo stimulation of cells. (a) A schematic diagram shows coaxial p-type/intrinsic/n-type (p-i-n) SiNWs for photoelectrochemical extracellular modulation of DRG neuron membrane potential. (b) Atom probe tomography shows the presence of diffused Au (yellow balls) on the sidewalls of p-i-n SiNWs (Si atoms: dark blur; O atoms: light blue). (a) and (b) Reproduced from ref.129 with permission from Springer Nature, copyright 2018. (c) Cross-section TEM image (left), scanning TEM (STEM) image (upper right) and the diffraction pattern of a p-i-n Si membrane nanostructure applied for the photostimulation of brain cortex and behavior control. Reproduced from ref.38 with permission from Springer Nature, copyright 2018. (d) Left: SEM image of nanostructures of replica Si from hexagonal mesoporous silica SBA-15, which were applied in the elicitation of action potential by photothermal effect. Right: TEM image shows the hexagonal packing of a Si nanowire. Reproduced from ref.67 with permission from Springer Nature, copyright 2016.
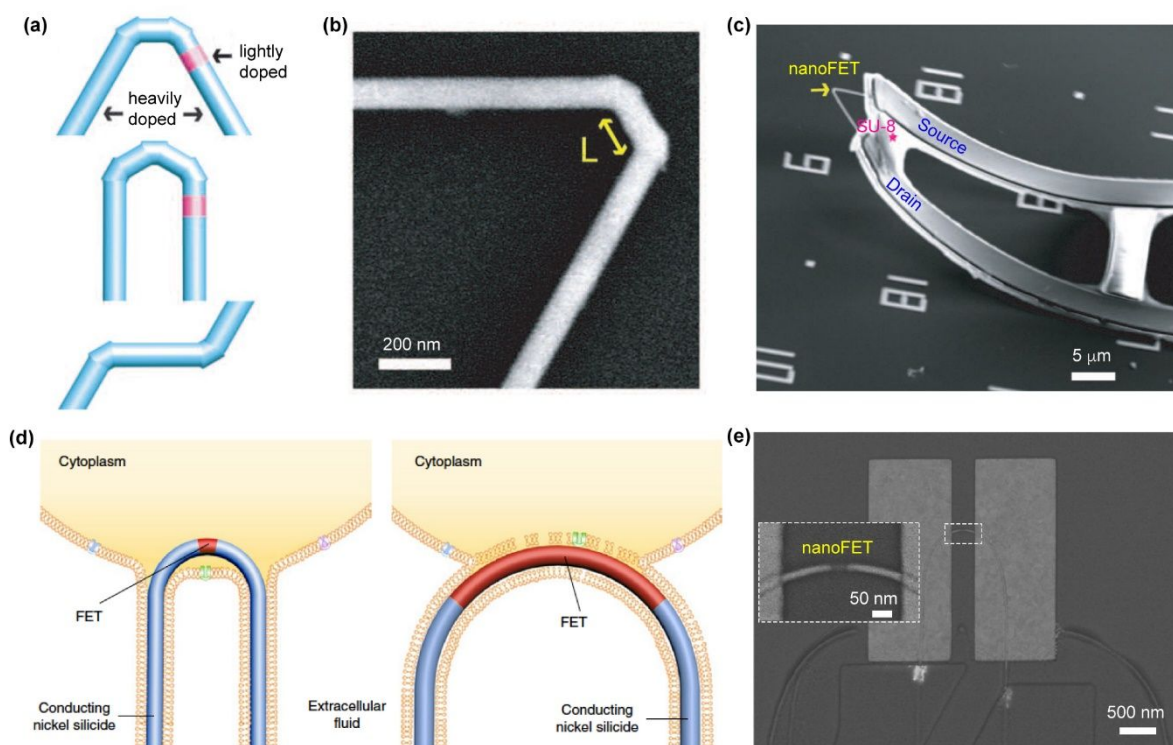
Figure 7. Si-based nanoFET for intracellular recordings. (a) A schematic diagram of the nano-sized FET region, which was introduced by dopant modulation on kinked nanowires. (b) A SEM image of a kinked Si nanowire. (c) NanoFET on an SU-8 microribbon support. (a) − (c) Reproduced from ref.43 with permission from the American Association for the Advancement of Science, copyright 2010. (d) A schematic diagram of probe internalization and intracellular recording by short channel nanoFETs. (e) SEM image of a U-shape nanoFET with atomically sharp nickel silicide interfaces. (d) and (e) Reproduced from ref.175 with permission from Springer Nature, copyright 2019.
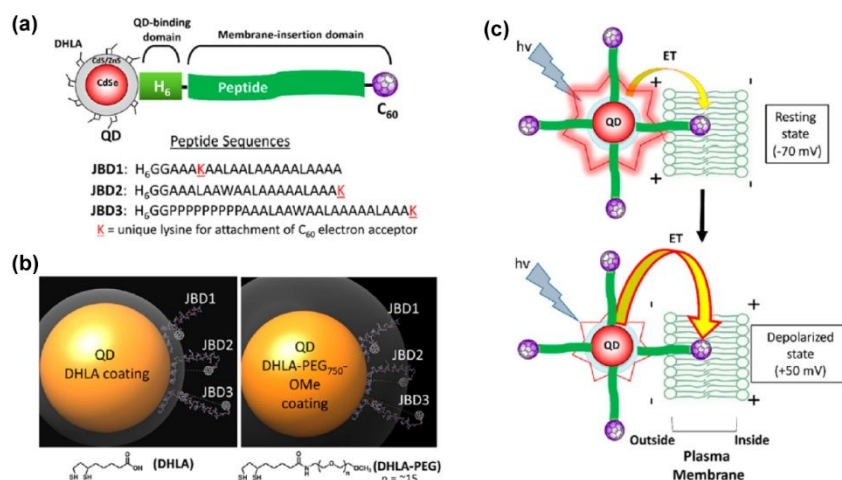
Figure 8. QD applied for bioelectronic voltage sensing in neural membranes. (a) A schematic diagram and (b) molecular models for the design of the QD (electron donor) − peptide-fullerene (electron acceptor) bioconjugated system. (c) A schematic diagram for the fluorescence change introduced by membrane depolarization process. The electrons transfer from the photoexcited QD donor to the fullerene acceptor when the plasma membrane is depolarized, giving rise to the quenching of PL. Reproduced from ref.225 with permission from the American Chemical Society, copyright 2017.
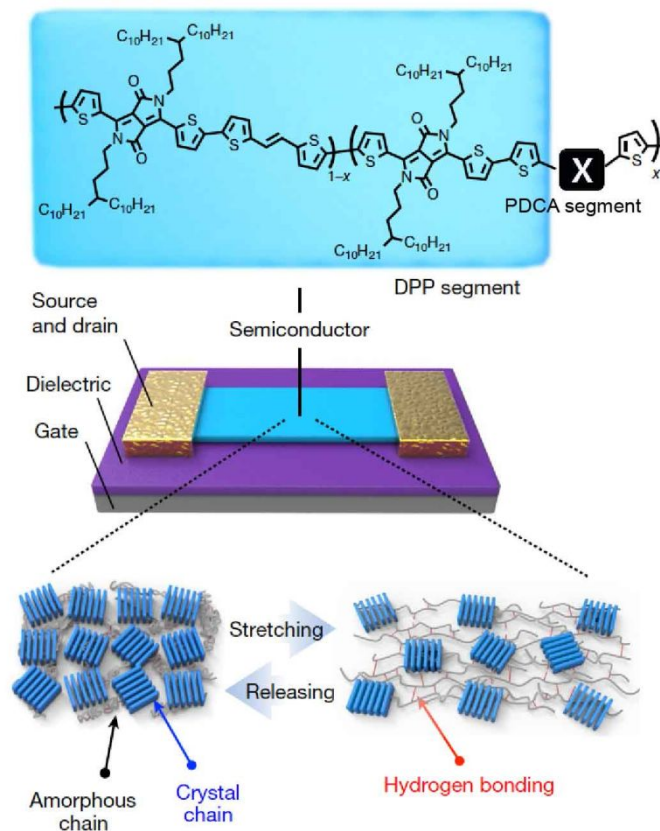
Figure 9. Intrinsically stretchable and healable polymers for fabricating stretchable organic thin-film field effect transistors (OTFTs). 2,6-pyridine dicarboxamide (PDCA) conjugation breaking spacers are integrated with the 3,6-di(thiophen-2-yl)-2,5-dihydropyrrolo[3,4-c]pyrrole-1,4-dione (DPP) semiconductor polymer. The polymer contains crystalline domains (blue) and amorphous polymer chains, where dynamic hydrogen bonds can break and reform. Reproduced from ref.273 with permission from Springer Nature, copyright 2016.
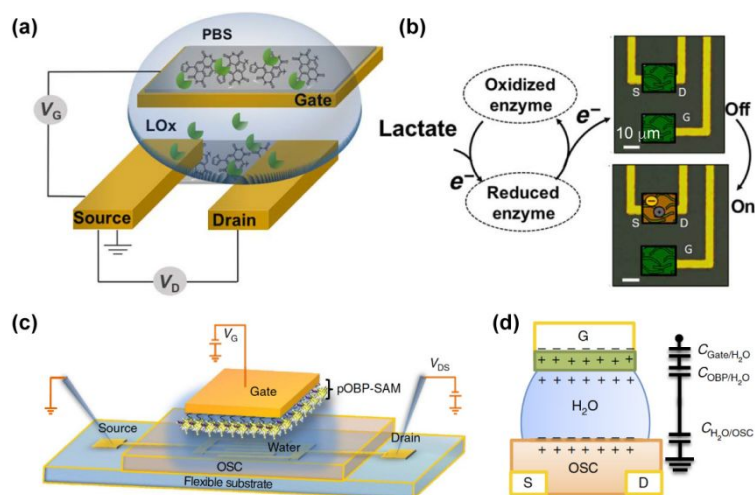
Figure 10. Surface modification of organic transistors for bioelectronic sensing. (a) A schematic diagram of the enzyme biofunctionalization on OECTs devices. (b) LOx enzyme immobilized on the gate electrode of transistors can enhance the sensing selectivity. (a) and (b) Reproduced from ref.294 with permission from the American Association for the Advancement of Science, copyright 2018. (c) A schematic diagram and (d) working mechanism of a capacitively coupled p-type organic FET with pOBPs as ligands. (c) and (d) Reproduced from ref.291 under the terms of the Creative Commons Attribution License from Springer Nature, copyright 2015.
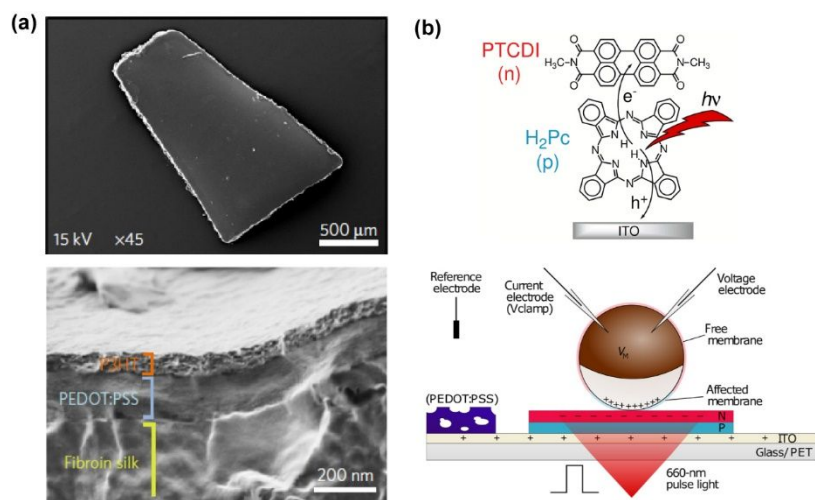
Figure 11. Organic semiconductors used for optical modulation of cells and tissues. (a) SEM images of photosensitive organic prosthetic implants composed of active P3HT layer, conductive PEDOT:PSS layer, and silk fibroin substrate. Reproduced from ref.308 with permission from Springer Nature, copyright 2017. (b) A schematic diagram of the organic electrolytic photocapacitors based on H2Pc / PTCDI junction for the X. laevis oocyte photoexcitation. Reproduced from ref.317 with permission from the American Association for the Advancement of Science, copyright 2019.
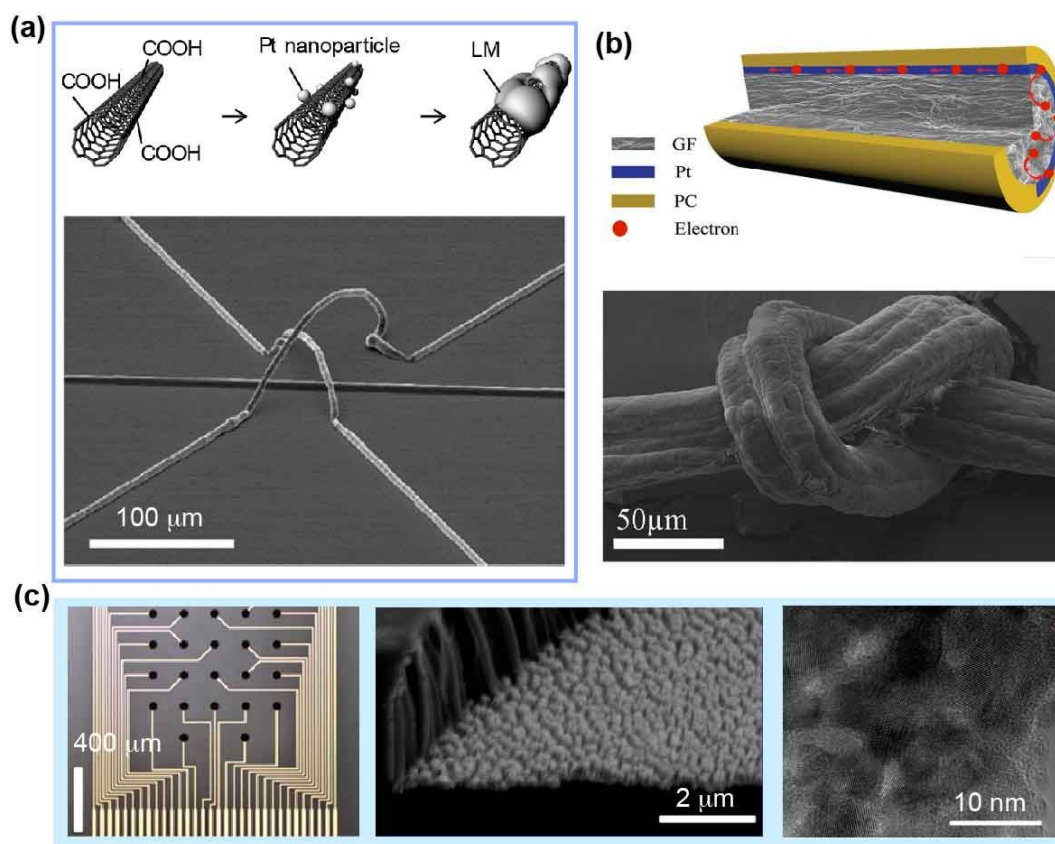
Figure 12. Pt nanostructures used for bioelectronics. (a) Top: A schematic diagram shows Pt nanoparticles as interface materials in the preparation of carbon nanotube/liquid metal (LM) composite. Bottom: SEM image of a 3D structure of printed Pt/CNTs/liquid metal composites. Reproduced from ref.336 with permission from the American Chemical Society, copyright 2019. (b) Top: the structure of a Pt coated graphene fiber (GF) with an as yet unrivalled charge injection capacity of ~10 mC·cm^{-2}. Graphene, as current collector, improved the charge injection capacity of the system via a strong synergistic effect. Bottom: SEM image of a tied knot shows the flexibility of the graphene microfibers. Reproduced from ref.342 with permission from Wiley, copyright 2019. (c) Optical image (left), cross-section SEM image (middle), and high-resolution TEM image (right) of the porous Pt nanorods obtained from dissolution Ag from a co-sputtered PtAg alloy. Reproduced from ref.352 with permission from the American Chemical Society, copyright 2019.
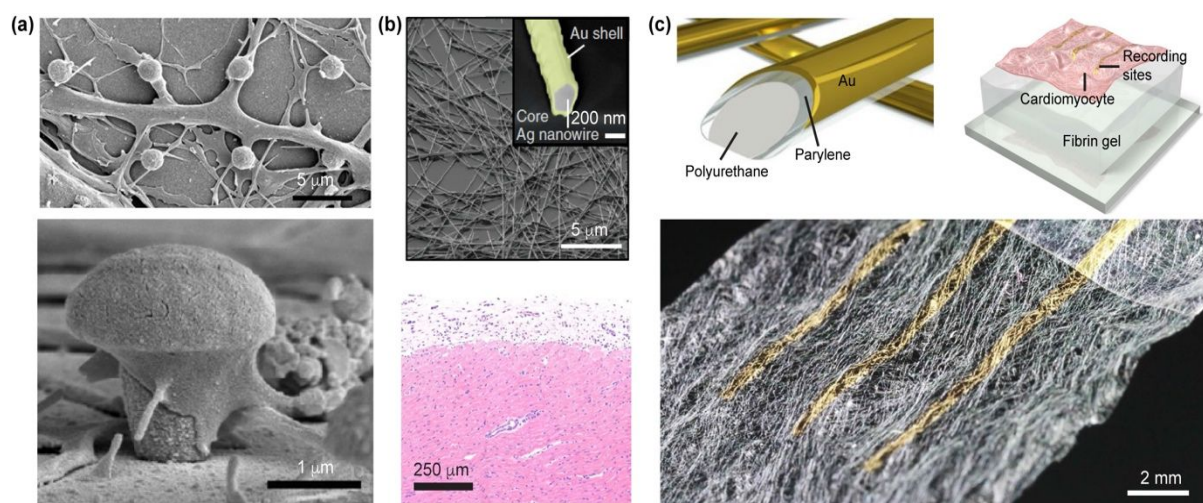
Figure 13. Au-based nanostructures used for bioelectronics. (a) SEM images of rat hippocampal cells cultured on Au mushroom microelectrodes. Reproduced from ref.353 under terms of the Creative Commons Attribution License from Frontiers, copyright 2011. (b) Top: SEM image and backscattered electron (BSE) image (inset) of Au–Ag nanocomposites. Bottom: haematoxylin & eosin (H&E) staining of Ag–Au nanowires implanted cardiac muscles shows little fibrotic reaction and inflammatory response. Reproduced from ref.358 with permission from Springer Nature, copyright 2018. (c) Top: A schematic diagram of the ultrasoft Au-deposited parylene–polyurethane nanomesh (left). This ultrasoft electronics can be used for mapping the electrophysiological dynamics during cardiomyocytes beating (right). Bottom: An optical image of the ultrasoft nanomesh. Reproduced from ref.362 with permission from Springer Nature, copyright 2018.
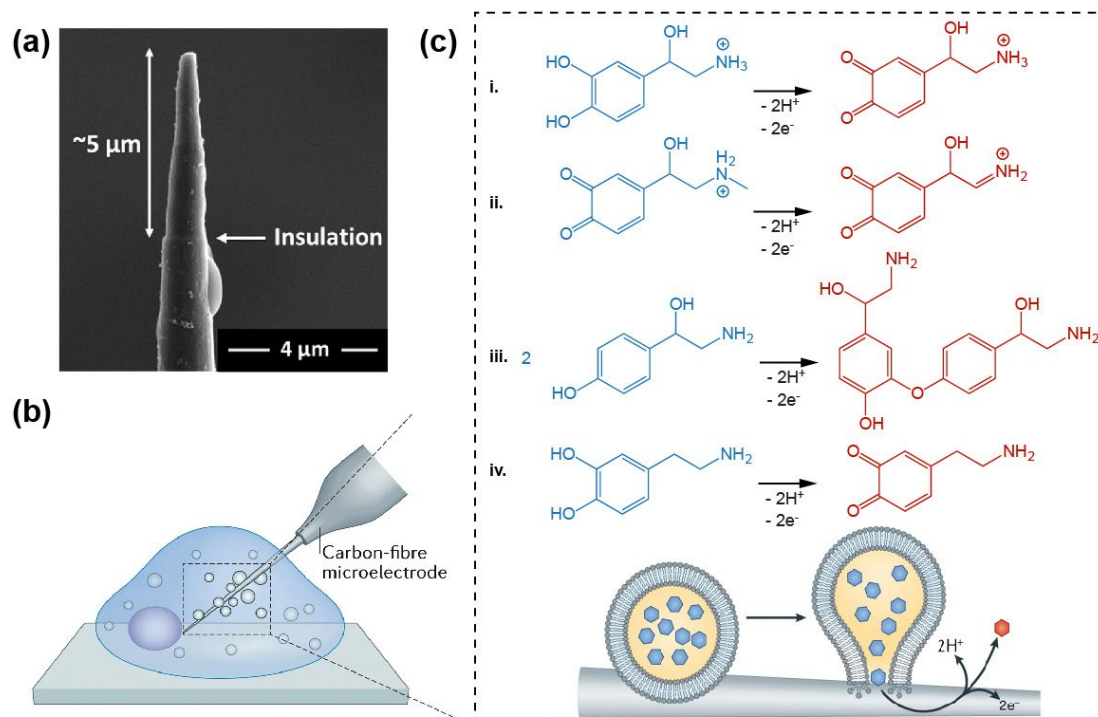
Figure 14. Carbon microfiber used for intracellular electrochemical detection. (a) SEM of an insulated carbon microelectrode with nanoscale tip. Reproduced from ref.407 with permission from the American Chemical Society, copyright 2020. (b) A schematic diagram shows single-cell intracellular measurements of vesicles and synaptic activities using a carbon-fiber microelectrode. (c) On a carbon electrode, vesicles rupture and expel contents, for example norepinephrine (i), epinephrine (ii), octopamine (iii) or dopamine (iv). The elicited oxidation currents can be electrochemically detected by the carbon microelectrode. (b) and (c) Adapted from ref.405 with permission from Springer Nature, copyright 2017.
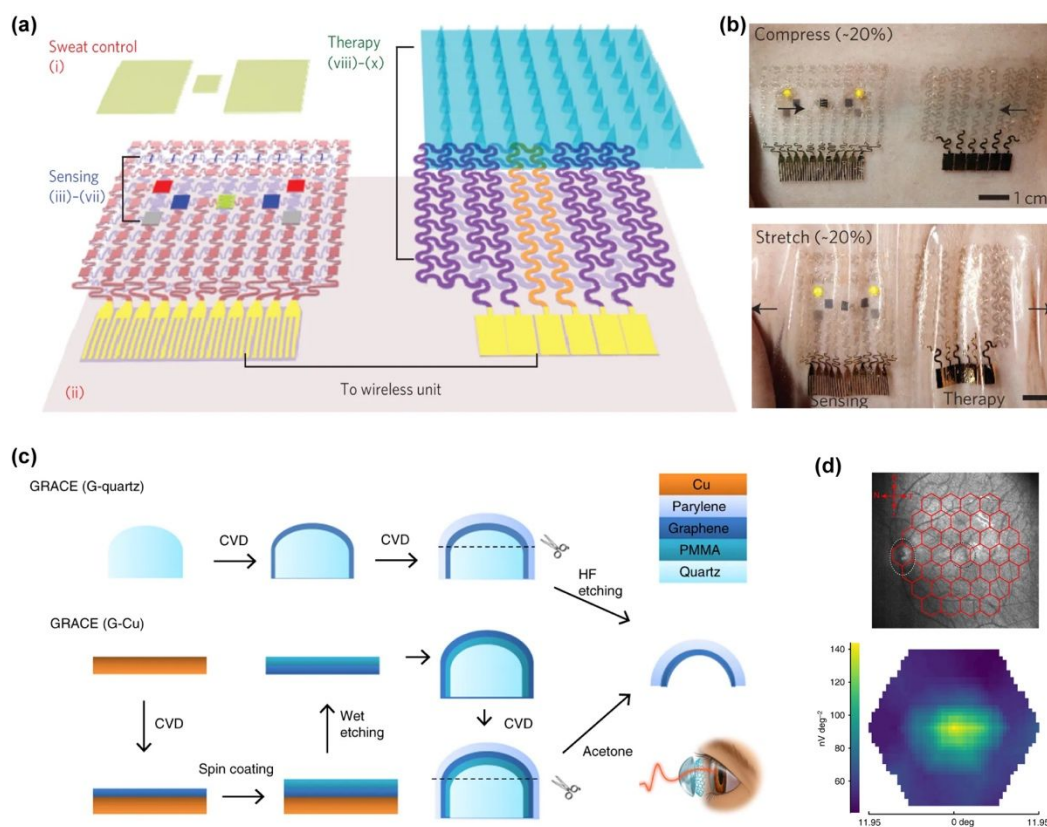
Figure 15. Graphene-based bioelectronics. (a) A schematic diagram of the serpentine Au mesh/graphene-based diabetes patch with sweat-control, sensing and therapy components. (b) Optical images of the compressed (top) and stretched (bottom) diabetes patches. (a) and (b) Reproduced from ref.404 with permission from Springer Nature, copyright 2016. (c) A schematic diagram shows the fabrication steps to obtain soft graphene contact lens on Parylene C. (d) Top: infrared fundus photo of a monkey eye taken during multifocal electroretinography (ERG) recording with a soft graphene contact lens (or GRACE device). Bottom: The response density plot of ERG signals in associated regions. (c) and (d) Reproduced from ref.427 under the terms of the Creative Commons Attribution License from Springer Nature, copyright 2018.
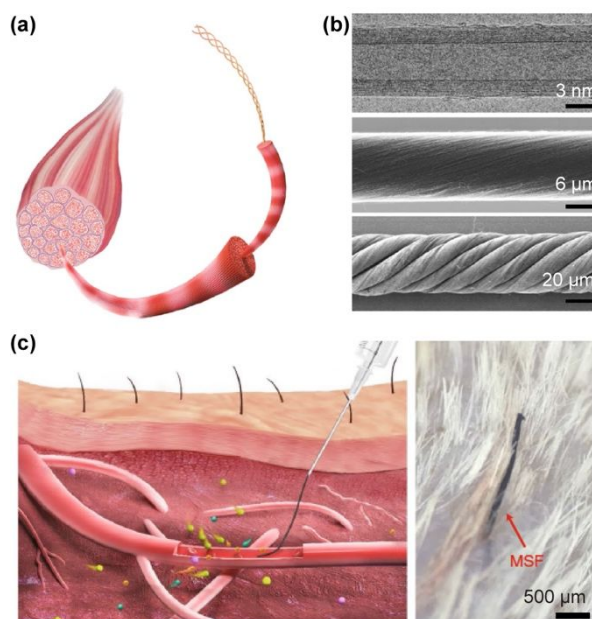
Figure 16. Hierarchical carbon fiber-based bioelectronics. (a) A schematic diagram shows the hierarchical helical bundles of muscle. (b) Top: TEM image of a multi-walled CNT, the building block for a CNT-based hierarchical helical bundle. Middle: SEM image of a primary CNT-based fibre. Bottom: SEM image of assembled hierarchical helical CNT bundles. (c) Left: a schematic diagram shows the CNT helical fibre bundles can be injected into blood vessel for *in vivo* monitoring. Right: photograph of the skin surface of a cat after injection with a CNT-based multiply sensing fibre. (a) − (c) Reproduced from ref.16 with permission from Springer Nature, copyright 2019.
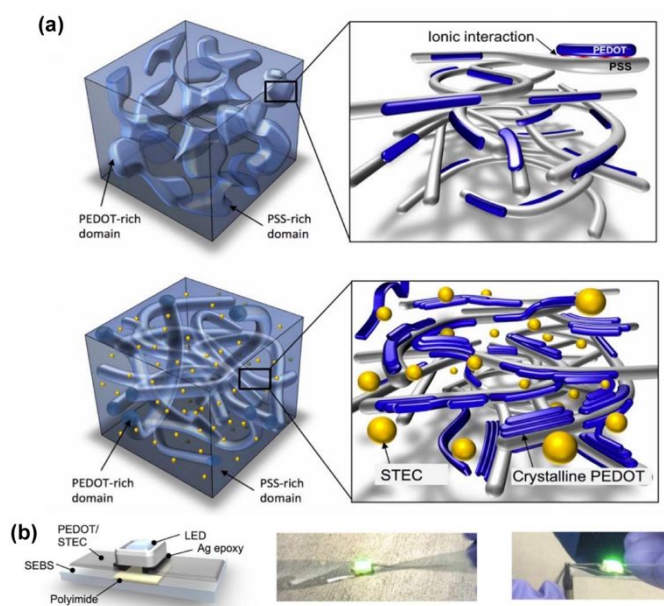
Figure 17. STEC-enabled PEDOT:PSS bioelectronics. (a) Schematic representations of PEDOT:PSS domains in a pristine polymer (top) and with an addition (bottom) of stretchability and electrical conductivity enhancer. (b) Left: schematic representation of LED device with interconnects made of PEDOT/STEC. Middle: photograph shows high LED brightness when the device is stretched and twisted. Right: photograph shows high LED brightness when the device is poked with a sharp object. (a) and (b) Reproduced from ref.465 with permission from the American Association for the Advancement of Science, copyright 2017.
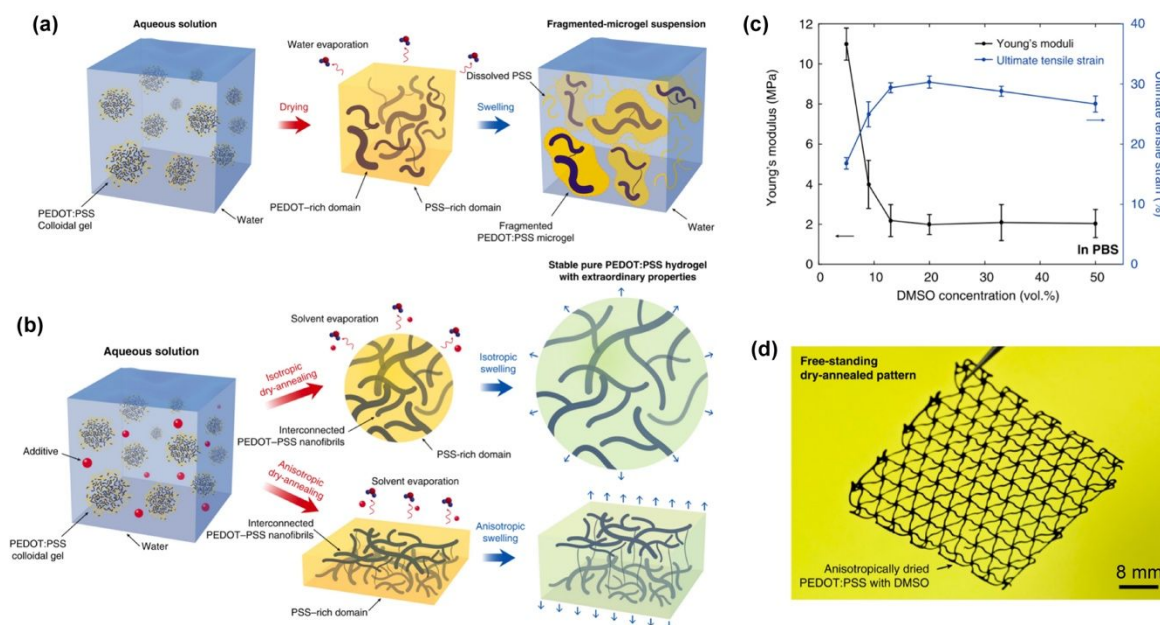
Figure 18. Pure PEDOT:PSS hydrogel and freestanding structure. (a) Schematic representation of PEDOT:PSS domains aggregation during water evaporation. (b) Schematic representation of fibril domain morphology in PEDOT:PSS hydrogel dried with DMSO as an additive. (c) DMSO dependent Young's moduli and ultimate tensile strains in the pure PEDOT:PSS gels. (d) Free-standing PEDOT:PSS pattern fabricated using inkjet printing. (a) − (d) Reproduced from ref.467 under the terms of the Creative Commons Attribution License from Springer Nature, copyright 2019.
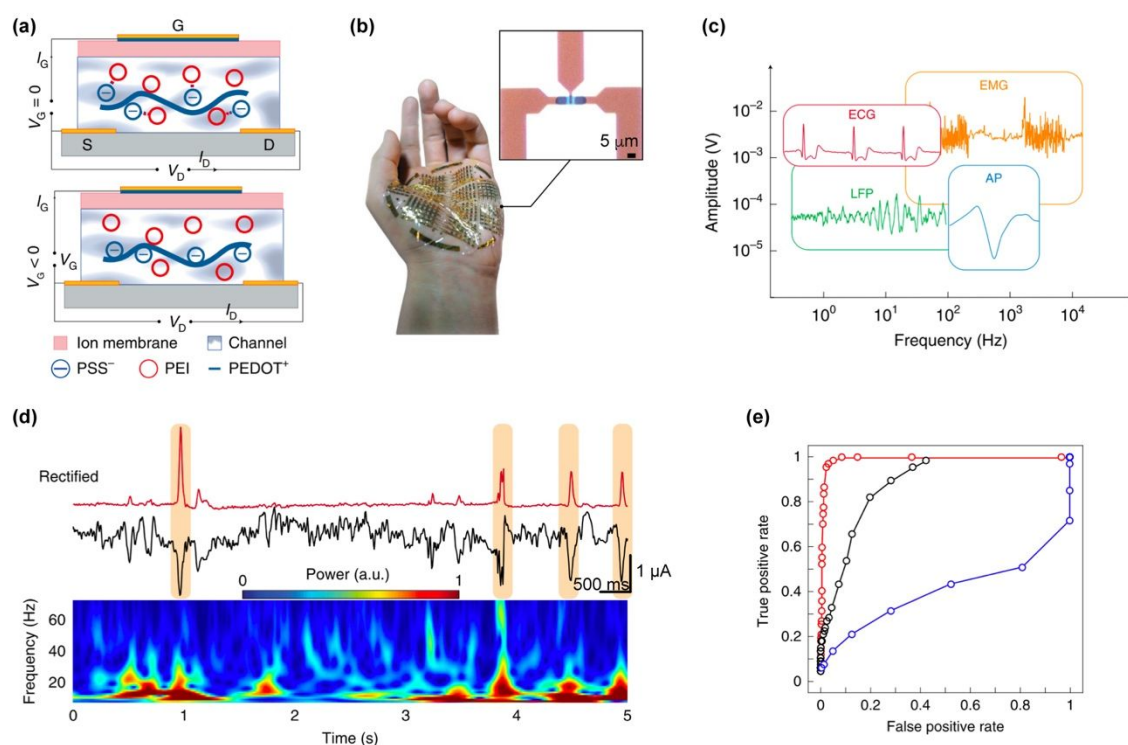
Figure 19. e-IGT for bioelectronics. (a) Schematic illustration of e-IGT device operation. Protonation of PEI+ under negative gate potential releases PSS- which upon binding to PEDOT reinstitutes its conductivity. (b) Photograph showing conformance of the ultra-thin e-IGT based device to the human hand. Inset shows the microphotograph of an individual junction. (c) Traces of sample signals recorded with e-IGT-based devices spanning through amplitude and frequency ranges. (d) Output of nonlinear rectifier made of IGT-based circuit. Top: marked spikes show epileptic discharges. Bottom: Power spectrogram of the recording. (e) Operating curves showing improved detection performance of nonlinear amplifier (red) over bandpass filter (black) and amplitude (blue) thresholding. (a) − (e) Reproduced from ref.469 with permission from Springer Nature, copyright 2020.
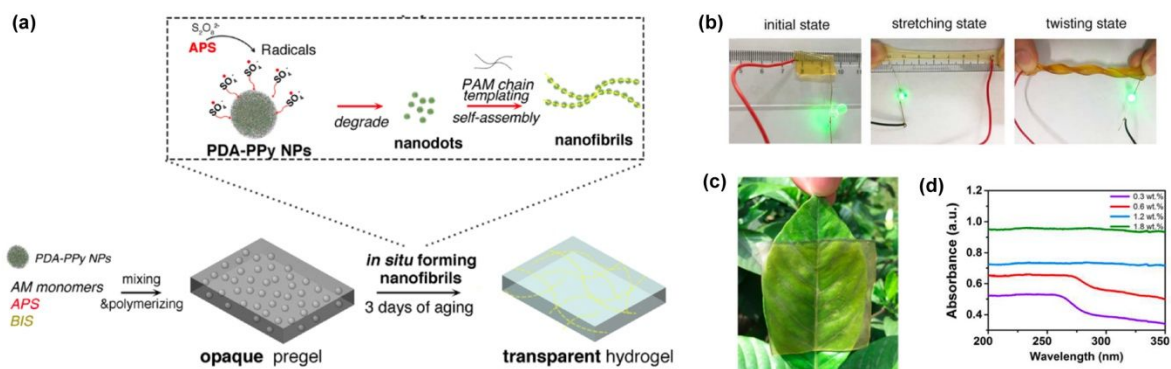
Figure 20. PDA-PPy hydrogels. (a) Schematic representation of in situ transformation of PDA-PPy nanoparticles into transparent fibrils. (b) Demonstration of the electrical conductivity of the hydrogel (6 wt. %) under stretching and twisting. (c) Photography of transparent hydrogel on a leaf. (d) UV-vis absorption spectra of hydrogels prepared with different PDA-PPy concentration. (a) − (d) Reproduced from ref.478 with permission from the American Chemical Society, copyright 2018.
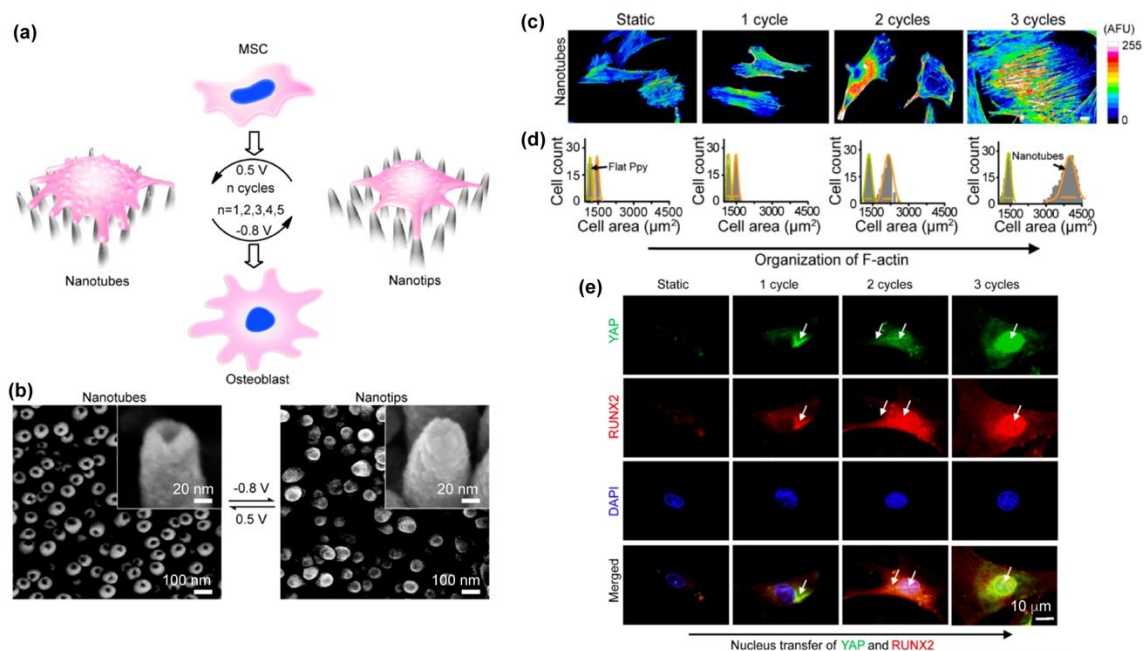
Figure 21. Structured PPy for mechanotransduction. (a) Schematic representation of structure switching in PPy array directing development of Mesenchymal stem cells. (b) SEM images of PPy array at the two redox states showing nanotube and nanotip geometry. Mechanotransduction effects on (c) distribution of actin filaments (pseudocoloured heat maps, scale bar 10 um), (d) cell area, and (e) nuclear translocation. (a) − (e) Reproduced from ref.482 with permission from the American Chemical Society, copyright 2017.
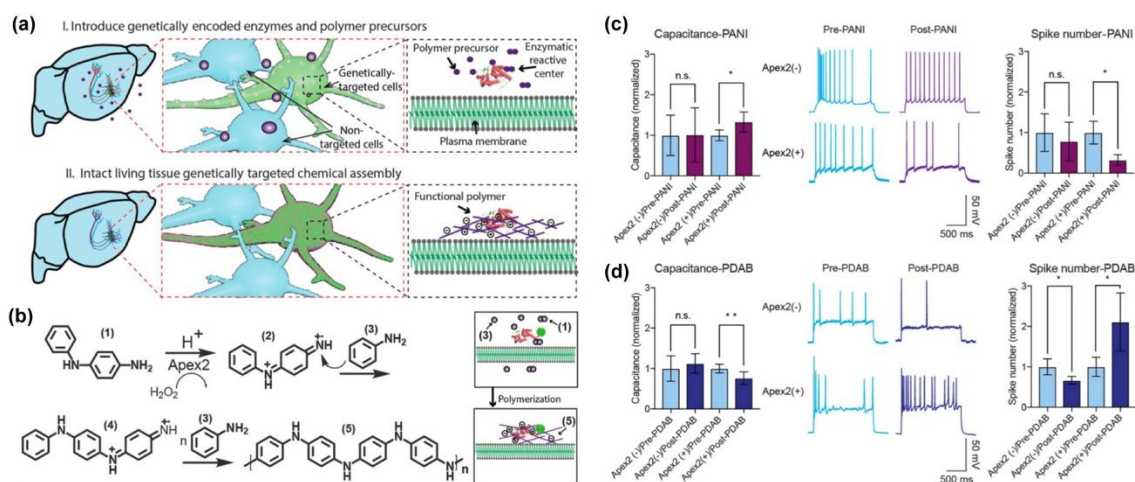
Figure 22. Genetically targeted chemical assembly of polymers. (a) A schematic diagram shows specific synthesis of functional polymer on membranes of genetically modified neurons. (b) Scheme of Apex2-catalyzed polymerization reaction initiated by oxidation of aniline dimer. Chemical species participating in a reaction are as follows: (1) aniline dimer, (2) aniline dimer radical cations, (3) aniline monomer, (4) aniline trimer radical cations, and (5) polyaniline (PANI). Patch clamp measurements of membrane capacitance and current potential spikes from neurons show that modification with conductive PANI increases transmembrane capacitance and decreases spike number (c) while modification with insulating poly(3,3'-diaminobenzidine) (PDAB) inversely reduces the capacitance and increases spike number. (a) − (d) Reproduced from ref.494 with permission from the American Association for the Advancement of Science, copyright 2020.
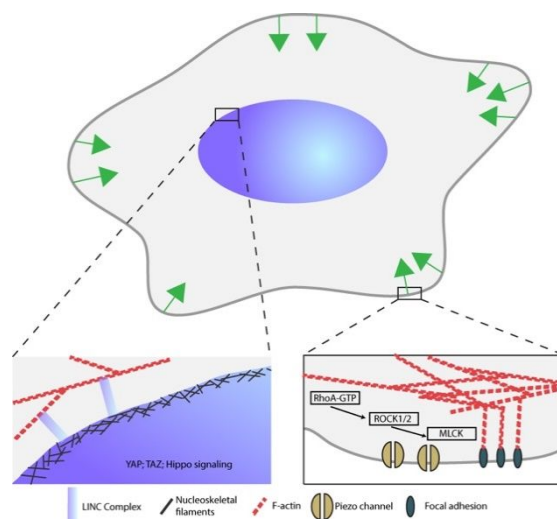
Figure 23. A minimal mechanical model of a cell. Top: schematic of an entire mammalian cell, with the nucleus shown in blue and the cytosol in grey. Green arrows indicate locations, orientations, and relative magnitudes of traction stresses. Lower left: mechanical components around the cell nucleus. The actin cytoskeleton is linked to the nucleoskeleton through the LINC complex. Within the nucleus, YAP/TAZ are effectors of Hippo signaling, which ultimately governs cell spreading and proliferation. Lower right: mechanical components at the cell edge. Traction stresses are transmitted from the cytoskeleton to the substrate through focal adhesions. The RhoA pathway is especially active at focal adhesions and modulates cell contractility by affecting the activity of myosin light chain kinase, MLCK. Piezo channels are both mechanically and electrically active, and therefore are integral parts of electromechanical coupling.
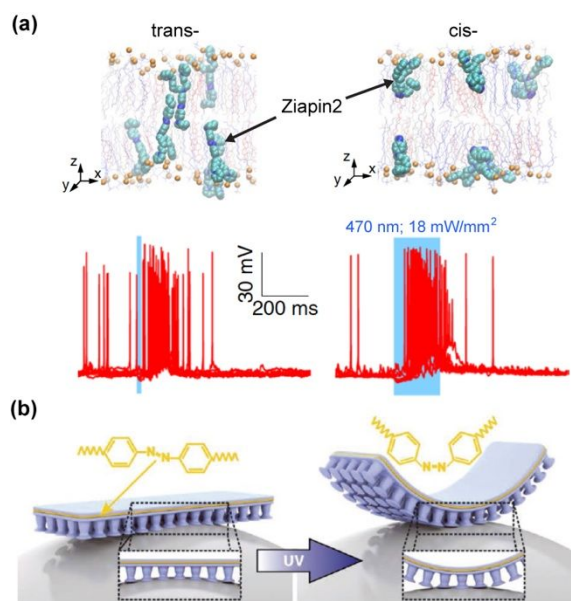
Figure 24. Photoisomerization-triggered neuromodulation. (a) Top: snapshots from MD simulations of a membrane-bound photoswitch, Ziapin2, in trans- and cis-conformations. Bottom: current-clamp traces from neurons incubated with Ziapin2. Illumination period is indicated with cyan shading. Reproduced from Ref.564 with permission from Springer Nature, copyright 2020. (b) Schematic of how photoisomerization can induce appreciable mechanical deformations in a material, useful for applications such as switchable adhesions and robotic actuators. Reproduced from Ref.565 with permission from Wiley, copyright 2019.
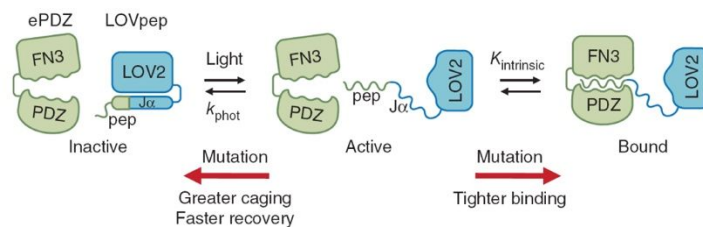
Figure 25. Schematic of LOVpep-based optogenetic dimerization. Illumination exposes the PDZ-binding domain of LOV2, thereby causing dimerization with PDZ domain proteins. Reproduced from Ref.573 with permission from Springer Nature, copyright 2012.

Figure 26. Schematic of remotely controlled chemomagnetic neuromodulation. (a) Magnetically responsive liposomes release chemical payloads upon magnetic heating and stimulate the receptors. (b) The liposomes can be injected into the ventral tegmental area, a region typically used for motivated behavior, reward and depression studies. (a) and (b) Reproduced from Ref.61 with permission from Springer Nature, copyright 2019.

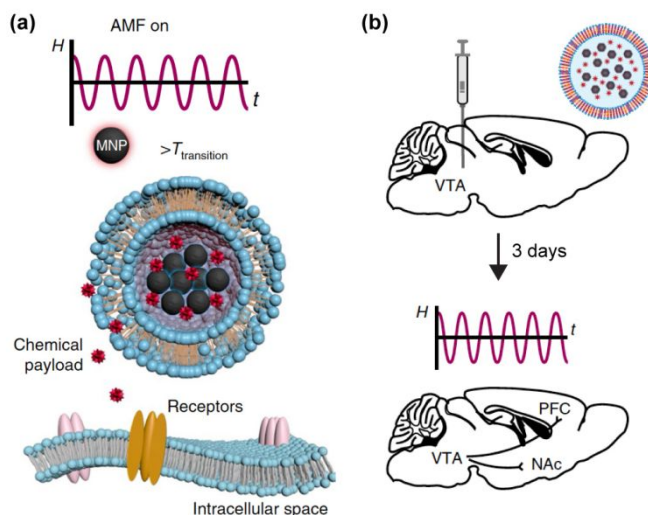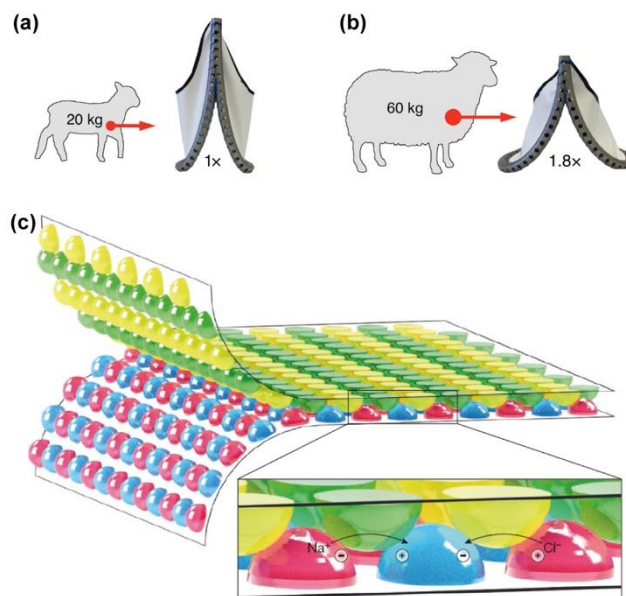**Figure 27.** Biomimetic targets and designs. (a) Schematic showing conformation of geometrically adaptable heart valve when implanted in a juvenile sheep, in the unextended conformation. (b) Schematic showing conformation of geometrically adaptable heart valve when implanted in mature sheep. In this case, the needed pulmonary valve dimensions are 1.8x larger than the juvenile case. (a) and (b) Reproduced from Ref.602 with permission from the American Association for the Advancement of Science, copyright 2020. (c) Electric eel-mimicking hydrogel array. Red gel is high concentration NaCl, blue gel is low concentration NaCl, green gel is cation-selective, and yellow gel is anion-selective. Reproduced from Ref.605 with permission from Springer Nature, copyright 2017.
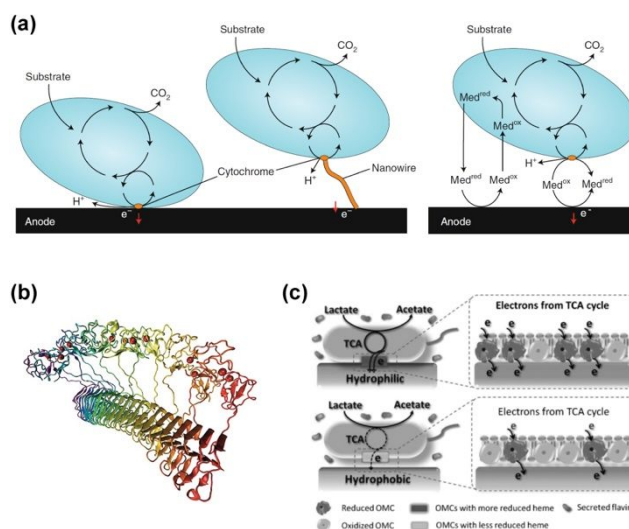
Figure 28. Chemical considerations in electron transfer and electrode selection for bioelectrocatalysis. (a) Direct electron transfer (DET) and mediated electron transfer (MET) schemes. DET is shown both wired and unwired. Reproduced from Ref.75 with permission from Springer Nature, copyright 2020. (b) A view of a protein chimera nanowire used for wiring in a synthetic redox film. Reproduced from Ref.610 with permission from Springer Nature, copyright 2016. (c) Diagram of how enhanced wettability of electrode surface can improve the electrochemical performance of a catalyst. Reproduced from Ref.612 with permission from the Wiley, copyright 2014.

.
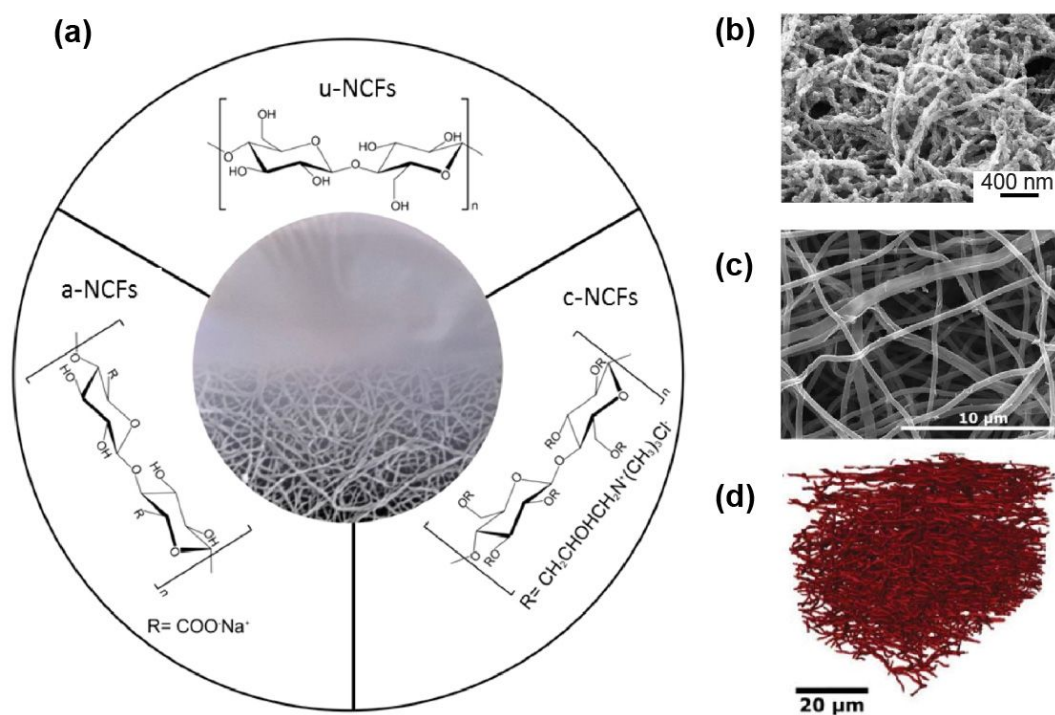
Figure 29. Nanofibrillar cellulose and lignin form good substrates for bioelectronic supercapacitors. (a) Photograph of nanocellulose fibrillar paper and molecular structures for different types of nanocellulose fibers. (b) SEM image of PPy-nanocellulose fiber composite material. (a) and (b) Reproduced from Ref.621 with permission from the American Chemical Society, copyright 2015. (c) SEM image of lignin-derived carbon nanofiber mat. (d) 3D visualization of lignin-derived carbon nanofiber maps obtained from computed tomography. (c) and (d) Reproduced from Ref.628 under the terms of the Creative Commons Attribution License from the Royal Society of Chemistry, copyright 2019.

Table 1. Summary of advantages, disadvantages and example applications of the material groups used for fabrication of bioelectronics devices.

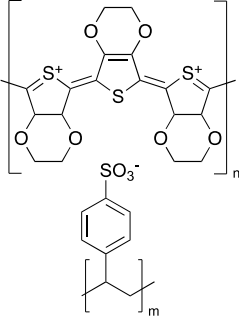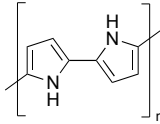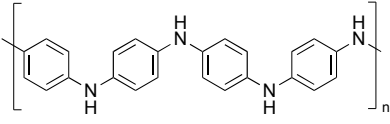|	Advantages	Disadvantages	Application Examples
Inorganic semiconductors	- Established industrial processing - Colloidal structures can be synthesized - Mostly crystalline material - Available surface modification methods - Tunable electrical and optical properties	- Larger material rigidity - Mechanical mismatch at the biointerfaces - Some materials are highly cytotoxic	- Resorbable devices[134, 157, 160] - Intracellular stimulation[38, 67, 129] - Intracellular recording[43, 175] - Membrane voltage sensor[225]
Organic semiconductors	- Solution processable - Flexible and can be intrinsically stretchable - Available surface and bulk modification methods - Tunable electrical and optical properties - Generally low cytotoxicity	- Lower carrier mobility - Stability *in air* and *in vivo* may be poor - May have low crystallinity	- Stretchable sensors[273] - Bioelectronic sensing[291, 294] - Optical modulation[308, 317]
Inorganic conductors	- Established fabrication methods - Good stability - Colloidal structures can be synthesized - Mostly crystalline material - Available surface modification methods - Excellent and stable electrical conductivity - Generally low cytotoxicity	- Larger material rigidity - Mechanical mismatch at the biointerfaces	- Recording microelectrodes[336, 342, 352, 353, 358, 362] - Intracellular electrochemical detection[405, 407] - Wearable electronics[404, 427] - *In vivo* monitoring[16]
Organic conductors	- Solution processable - Suitable for additive manufacturing (*e.g.*, inkjet printing, 3D printing) - Flexible and can be intrinsically stretchable - Can have high water content - Available surface and bulk modification methods - Tunable electrical conductivity - Generally low cytotoxicity	- Low chemical stability - May need to manage the conductive phases within the material - May have low crystallinity	- Stretchable electronics[465] - *In vivo* recording[469] - Transparent electronics[478] - Chemical assembly in living cells[494]

Table 2. Characteristics of common inorganic conductors used for bioelectronics.

	Characteristics
Platinum	- Most widely used material for bioelectronic probes - Good electrical conductivity, stability and biocompatibility - Established fabrication and surface modification methods - Can be alloyed with iridium to increase charge injection current
Gold	- Excellent electrical conductivity, stability, malleability, and biocompatibility - Established fabrication and surface modification methods - Gold nanostructures exhibit plasmonic properties
Liquid metal	- Focuses on low melting point gallium alloys - Can be used to fabricate all soft and self-healing circuits
Other metals: - **Silver**	- Excellent conductivity - Antimicrobial properties
- **Stainless steel**	- Cheap alternative to noble metals - Great chemical stability - Nonmagnetic and MRI safe
- **Copper**	- Alternative to gold with excellent conductivity
Carbon	- Used mostly in the form of graphene or carbon nanotubes - High chemical stability - Can be mechanically flexible - Large surface area - Wide-range of conductivities - Nanostructured carbon can be cytotoxic
Oxides, nitride, carbides	- Wide range of physical and chemical properties - New opportunities for future bioelectronics

Table 3. Characteristics of common organic conductors used for bioelectronics.

	PEDOT:PSS	PPy	PANI
Systematic name	Poly(3,4-ethylenedioxythiophene):poly(styrene sulfonate)	Polypyrrole	Polyanilline
Chemical structure[*]			
Characteristics	- The most studied conductive polymer - Mixture of two ionomers - Poor mechanical stability, requires fixing or composite formulation	- pH-sensitive conductivity - Mechanoelectric properties - Can be synthesized through photopolymerization	- Low-cost precursor and synthesis - pH-sensitive conductivity - Can be synthesized *in situ* onto biological structures

* The exact structure depends on protonation and oxidation states and will vary depending on the conditions.

References

1.　A. Zhang and C. M. Lieber, *Chemical Reviews*, 2016, **116**, 215-257.
2.　A. Chortos, J. Liu and Z. Bao, *Nature Materials*, 2016, **15**, 937-950.
3.　A. Jonsson, S. Inal, I. Uguz, A. J. Williamson, L. Kergoat, J. Rivnay, D. Khodagholy, M. Berggren, C. Bernard, G. G. Malliaras and D. T. Simon, *Proceedings of the National Academy of Sciences*, 2016, **113**, 9440.
4.　A. D. Mickle, S. M. Won, K. N. Noh, J. Yoon, K. W. Meacham, Y. Xue, L. A. McIlvried, B. A. Copits, V. K. Samineni, K. E. Crawford, D. H. Kim, P. Srivastava, B. H. Kim, S. Min, Y. Shiuan, Y. Yun, M. A. Payne, J. Zhang, H. Jang, Y. Li, H. H. Lai, Y. Huang, S. I. Park, R. W. Gereau and J. A. Rogers, *Nature*, 2019, **565**, 361-365.
5.　E. Cingolani, J. I. Goldhaber and E. Marbán, *Nature Reviews Cardiology*, 2018, **15**, 139-150.
6.　R. Feiner, L. Engel, S. Fleischer, M. Malki, I. Gal, A. Shapira, Y. Shacham-Diamand and T. Dvir, *Nature Materials*, 2016, **15**, 679-685.
7.　M. H. Yacoub and C. McLeod, *Nature Reviews Cardiology*, 2018, **15**, 770-779.
8.　B. Freedman, G. Boriani, T. V. Glotzer, J. S. Healey, P. Kirchhof and T. S. Potpara, *Nature Reviews Cardiology*, 2017, **14**, 701-714.
9.　G. Hong, X. Yang, T. Zhou and C. M. Lieber, *Curr Opin Neurobiol*, 2018, **50**, 33-41.
10.　T. M. Fu, G. Hong, T. Zhou, T. G. Schuhmann, R. D. Viveros and C. M. Lieber, *Nat Methods*, 2016, **13**, 875-882.
11.　G. S. Hong, T. M. Fu, M. Qiao, R. D. Viveros, X. Yang, T. Zhou, J. M. Lee, H. G. Park, J. R. Sanes and C. M. Lieber, *Science*, 2018, **360**, 1447-+.
12.　G. S. Hong and C. M. Lieber, *Nature Reviews Neuroscience*, 2019, **20**, 330-345.
13.　W. Gao, S. Emaminejad, H. Y. Y. Nyein, S. Challa, K. Chen, A. Peck, H. M. Fahad, H. Ota, H. Shiraki, D. Kiriya, D. H. Lien, G. A. Brooks, R. W. Davis and A. Javey, *Nature*, 2016, **529**, 509-514.
14.　A. J. Bandodkar, W. J. Jeang, R. Ghaffari and J. A. Rogers, *Annual Review of Analytical Chemistry*, 2019, **12**, 1-22.
15.　K. Kalantar-Zadeh, K. J. Berean, N. Ha, A. F. Chrimes, K. Xu, D. Grando, J. Z. Ou, N. Pillai, J. L. Campbell, R. Brkljača, K. M. Taylor, R. E. Burgell, C. K. Yao, S. A. Ward, C. S. McSweeney, J. G. Muir and P. R. Gibson, *Nature Electronics*, 2018, **1**, 79-87.
16.　L. Wang, S. Xie, Z. Wang, F. Liu, Y. Yang, C. Tang, X. Wu, P. Liu, Y. Li, H. Saiyin, S. Zheng, X. Sun, F. Xu, H. Yu and H. Peng, *Nature Biomedical Engineering*, 2019, DOI: 10.1038/s41551-019-0462-8.
17.　S. P. Lacour, G. Courtine and J. Guck, *Nature Reviews Materials*, 2016, **1**.
18.　N. Wenger, E. M. Moraud, J. Gandar, P. Musienko, M. Capogrosso, L. Baud, C. G. Le Goff, Q. Barraud, N. Pavlova, N. Dominici, I. R. Minev, L. Asboth, A. Hirsch, S. Duis, J. Kreider, A. Mortera, O. Haverbeck, S. Kraus, F. Schmitz, J. DiGiovanna, R. van den Brand, J. Bloch, P. Detemple, S. P. Lacour, E. Bézard, S. Micera and G. Courtine, *Nature Medicine*, 2016, **22**, 138-145.
19.　F. B. Wagner, J.-B. Mignardot, C. G. Le Goff-Mignardot, R. Demesmaeker, S. Komi, M. Capogrosso, A. Rowald, I. Seáñez, M. Caban, E. Pirondini, M. Vat, L. A. McCracken, R. Heimgartner, I. Fodor, A. Watrin, P. Seguin, E. Paoles, K. Van Den Keybus, G. Eberle, B. Schurch, E. Pralong, F. Becce, J. Prior, N. Buse, R. Buschman, E. Neufeld, N. Kuster, S. Carda, J. von Zitzewitz, V. Delattre, T. Denison, H. Lambert, K. Minassian, J. Bloch and G. Courtine, *Nature*, 2018, **563**, 65-71.

20. E. Formento, K. Minassian, F. Wagner, J. B. Mignardot, C. G. Le Goff-Mignardot, A. Rowald, J. Bloch, S. Micera, M. Capogrosso and G. Courtine, *Nature Neuroscience*, 2018, **21**, 1728-1741.

21. M. L. Gill, P. J. Grahn, J. S. Calvert, M. B. Linde, I. A. Lavrov, J. A. Strommen, L. A. Beck, D. G. Sayenko, M. G. Van Straaten, D. I. Drubach, D. D. Veith, A. R. Thoreson, C. Lopez, Y. P. Gerasimenko, V. R. Edgerton, K. H. Lee and K. D. Zhao, *Nature Medicine*, 2018, **24**, 1677-1682.

22. H. Acarón Ledesma, X. Li, J. L. Carvalho-de-Souza, W. Wei, F. Bezanilla and B. Tian, *Nature Nanotechnology*, 2019, **14**, 645-657.

23. R. Chen, A. Canales and P. Anikeeva, *Nature Reviews Materials*, 2017, **2**, 1-16.

24. N. Obidin, F. Tasnim and C. Dagdeviren, *Advanced Materials*, 2019, **1901482**, 1-26.

25. J. A. Frank, M. J. Antonini and P. Anikeeva, *Nature Biotechnology*, 2019, **37**, 1013-1023.

26. J. Rivnay, H. Wang, L. Fenno, K. Deisseroth and G. G. Malliaras, *Sci Adv*, 2017, **3**, e1601649.

27. P. Cai, W. R. Leow, X. Wang, Y. L. Wu and X. Chen, *Adv Mater*, 2017, **29**.

28. M. Wang, G. Mi, D. Shi, N. Bassous, D. Hickey and T. J. Webster, *Advanced Functional Materials*, 2018, **28**, 1700905.

29. S. M. Won, E. Song, J. Zhao, J. Li, J. Rivnay and J. A. Rogers, *Adv Mater*, 2018, **30**, e1800534.

30. T. Wang, M. Wang, L. Yang, Z. Li, X. J. Loh and X. Chen, *Adv Mater*, 2020, **32**, e1905522.

31. W. Gao, H. Ota, D. Kiriya, K. Takei and A. Javey, *Acc Chem Res*, 2019, **52**, 523-533.

32. T. R. Ray, J. Choi, A. J. Bandodkar, S. Krishnan, P. Gutruf, L. Tian, R. Ghaffari and J. A. Rogers, *Chem Rev*, 2019, **119**, 5461-5533.

33. A. H. Moffa, D. Martin, A. Alonzo, D. Bennabi, D. M. Blumberger, I. M. Benseñor, Z. Daskalakis, F. Fregni, E. Haffen, S. H. Lisanby, F. Padberg, U. Palm, L. B. Razza, B. Sampaio-Jr, C. Loo and A. R. Brunoni, *Progress in Neuro-Psychopharmacology and Biological Psychiatry*, 2020, **99**.

34. X. C. Dai, G. S. Hong, T. Gao and C. M. Lieber, *Accounts of Chemical Research*, 2018, **51**, 309-318.

35. T. M. Fu, G. S. Hong, R. D. Viveros, T. Zhou and C. M. Lieber, *Proceedings of the National Academy of Sciences of the United States of America*, 2017, **114**, E10046-E10055.

36. T. M. Fu, G. S. Hong, T. Zhou, T. G. Schuhmann, R. D. Viveros and C. M. Lieber, *Nature Methods*, 2016, **13**, 875-+.

37. G. S. Hong, T. M. Fu, T. Zhou, T. G. Schuhmann, J. L. Huang and C. M. Lieber, *Nano Letters*, 2015, **15**, 6979-6984.

38. Y. Jiang, X. Li, B. Liu, J. Yi, Y. Fang, F. Shi, X. Gao, E. Sudzilovsky, R. Parameswaran, K. Koehler, V. Nair, J. Yue, K. Guo, Y. Fang, H.-M. Tsai, G. Freyermuth, R. C. S. Wong, C.-M. Kao, C.-T. Chen, A. W. Nicholls, X. Wu, G. M. G. Shepherd and B. Tian, *Nature Biomedical Engineering*, 2018, **2**, 508-521.

39. T. Someya, Z. Bao and G. G. Malliaras, *Nature*, 2016, **540**, 379-385.

40. Q. Li, K. W. Nan, P. Le Floch, Z. W. Lin, H. Sheng, T. S. Blum and J. Liu, *Nano Letters*, 2019, **19**, 5781-5789.

41. T. Cohen-Karni, B. P. Timko, L. E. Weiss and C. M. Lieber, *Proceedings of the National Academy of Sciences of the United States of America*, 2009, **106**, 7309-7313.

42. X. Duan, R. Gao, P. Xie, T. Cohen-Karni, Q. Qing, H. S. Choe, B. Tian, X. Jiang and C. M. Lieber, *Nature Nanotechnology*, 2012, **7**, 174-179.

43.   B. Tian, T. Cohen-Karni, Q. Qing, X. Duan, P. Xie and C. M. Lieber, *Science*, 2010, **329**, 830-834.

44.   L. Xiang, K. Chen, R. Yan, W. Li and K. Xu, *Nature Methods*, 2020, DOI: 10.1038/s41592-020-0793-0.

45.   R. Phillips and S. R. Quake, *Physics Today*, 2006, **59**, 38-43.

46.   E. Musk, *Journal of Medical Internet Research*, 2019, **21**, e16194-e16194.

47.   K. L. Drake, K. D. Wise, J. Farraye, D. J. Anderson and S. L. BeMent, *IEEE Transactions on Biomedical Engineering*, 1988, **35**, 719-732.

48.   K. E. Jones, P. K. Campbell and R. A. Normann, *Annals of Biomedical Engineering*, 1992, **20**, 423-437.

49.   E. M. Maynard, C. T. Nordhausen and R. A. Normann, *Electroencephalography and Clinical Neurophysiology*, 1997, **102**, 228-239.

50.   R. J. Vetter, J. C. Williams, J. F. Hetke, E. A. Nunamaker and D. R. Kipke, *IEEE Transactions on Biomedical Engineering*, 2004, **51**, 896-904.

51.   K. D. Wise, *IEEE Engineering in Medicine and Biology Magazine*, 2005, **24**, 22-29.

52.   P. K. Campbell, K. E. Jones, R. J. Huber, K. W. Horch and R. A. Normann, *IEEE Transactions on Biomedical Engineering*, 1991, **38**, 758-768.

53.   H. Spoendlin and A. Schrott, *Hearing Research*, 1989, **43**, 25-38.

54.   J. B. Jonas, A. M. Schmidt, J. A. Muller-Bergh, U. M. Schlotzer-Schrehardt and G. O. H. Naumann, *Investigative Ophthalmology and Visual Science*, 1992, **33**, 2012-2018.

55.   F. R. Willett, D. R. Deo, D. T. Avansino, P. Rezaii, L. R. Hochberg, J. M. Henderson and K. V. Shenoy, *Cell*, 2020, **181**, 396-409.e326.

56.   J.-B. Eichenlaub, B. Jarosiewicz, J. Saab, B. Franco, J. Kelemen, E. Halgren, L. R. Hochberg and S. S. Cash, *Cell Reports*, 2020, **31**, 107581.

57.   A. Obaid, M.-E. Hanna, Y.-W. Wu, M. Kollo, R. Racz, M. R. Angle, J. Müller, N. Brackbill, W. Wray, F. Franke, E. J. Chichilnisky, A. Hierlemann, J. B. Ding, A. T. Schaefer and N. A. Melosh, *Science Advances*, 2020, **6**, eaay2789.

58.   Y. Zhang, Z. Zheng, M. Yu, C. Hsu, E. A. Berthiaume, H. Pan, X. Zhang, A. Z. Stieg, B. Wu, H. Wang, K. Ting and C. Soo, *ACS Applied Materials & Interfaces*, 2018, **10**, 15449-15460.

59.   Y. Zhang, A. D. Mickle, P. Gutruf, L. A. McIlvried, H. Guo, Y. Wu, J. P. Golden, Y. Xue, J. G. Grajales-Reyes, X. Wang, S. Krishnan, Y. Xie, D. Peng, C. J. Su, F. Zhang, J. T. Reeder, S. K. Vogt, Y. Huang, J. A. Rogers and R. W. Gereau, *Science Advances*, 2019, **5**, 1-12.

60.   R. Chen, G. Romero, M. G. Christiansen, A. Mohr and P. Anikeeva, *Science*, 2015, **347**, 1477-1480.

61.   S. Y. Rao, R. Chen, A. A. LaRocca, M. G. Christiansen, A. W. Senko, C. H. Shi, P. H. Chiang, G. Varnavides, J. Xue, Y. Zhou, S. Park, R. H. Ding, J. Moon, G. P. Feng and P. Anikeeva, *Nature Nanotechnology*, 2019, **14**, 967-+.

62.   Y. Jiang, R. Parameswaran, X. Li, J. L. Carvalho-de-Souza, X. Gao, L. Meng, F. Bezanilla, G. M. G. Shepherd and B. Tian, *Nature Protocols*, 2019, **14**, 1339-1376.

63.   R. Parameswaran, K. Koehler, M. Y. Rotenberg, M. J. Burke, J. Kim, K.-Y. Jeong, B. Hissa, M. D. Paul, K. Moreno, N. Sarma, T. Hayes, E. Sudzilovsky, H.-G. Park and B. Tian, *Proc Natl Acad Sci USA*, 2019, **116**, 413-421.

64.   S. Yoo, S. Hong, Y. Choi, J. H. Park and Y. Nam, *ACS Nano*, 2014, **8**, 8040-8049.

65.   J. L. Carvalho-de-Souza, B. I. Pinto, D. R. Pepperberg and F. Bezanilla, *Biophysical Journal*, 2018, **114**, 283-288.

66.   J. L. Carvalho-de-Souza, J. S. Treger, B. Dang, S. B. Kent, D. R. Pepperberg and F. Bezanilla, *Neuron*, 2015, **86**, 207-217.

67. Y. Jiang, J. L. Carvalho-de-Souza, R. C. S. Wong, Z. Luo, D. Isheim, X. Zuo, A. W. Nicholls, I. W. Jung, J. Yue, D.-J. Liu, Y. Wang, V. De Andrade, X. Xiao, L. Navrazhnykh, D. E. Weiss, X. Wu, D. N. Seidman, F. Bezanilla and B. Tian, *Nature Materials*, 2016, **15**, 1023-1030.

68. J. Kubanek, P. Shukla, A. Das, S. A. Baccus and M. B. Goodman, *Journal of Neuroscience*, 2018, **38**, 3081-3091.

69. R. Plonsey and R. C. Barr, *Bioelectricity: a quantitative approach*, Springer Science & Business Media, 2007.

70. L. P. Savtchenko, M. M. Poo and D. A. Rusakov, *Nature Reviews Neuroscience*, 2017, **18**, 598-612.

71. H. Yuk, B. Lu and X. Zhao, *Chemical Society Reviews*, 2019, **48**, 1642-1667.

72. P. Sanjuan-Alberte, M. R. Alexander, R. J. M. Hague and F. J. Rawson, *Bioelectronic Medicine*, 2018, **4**, 1-7.

73. C. Choi, D. S. Ashby, D. M. Butts, R. H. DeBlock, Q. Wei, J. Lau and B. Dunn, *Nature Reviews Materials*, 2020, **5**, 5-19.

74. A. Ruff, F. Conzuelo and W. Schuhmann, *Nature Catalysis*, 2020, **3**, 214-224.

75. H. Chen, F. Dong and S. D. Minteer, *Nature Catalysis*, 2020, **3**, 225-244.

76. T. K. Rudolph and B. A. Freeman, *Science Signaling*, 2009, **2**, re7-re7.

77. B. C. Dickinson and C. J. Chang, *Nature Chemical Biology*, 2011, **7**, 504-511.

78. A. Burton, S. N. Obaid, A. Vazquez-Guardado, M. B. Schmit, T. Stuart, L. Cai, Z. Chen, I. Kandela, C. R. Haney, E. A. Waters, H. Cai, J. A. Rogers, L. Lu and P. Gutruf, *Proc Natl Acad Sci U S A*, 2020, **117**, 2835-2845.

79. L. Lu, P. Gutruf, L. Xia, D. L. Bhatti, X. Wang, A. Vazquez-Guardado, X. Ning, X. Shen, T. Sang, R. Ma, G. Pakeltis, G. Sobczak, H. Zhang, D.-o. Seo, M. Xue, L. Yin, D. Chanda, X. Sheng, M. R. Bruchas and J. A. Rogers, *Proc Natl Acad Sci U S A*, 2018, **115**, E1374-E1383.

80. Z. Zhang and J. T. Yates, *Chemical Reviews*, 2012, **112**, 5520-5551.

81. A. Vilan and D. Cahen, *Chemical Reviews*, 2017, **117**, 4624-4666.

82. J. I. Pankove, *Optical processes in semiconductors*, Prentice-Hall, Englewood Cliffs, N.J.,, 1971.

83. K. M. Mayer and J. H. Hafner, *Chem Rev*, 2011, **111**, 3828-3857.

84. L. Jauffred, A. Samadi, H. Klingberg, P. M. Bendix and L. B. Oddershede, *Chem Rev*, 2019, **119**, 8087-8130.

85. J. S. Donner, S. A. Thompson, M. P. Kreuzer, G. Baffou and R. Quidant, *Nano Lett*, 2012, **12**, 2107-2111.

86. T. Bai and N. Gu, *Small*, 2016, **12**, 4590-4610.

87. M. J. Dalby, N. Gadegaard, P. Herzyk, D. Sutherland, H. Agheli, C. D. W. Wilkinson and A. S. G. Curtis, *Journal of Cellular Biochemistry*, 2007, **102**, 1234-1244.

88. P. Beard, *Interface Focus*, 2011, **1**, 602-631.

89. S. Park, J. A. Frank and P. Anikeeva, *Nature Biomedical Engineering*, 2018, **2**, 471-472.

90. M. Dipalo, G. Melle, L. Lovato, A. Jacassi, F. Santoro, V. Caprettini, A. Schirato, A. Alabastri, D. Garoli, G. Bruno, F. Tantussi and F. De Angelis, *Nat Nanotechnol*, 2018, **13**, 965-971.

91. Q. Li, N. Lu, L. Wang and C. Fan, *Small Methods*, 2018, **2**, 1700263.

92. M. J. Schöning and A. Poghossian, *Analyst*, 2002, **127**, 1137-1151.

93. P. Fromherz, A. Offenhausser, T. Vetter and J. Weis, *Science*, 1991, **252**, 1290.

94. D. A. Bernards and G. G. Malliaras, *Advanced Functional Materials*, 2007, **17**, 3538-3544.

95.   J. Rivnay, S. Inal, A. Salleo, R. M. Owens, M. Berggren and G. G. Malliaras, *Nature Reviews Materials*, 2018, **3**.

96.   D. Khodagholy, J. Rivnay, M. Sessolo, M. Gurfinkel, P. Leleux, L. H. Jimison, E. Stavrinidou, T. Herve, S. Sanaur, R. M. Owens and G. G. Malliaras, *Nature Communications*, 2013, **4**, 1-6.

97.   M. Ghittorelli, L. Lingstedt, P. Romele, N. I. Crăciun, Z. M. Kovács-Vajna, P. W. M. Blom and F. Torricelli, *Nature Communications*, 2018, **9**, 1441.

98.   M. Jakešová, T. A. Sjöström, V. Đerek, D. Poxson, M. Berggren, E. D. Głowacki and D. T. Simon, *npj Flexible Electronics*, 2019, **3**.

99.   J. Isaksson, P. Kjäll, D. Nilsson, N. Robinson, M. Berggren and A. Richter-Dahlfors, *Nature Materials*, 2007, **6**, 673-679.

100.   A. Williamson, J. Rivnay, L. Kergoat, A. Jonsson, S. Inal, I. Uguz, M. Ferro, A. Ivanov, T. A. Sjöström, D. T. Simon, M. Berggren, G. G. Malliaras and C. Bernard, *Advanced Materials*, 2015, **27**, 3138-3144.

101.   M. Seitanidou, R. Blomgran, G. Pushpamithran, M. Berggren and D. T. Simon, *Advanced Healthcare Materials*, 2019, **8**, 1900813.

102.   M. Berggren, X. Crispin, S. Fabiano, M. P. Jonsson, D. T. Simon, E. Stavrinidou, K. Tybrandt and I. Zozoulenko, *Advanced Materials*, 2019, **31**, 1805813.

103.   T. Arbring Sjöström, M. Berggren, E. O. Gabrielsson, P. Janson, D. J. Poxson, M. Seitanidou and D. T. Simon, *Advanced Materials Technologies*, 2018, **3**, 1700360.

104.   A. Jonsson, Z. Song, D. Nilsson, B. A. Meyerson, D. T. Simon, B. Linderoth and M. Berggren, *Science Advances*, 2015, **1**, 1-6.

105.   A. Cobo, R. Sheybani and E. Meng, *Advanced Healthcare Materials*, 2015, **4**, 969-982.

106.   E. Meng and T. Hoang, *Advanced Drug Delivery Reviews*, 2012, **64**, 1628-1638.

107.   E. S. Boyden, F. Zhang, E. Bamberg, G. Nagel and K. Deisseroth, *Nature Neuroscience*, 2005, **8**, 1263-1268.

108.   J. Levitz, J. Broichhagen, P. Leippe, D. Konrad, D. Trauner and E. Y. Isacoff, *Proceedings of the National Academy of Sciences of the United States of America*, 2017, **114**, E3546-E3554.

109.   J. Delbeke, L. Hoffman, K. Mols, D. Braeken and D. Prodanov, *Frontiers in Neuroscience*, 2017, **11**, 1-20.

110.   J. P. Seymour, F. Wu, K. D. Wise and E. Yoon, *Microsystems and Nanoengineering*, 2017, **3**, 1-16.

111.   R. Qazi, A. M. Gomez, D. C. Castro, Z. Zou, J. Y. Sim, Y. Xiong, J. Abdo, C. Y. Kim, A. Anderson, F. Lohner, S. H. Byun, B. Chul Lee, K. I. Jang, J. Xiao, M. R. Bruchas and J. W. Jeong, *Nature Biomedical Engineering*, 2019, **3**, 655-669.

112.   N. Wang, *Journal of Physics D: Applied Physics*, 2017, **50**.

113.   Y. Li, Y. Xiao and C. Liu, *Chemical Reviews*, 2017, **117**, 4376-4421.

114.   M. Hernandez, J. Patzig, S. R. Mayoral, K. D. Costa, J. R. Chan and P. Casaccia, *Journal of Neuroscience*, 2016, **36**, 806-813.

115.   W. Zhao, L. Hanson, H.-Y. Lou, M. Akamatsu, P. D. Chowdary, F. Santoro, J. R. Marks, A. Grassart, D. G. Drubin, Y. Cui and B. Cui, *Nature Nanotechnology*, 2017, **12**, 750-756.

116.   C. F. Guimarães, L. Gasperini, A. P. Marques and R. L. Reis, *Nature Reviews Materials*, 2020, DOI: 10.1038/s41578-019-0169-1, 1-20.

117.   J. W. Salatino, K. A. Ludwig, T. D. Y. Kozai and E. K. Purcell, *Nature Biomedical Engineering*, 2017, **1**, 862-877.

118.   B. A. Copits, M. Y. Pullen and R. W. Gereau, *PAIN*, 2016, **157**, 2424-2433.

119.   D. J. McFarland and J. R. Wolpaw, *Communications of the ACM*, 2011, **54**, 60-66.

120.   S. Micera, M. Caleo, C. Chisari, F. C. Hummel and A. Pedrocchi, *Neuron*, 2020, **105**, 604-620.

121.   J. A. Rogers, T. Someya and Y. Huang, *Science*, 2010, **327**, 1603-1607.

122.   Z. Xue, H. Song, J. A. Rogers, Y. Zhang and Y. Huang, *Advanced Materials*, 2019, **1902254**, 1-32.

123.   C. Zhu, D. Du and Y. Lin, *Biosensors and Bioelectronics*, 2017, **89**, 43-55.

124.   G. M. Taboada, K. Yang, M. J. N. Pereira, S. S. Liu, Y. Hu, J. M. Karp, N. Artzi and Y. Lee, *Nature Reviews Materials*, 2020, DOI: 10.1038/s41578-019-0171-7.

125.   J. Koo, M. R. MacEwan, S. K. Kang, S. M. Won, M. Stephen, P. Gamble, Z. Xie, Y. Yan, Y. Y. Chen, J. Shin, N. Birenbaum, S. Chung, S. B. Kim, J. Khalifeh, D. V. Harburg, K. Bean, M. Paskett, J. Kim, Z. S. Zohny, S. M. Lee, R. Zhang, K. Luo, B. Ji, A. Banks, H. M. Lee, Y. Huang, W. Z. Ray and J. A. Rogers, *Nature Medicine*, 2018, **24**, 1830-1836.

126.   M. Irimia-Vladu, *Chem. Soc. Rev.*, 2014, **43**, 588-610.

127.   A. Hoppe, N. S. Güldal and A. R. Boccaccini, *Biomaterials*, 2011, **32**, 2757-2774.

128.   S. Han, J. Kim, S. M. Won, Y. Ma, D. Kang, Z. Xie, K.-T. Lee, H. U. Chung, A. Banks, S. Min, S. Y. Heo, C. R. Davies, J. W. Lee, C.-H. Lee, B. H. Kim, K. Li, Y. Zhou, C. Wei, X. Feng, Y. Huang and J. A. Rogers, *Sci. Transl. Med.*, 2018, **10**, eaan4950.

129.   R. Parameswaran, J. L. Carvalho-De-Souza, Y. Jiang, M. J. Burke, J. F. Zimmerman, K. Koehler, A. W. Phillips, J. Yi, E. J. Adams, F. Bezanilla and B. Tian, *Nature Nanotechnology*, 2018, **13**, 260-266.

130.   M. Y. Rotenberg, N. Yamamoto, E. N. Schaumann, L. Matino, F. Santoro and B. Tian, *Proc Natl Acad Sci USA*, 2019, **116**, 22531-22539.

131.   F. Patolsky, G. Zheng and C. M. Lieber, *Nat Protoc*, 2006, **1**, 1711-1724.

132.   T. Shimoda, Y. Matsuki, M. Furusawa, T. Aoki, I. Yudasaka, H. Tanaka, H. Iwasawa, D. Wang, M. Miyasaka and Y. Takeuchi, *Nature*, 2006, **440**, 783-786.

133.   P. D. Tran, V. Artero and M. Fontecave, *Energy Environ. Sci.*, 2010, **3**, 727-747.

134.   S. W. Hwang, H. Tao, D. H. Kim, H. Cheng, J. K. Song, E. Rill, M. A. Brenckle, B. Panilaitis, S. M. Won, Y. S. Kim, Y. M. Song, K. J. Yu, A. Ameen, R. Li, Y. Su, M. Yang, D. L. Kaplan, M. R. Zakin, M. J. Slepian, Y. Huang, F. G. Omenetto and J. A. Rogers, *Science*, 2012, **337**, 1640-1644.

135.   Y. Fang, Y. Jiang, H. Acaron Ledesma, J. Yi, X. Gao, D. E. Weiss, F. Shi and B. Tian, *Nano Letters*, 2018, **18**, 4487-4492.

136.   A. I. Hochbaum, D. Gargas, Y. J. Hwang and P. Yang, *Nano Letters*, 2009, **9**, 3550-3554.

137.   C. Chiappini, E. De Rosa, J. O. Martinez, X. Liu, J. Steele, M. M. Stevens and E. Tasciotti, *Nature Materials*, 2015, **14**, 532-539.

138.   J. Salonen and E. Mäkilä, *Advanced Materials*, 2018, **30**, 1703819.

139.   M. M. Orosco, C. Pacholski and M. J. Sailor, *Nature Nanotechnology*, 2009, **4**, 255-258.

140.   R. Vilensky, M. Bercovici and E. Segal, *Advanced Functional Materials*, 2015, **25**, 6725-6732.

141.   H. Acaron Ledesma and B. Tian, *J. Mater. Chem. B*, 2017, **5**, 4276-4289.

142.   S. Kim and J. F. Cahoon, *Accounts of Chemical Research*, 2019, **52**, 3511-3520.

143.   Y. Fang, Y. Jiang, M. J. Cherukara, F. Shi, K. Koehler, G. Freyermuth, D. Isheim, B. Narayanan, A. W. Nicholls, D. N. Seidman, S. K. R. S. Sankaranarayanan and B. Tian, *Nature Communications*, 2017, **8**, 2014.

144. Z. Luo, Y. Jiang, B. D. Myers, D. Isheim, J. Wu, J. F. Zimmerman, Z. Wang, Q. Li, Y. Wang, X. Chen, V. P. Dravid, D. N. Seidman and B. Tian, *Science*, 2015, **348**, 1451-1455.

145. D. J. Hill, T. S. Teitsworth, E. T. Ritchie, J. M. Atkin and J. F. Cahoon, *ACS Nano*, 2018, **12**, 10554-10563.

146. S. Kim, D. J. Hill, C. W. Pinion, J. D. Christesen, J. R. McBride and J. F. Cahoon, *ACS Nano*, 2017, **11**, 4453-4462.

147. C. W. Pinion, J. D. Christesen and J. F. Cahoon, *J. Mater. Chem. C*, 2016, **4**, 3890-3897.

148. X. Gao, Y. Jiang, Y. Lin, K. H. Kim, Y. Fang, J. Yi, L. Meng, H. C. Lee, Z. Lu, O. Leddy, R. Zhang, Q. Tu, W. Feng, V. Nair, P. J. Griffin, F. Shi, G. S. Shekhawat, A. R. Dinner, H. G. Park and B. Tian, *Sci Adv*, 2020, **6**, eaay2760.

149. G. Dhanaraj, *Springer handbook of crystal growth*, Springer, Heidelberg ; New York, 2010.

150. W. N. Borle and R. K. Bagai, *Journal of Crystal Growth*, 1976, **36**, 259-262.

151. C. Li, C. Guo, V. Fitzpatrick, A. Ibrahim, M. J. Zwierstra, P. Hanna, A. Lechtig, A. Nazarian, S. J. Lin and D. L. Kaplan, *Nature Reviews Materials*, 2020, **5**, 61-81.

152. J.-K. Chang, H. Fang, C. A. Bower, E. Song, X. Yu and J. A. Rogers, *Proc Natl Acad Sci USA*, 2017, **114**, E5522-E5529.

153. M. Irimia-Vladu, E. D. Glowacki, N. S. Sariciftci and S. Bauer, *Green Materials for Electronics*, Wiley-VCH Verlag GmbH & Co. KGaA, Weinheim, Germany, 2017.

154. J.-H. Park, L. Gu, G. von Maltzahn, E. Ruoslahti, S. N. Bhatia and M. J. Sailor, *Nature Materials*, 2009, **8**, 331-336.

155. C. M. Dekeyser, C. C. Buron, S. R. Derclaye, A. M. Jonas, J. Marchand-Brynaert and P. G. Rouxhet, *Journal of Colloid and Interface Science*, 2012, **378**, 77-82.

156. D. A. Wilcox, J. Snaider, S. Mukherjee, L. Yuan, L. Huang, B. M. Savoie and B. W. Boudouris, *Soft Matter*, 2019, **15**, 1413-1422.

157. J. Shin, Z. Liu, W. Bai, Y. Liu, Y. Yan, Y. Xue, I. Kandela, M. Pezhouh, M. R. MacEwan, Y. Huang, W. Z. Ray, W. Zhou and J. A. Rogers, *Science Advances*, 2019, **5**, eaaw1899.

158. J. Shin, Y. Yan, W. Bai, Y. Xue, P. Gamble, L. Tian, I. Kandela, C. R. Haney, W. Spees, Y. Lee, M. Choi, J. Ko, H. Ryu, J.-K. Chang, M. Pezhouh, S.-K. Kang, S. M. Won, K. J. Yu, J. Zhao, Y. K. Lee, M. R. MacEwan, S.-K. Song, Y. Huang, W. Z. Ray and J. A. Rogers, *Nature Biomedical Engineering*, 2019, **3**, 37-46.

159. C. Chiappini, J. O. Martinez, E. De Rosa, C. S. Almeida, E. Tasciotti and M. M. Stevens, *ACS Nano*, 2015, **9**, 5500-5509.

160. W. Bai, J. Shin, R. Fu, I. Kandela, D. Lu, X. Ni, Y. Park, Z. Liu, T. Hang, D. Wu, Y. Liu, C. R. Haney, I. Stepien, Q. Yang, J. Zhao, K. R. Nandoliya, H. Zhang, X. Sheng, L. Yin, K. MacRenaris, A. Brikha, F. Aird, M. Pezhouh, J. Hornick, W. Zhou and J. A. Rogers, *Nat Biomed Eng*, 2019, **3**, 644-654.

161. S. Hu, M. R. Shaner, J. A. Beardslee, M. Lichterman, B. S. Brunschwig and N. S. Lewis, *Science*, 2014, **344**, 1005-1009.

162. A. Peled, A. Pevzner, H. Peretz Soroka and F. Patolsky, *J Nanobiotechnol*, 2014, **12**, 7.

163. H. Fang, K. J. Yu, C. Gloschat, Z. Yang, E. Song, C.-H. Chiang, J. Zhao, S. M. Won, S. Xu, M. Trumpis, Y. Zhong, S. W. Han, Y. Xue, D. Xu, S. W. Choi, G. Cauwenberghs, M. Kay, Y. Huang, J. Viventi, I. R. Efimov and J. A. Rogers, *Nature Biomedical Engineering*, 2017, **1**, 0038.

164. Y. W. Chen, J. D. Prange, S. Dühnen, Y. Park, M. Gunji, C. E. D. Chidsey and P. C. McIntyre, *Nature Materials*, 2011, **10**, 539-544.

165. L. Ji, M. D. McDaniel, S. Wang, A. B. Posadas, X. Li, H. Huang, J. C. Lee, A. A. Demkov, A. J. Bard, J. G. Ekerdt and E. T. Yu, *Nature Nanotechnology*, 2015, **10**, 84-90.

166. K. Mathieson, J. Loudin, G. Goetz, P. Huie, L. Wang, T. I. Kamins, L. Galambos, R. Smith, J. S. Harris, A. Sher and D. Palanker, *Nature Photon*, 2012, **6**, 391-397.

167. H. Lorach, G. Goetz, R. Smith, X. Lei, Y. Mandel, T. Kamins, K. Mathieson, P. Huie, J. Harris, A. Sher and D. Palanker, *Nature Medicine*, 2015, **21**, 476-482.

168. L. Wang, K. Mathieson, T. I. Kamins, J. D. Loudin, L. Galambos, G. Goetz, A. Sher, Y. Mandel, P. Huie, D. Lavinsky, J. S. Harris and D. V. Palanker, *Journal of Neural Engineering*, 2012, **9**, 046014.

169. T. Yokota, T. Nakamura, H. Kato, M. Mochizuki, M. Tada, M. Uchida, S. Lee, M. Koizumi, W. Yukita, A. Takimoto and T. Someya, *Nature Electronics*, 2020, **3**, 113-121.

170. F. Patolsky, G. Zheng, O. Hayden, M. Lakadamyali, X. Zhuang and C. M. Lieber, *Proc Natl Acad Sci U S A*, 2004, **101**, 14017-14022.

171. Y. Cui, *Science*, 2001, **293**, 1289-1292.

172. Y. Cui, Z. Zhong, D. Wang, W. U. Wang and C. M. Lieber, *Nano Letters*, 2003, **3**, 149-152.

173. Y. Wu, J. Xiang, C. Yang, W. Lu and C. M. Lieber, *Nature*, 2004, **430**, 61-65.

174. Y. Zhao, J. Yao, L. Xu, M. N. Mankin, Y. Zhu, H. Wu, L. Mai, Q. Zhang and C. M. Lieber, *Nano Letters*, 2016, **16**, 2644-2650.

175. Y. Zhao, S. S. You, A. Zhang, J.-H. Lee, J. Huang and C. M. Lieber, *Nat. Nanotechnol.*, 2019, **14**, 783-790.

176. H. Fang, K. J. Yu, C. Gloschat, Z. Yang, C. H. Chiang, J. Zhao, S. M. Won, S. Xu, M. Trumpis, Y. Zhong, E. Song, S. W. Han, Y. Xue, D. Xu, G. Cauwenberghs, M. Kay, Y. Huang, J. Viventi, I. R. Efimov and J. A. Rogers, *Nat Biomed Eng*, 2017, **1**.

177. H. Fang, J. Zhao, K. J. Yu, E. Song, A. B. Farimani, C. H. Chiang, X. Jin, Y. Xue, D. Xu, W. Du, K. J. Seo, Y. Zhong, Z. Yang, S. M. Won, G. Fang, S. W. Choi, S. Chaudhuri, Y. Huang, M. A. Alam, J. Viventi, N. R. Aluru and J. A. Rogers, *Proc Natl Acad Sci U S A*, 2016, **113**, 11682-11687.

178. J. Li, E. Song, C. H. Chiang, K. J. Yu, J. Koo, H. Du, Y. Zhong, M. Hill, C. Wang, J. Zhang, Y. Chen, L. Tian, Y. Zhong, G. Fang, J. Viventi and J. A. Rogers, *Proc Natl Acad Sci U S A*, 2018, **115**, E9542-E9549.

179. J. Veerbeek and J. Huskens, *Small Methods*, 2017, **1**, 1700072.

180. K. Huang, F. Duclairoir, T. Pro, J. Buckley, G. Marchand, E. Martinez, J.-C. Marchon, B. De Salvo, G. Delapierre and F. Vinet, *ChemPhysChem*, 2009, **10**, 963-971.

181. B. Fabre, *Accounts of Chemical Research*, 2010, **43**, 1509-1518.

182. B. Fabre, Y. Li, L. Scheres, S. P. Pujari and H. Zuilhof, *Angewandte Chemie International Edition*, 2013, **52**, 12024-12027.

183. Y. Yang, S. Ciampi, Y. Zhu and J. J. Gooding, *The Journal of Physical Chemistry C*, 2016, **120**, 13032-13038.

184. H. Liu, F. Duclairoir, B. Fleury, L. Dubois, Y. Chenavier and J.-C. Marchon, *Dalton Transactions*, 2009, DOI: 10.1039/B901309A, 3793-3799.

185. A. Vacher, M. Auffray, F. Barrière, T. Roisnel and D. Lorcy, *Organic Letters*, 2017, **19**, 6060-6063.

186. G. Yzambart, B. Fabre and D. Lorcy, *Langmuir*, 2012, **28**, 3453-3459.

187. F. Gao and A. V. Teplyakov, *Langmuir*, 2017, **33**, 8632-8639.

188. W. Feng and B. Miller, *Langmuir*, 1999, **15**, 3152-3156.

189. Y. L. Bunimovich, Y. S. Shin, W.-S. Yeo, M. Amori, G. Kwong and J. R. Heath, *J. Am. Chem. Soc.*, 2006, **128**, 16323-16331.

190. R. Har-Lavan, O. Yaffe, P. Joshi, R. Kazaz, H. Cohen and D. Cahen, *AIP Advances*, 2012, **2**, 012164.

191. E. J. Faber, L. C. P. M. de Smet, W. Olthuis, H. Zuilhof, E. J. R. Sudhölter, P. Bergveld and A. van den Berg, *ChemPhysChem*, 2005, **6**, 2153-2166.

192. K. M. Roth, A. A. Yasseri, Z. Liu, R. B. Dabke, V. Malinovskii, K.-H. Schweikart, L. Yu, H. Tiznado, F. Zaera, J. S. Lindsey, W. G. Kuhr and D. F. Bocian, *J. Am. Chem. Soc.*, 2003, **125**, 505-517.

193. S. H. Lee, J. S. Kang and D. Kim, *Materials (Basel)*, 2018, **11**, 2557.

194. W. Peng, S. M. Rupich, N. Shafiq, Y. N. Gartstein, A. V. Malko and Y. J. Chabal, *Chemical Reviews*, 2015, **115**, 12764-12796.

195. J. Politi, S. Zappavigna, I. Rea, P. Grieco, A. Caliò, A. Luce, M. Caraglia and L. De Stefano, *Journal of Sensors*, 2017, **2017**, 6792396.

196. Z. Pápa, S. K. Ramakrishnan, M. Martin, T. Cloitre, L. Zimányi, J. Márquez, J. Budai, Z. Tóth and C. Gergely, *Langmuir*, 2016, **32**, 7250-7258.

197. Z.-H. Wang and G. Jin, *Colloids and Surfaces B: Biointerfaces*, 2004, **34**, 173-177.

198. N. Aissaoui, L. Bergaoui, J. Landoulsi, J.-F. Lambert and S. Boujday, *Langmuir*, 2012, **28**, 656-665.

199. Q. Hong, C. Rogero, J. H. Lakey, B. A. Connolly, A. Houlton and B. R. Horrocks, *Analyst*, 2009, **134**, 593-601.

200. J.-H. Lee, A. Zhang, S. S. You and C. M. Lieber, *Nano Letters*, 2016, **16**, 1509-1513.

201. X. Li, X. Chen, J. Tan, X. Liang and J. Wu, *Analyst*, 2017, **142**, 586-590.

202. X. Ji, H. Wang, B. Song, B. Chu and Y. He, *Frontiers in Chemistry*, 2018, **6**, 38.

203. F. Patolsky, B. P. Timko, G. Yu, Y. Fang, A. B. Greytak, G. Zheng and C. M. Lieber, *Science*, 2006, **313**, 1100-1104.

204. W. Zhang, L. Tong and C. Yang, *Nano Lett*, 2012, **12**, 1002-1006.

205. X. Gan, H. Zhao and X. Quan, *Biosensors and Bioelectronics*, 2017, **89**, 56-71.

206. M. Xiong, Q. Rong, H.-m. Meng and X.-b. Zhang, *Biosensors and Bioelectronics*, 2017, **89**, 212-223.

207. D. Son, S. I. Chae, M. Kim, M. K. Choi, J. Yang, K. Park, V. S. Kale, J. H. Koo, C. Choi, M. Lee, J. H. Kim, T. Hyeon and D.-H. Kim, *Advanced Materials*, 2016, **28**, 9326-9332.

208. M. F. Reynolds, M. H. D. Guimarães, H. Gao, K. Kang, A. J. Cortese, D. C. Ralph, J. Park and P. L. McEuen, *Science Advances*, 2019, **5**, eaat9476.

209. X. Huang, K. Kumar, M. K. Jawed, A. Mohammadi Nasab, Z. Ye, W. Shan and C. Majidi, *Adv. Mater. Technol.*, 2019, **4**, 1800540.

210. K. Kang, S. Xie, L. Huang, Y. Han, P. Y. Huang, K. F. Mak, C.-J. Kim, D. Muller and J. Park, *Nature*, 2015, **520**, 656-660.

211. I. Datta, S. H. Chae, G. R. Bhatt, M. A. Tadayon, B. Li, Y. Yu, C. Park, J. Park, L. Cao, D. N. Basov, J. Hone and M. Lipson, *Nature Photon*, 2020, DOI: 10.1038/s41566-020-0590-4.

212. S. Xie, L. Tu, Y. Han, L. Huang, K. Kang, K. U. Lao, P. Poddar, C. Park, D. A. Muller, R. A. DiStasio and J. Park, *Science*, 2018, **359**, 1131-1136.

213. S. Choi, S. H. Tan, Z. Li, Y. Kim, C. Choi, P.-Y. Chen, H. Yeon, S. Yu and J. Kim, *Nature Materials*, 2018, **17**, 335-340.

214. Y. Kim, S. S. Cruz, K. Lee, B. O. Alawode, C. Choi, Y. Song, J. M. Johnson, C. Heidelberger, W. Kong, S. Choi, K. Qiao, I. Almansouri, E. A. Fitzgerald, J. Kong, A. M. Kolpak, J. Hwang and J. Kim, *Nature*, 2017, **544**, 340-343.

215. S.-H. Bae, K. Lu, Y. Han, S. Kim, K. Qiao, C. Choi, Y. Nie, H. Kim, H. S. Kum, P. Chen, W. Kong, B.-S. Kang, C. Kim, J. Lee, Y. Baek, J. Shim, J. Park, M. Joo, D. A.

Muller, K. Lee and J. Kim, *Nature Nanotechnology*, 2020, DOI: 10.1038/s41565-020-0633-5.

216. W. Kong, H. Li, K. Qiao, Y. Kim, K. Lee, Y. Nie, D. Lee, T. Osadchy, R. J. Molnar, D. K. Gaskill, R. L. Myers-Ward, K. M. Daniels, Y. Zhang, S. Sundram, Y. Yu, S.-h. Bae, S. Rajan, Y. Shao-Horn, K. Cho, A. Ougazzaden, J. C. Grossman and J. Kim, *Nature Materials*, 2018, **17**, 999-1004.

217. S. R. Shin, B. Migliori, B. Miccoli, Y.-C. Li, P. Mostafalu, J. Seo, S. Mandla, A. Enrico, S. Antona, R. Sabarish, T. Zheng, L. Pirrami, K. Zhang, Y. S. Zhang, K.-t. Wan, D. Demarchi, M. R. Dokmeci and A. Khademhosseini, *Adv. Mater.*, 2018, 13.

218. M. Nurunnabi, *Biomedical applications of graphene and 2D nanomaterials*, Elsevier, Cambridge, CA, 1st edition. edn., 2019.

219. F. Wang and X. Liu, *Chemical Society Reviews*, 2009, **38**, 976-989.

220. D. Kang, T. W. Kim, S. R. Kubota, A. C. Cardiel, H. G. Cha and K.-S. Choi, *Chemical Reviews*, 2015, **115**, 12839-12887.

221. T. Holtus, L. Helmbrecht, H. C. Hendrikse, I. Baglai, S. Meuret, G. W. P. Adhyaksa, E. C. Garnett and W. L. Noorduin, *Nat Chem*, 2018, **10**, 740-745.

222. M. Montalti, A. Cantelli and G. Battistelli, *Chemical Society Reviews*, 2015, **44**, 4853-4921.

223. A. L. Efros, J. B. Delehanty, A. L. Huston, I. L. Medintz, M. Barbic and T. D. Harris, *Nature Nanotechnology*, 2018, **13**, 278-288.

224. M. Caglar, R. Pandya, J. Xiao, S. K. Foster, G. Divitini, R. Y. S. Chen, N. C. Greenham, K. Franze, A. Rao and U. F. Keyser, *Nano Letters*, 2019, **19**, 8539-8549.

225. O. K. Nag, M. H. Stewart, J. R. Deschamps, K. Susumu, E. Oh, V. Tsytsarev, Q. Tang, A. L. Efros, R. Vaxenburg, B. J. Black, Y. Chen, T. J. O'Shaughnessy, S. H. North, L. D. Field, P. E. Dawson, J. J. Pancrazio, I. L. Medintz, Y. Chen, R. S. Erzurumlu, A. L. Huston and J. B. Delehanty, *ACS Nano*, 2017, **11**, 5598-5613.

226. S. Cestellos-Blanco, H. Zhang and P. D. Yang, *Faraday Discussions*, 2019, **215**, 54-65.

227. K. K. Sakimoto, A. B. Wong and P. D. Yang, *Science*, 2016, **351**, 74-77.

228. K. K. Saldrnoto, N. Kornienko and P. D. Yang, *Accounts of Chemical Research*, 2017, **50**, 476-481.

229. H. Zhang, H. Liu, Z. Q. Tian, D. Lu, Y. Yu, S. Cestellos-Blanco, K. K. Sakimoto and P. D. Yang, *Nature Nanotechnology*, 2018, **13**, 900-+.

230. J. L. Guo, M. Suastegui, K. K. Sakimoto, V. M. Moody, G. Xiao, D. G. Nocera and N. S. Joshi, *Science*, 2018, **362**, 813-+.

231. X. Wu, X. J. Zhu, P. Chong, J. L. Liu, L. N. Andre, K. S. Ong, K. Brinson, A. I. Mahdi, J. C. Li, L. E. Fenno, H. L. Wang and G. S. Hong, *Proceedings of the National Academy of Sciences of the United States of America*, 2019, **116**, 26332-26342.

232. D. Sarkar, W. Liu, X. Xie, A. C. Anselmo, S. Mitragotri and K. Banerjee, *ACS Nano*, 2014, **8**, 3992-4003.

233. K. F. Mak and J. Shan, *Nature Photon*, 2016, **10**, 216-226.

234. L. Wang, Y. Wang, J. I. Wong, T. Palacios, J. Kong and H. Y. Yang, *Small*, 2014, **10**, 1101-1105.

235. S. Manzeli, A. Allain, A. Ghadimi and A. Kis, *Nano Letters*, 2015, **15**, 5330-5335.

236. C. Liu, D. Kong, P. C. Hsu, H. Yuan, H. W. Lee, Y. Liu, H. Wang, S. Wang, K. Yan, D. Lin, P. A. Maraccini, K. M. Parker, A. B. Boehm and Y. Cui, *Nat Nanotechnol*, 2016, **11**, 1098-1104.

237.   C. Choi, M. K. Choi, S. Liu, M. S. Kim, O. K. Park, C. Im, J. Kim, X. Qin, G. J. Lee, K. W. Cho, M. Kim, E. Joh, J. Lee, D. Son, S. H. Kwon, N. L. Jeon, Y. M. Song, N. Lu and D. H. Kim, *Nature Communications*, 2017, **8**.

238.   N. Gao and X. Fang, *Chemical Reviews*, 2015, **115**, 8294-8343.

239.   W.-J. Ong, L.-L. Tan, Y. H. Ng, S.-T. Yong and S.-P. Chai, *Chemical Reviews*, 2016, **116**, 7159-7329.

240.   Z. Zhang, R. Xu, Z. Wang, M. Dong, B. Cui and M. Chen, *ACS Appl. Mater. Interfaces*, 2017, **9**, 34736-34743.

241.   J. Huang, M. Antonietti and J. Liu, *J. Mater. Chem. A*, 2014, **2**, 7686-7693.

242.   J. Liu and M. Antonietti, *Energy Environ. Sci.*, 2013, **6**, 1486.

243.   D. Yang, H. Zou, Y. Wu, J. Shi, S. Zhang, X. Wang, P. Han, Z. Tong and Z. Jiang, *Ind. Eng. Chem. Res.*, 2017, **56**, 6247-6255.

244.   J. H. Appel, D. O. Li, J. D. Podlevsky, A. Debnath, A. A. Green, Q. H. Wang and J. Chae, *ACS Biomaterials Science & Engineering*, 2016, **2**, 361-367.

245.   P. Shah, T. N. Narayanan, C.-Z. Li and S. Alwarappan, *Nanotechnology*, 2015, **26**, 315102.

246.   W. Z. Teo, E. L. K. Chng, Z. Sofer and M. Pumera, *Chemistry – A European Journal*, 2014, **20**, 9627-9632.

247.   L. M. Guiney, X. Wang, T. Xia, A. E. Nel and M. C. Hersam, *ACS nano*, 2018, **12**, 6360-6377.

248.   H. L. Chia, N. M. Latiff, R. Gusmão, Z. Sofer and M. Pumera, *Chemistry – A European Journal*, 2019, **25**, 2242-2249.

249.   N. Nakatsuka, K. A. Yang, J. M. Abendroth, K. M. Cheung, X. Xu, H. Yang, C. Zhao, B. Zhu, Y. S. Rim, Y. Yang, P. S. Weiss, M. N. Stojanović and A. M. Andrews, *Science*, 2018, **362**, 319-324.

250.   J. Tang, N. Qin, Y. Chong, Y. Diao, Yiliguma, Z. Wang, T. Xue, M. Jiang, J. Zhang and G. Zheng, *Nat Commun*, 2018, **9**, 786.

251.   S. Chai, Y. J. Kim and W. Lee, *Journal of Electroceramics - J ELECTROCERAM*, 2006, **17**, 909-912.

252.   L. Jiang, F.-C. Lv, R. Yang, D.-C. Hu and X. Guo, *Journal of Materiomics*, 2019, **5**, 296-302.

253.   M. Karbalaei Akbari and S. Zhuiykov, *Nat Commun*, 2019, **10**, 3873.

254.   P. Gao, H. Wang, P. Li, W. Gao, Y. Zhang, J. Chen and N. Jia, *Biosensors and Bioelectronics*, 2018, **121**, 104-110.

255.   Y. Wang, J. Guo, T. Wang, J. Shao, D. Wang and Y. W. Yang, *Nanomaterials (Basel)*, 2015, **5**, 1667-1689.

256.   K. N. Manukumar, R. Viswanatha and G. Nagaraju, *Ionics*, 2020, **26**, 1197-1202.

257.   J. Park, J. Kim, S. Y. Kim, W. H. Cheong, J. Jang, Y. G. Park, K. Na, Y. T. Kim, J. H. Heo and C. Y. Lee, *Sci. Adv.*, 2018, **4**, eaap9841.

258.   Z. Ma, D. Kong, L. Pan and Z. Bao, *Journal of Semiconductors*, 2020, Inpress.

259.   S. Wang, J. Xu, W. Wang, G.-J. N. Wang, R. Rastak, F. Molina-Lopez, J. W. Chung, S. Niu, V. R. Feig, J. Lopez, T. Lei, S.-K. Kwon, Y. Kim, A. M. Foudeh, A. Ehrlich, A. Gasperini, Y. Yun, B. Murmann, J. B. H. Tok and Z. Bao, *Nature*, 2018, **555**, 83-88.

260.   S. M. Wellman, J. R. Eles, K. A. Ludwig, J. P. Seymour, N. J. Michelson, W. E. McFadden, A. L. Vazquez and T. D. Y. Kozai, *Advanced Functional Materials*, 2018, **28**, 1701269.

261.   C. M. Boutry, L. Beker, Y. Kaizawa, C. Vassos, H. Tran, A. C. Hinckley, R. Pfattner, S. Niu, J. Li and J. Claverie, *Nature Biomedical Engineering*, 2019, **3**, 47.

262. J. Y. Oh, D. Son, T. Katsumata, Y. Lee, Y. Kim, J. Lopez, H.-C. Wu, J. Kang, J. Park, X. Gu, J. Mun, N. G.-J. Wang, Y. Yin, W. Cai, Y. Yun, J. B. H. Tok and Z. Bao, *Science Advances*, 2019, **5**, eaav3097.

263. M. Ashizawa, Y. Zheng, H. Tran and Z. Bao, *Progress in Polymer Science*, 2020, **100**, 101181.

264. K. Sim, Z. Rao, F. Ershad and C. Yu, *Adv Mater*, 2019, DOI: 10.1002/adma.201902417, e1902417.

265. J. Mun, J. Kang, Y. Zheng, S. Luo, H. C. Wu, N. Matsuhisa, J. Xu, G. J. N. Wang, Y. Yun, G. Xue, J. B. H. Tok and Z. Bao, *Advanced Materials*, 2019, **31**, 1903912.

266. N. Matsuhisa, X. Chen, Z. Bao and T. Someya, *Chemical Society Reviews*, 2019, **48**, 2946-2966.

267. S. E. Root, S. Savagatrup, A. D. Printz, D. Rodriquez and D. J. Lipomi, *Chem. Rev.*, 2017, **117**, 6467.

268. S. Savagatrup, A. S. Makaram, D. J. Burke and D. J. Lipomi, *Advanced Functional Materials*, 2014, **24**, 1169-1181.

269. H.-F. Wen, H.-C. Wu, J. Aimi, C.-C. Hung, Y.-C. Chiang, C.-C. Kuo and W.-C. Chen, *Macromolecules*, 2017, **50**, 4982-4992.

270. J. Xu, H.-C. Wu, C. Zhu, A. Ehrlich, L. Shaw, M. Nikolka, S. Wang, F. Molina-Lopez, X. Gu, S. Luo, D. Zhou, Y.-H. Kim, G.-J. N. Wang, K. Gu, V. R. Feig, S. Chen, Y. Kim, T. Katsumata, Y.-Q. Zheng, H. Yan, J. W. Chung, J. Lopez, B. Murmann and Z. Bao, *Nature Materials*, 2019, **18**, 594-601.

271. J. Xu, S. Wang, G.-J. N. Wang, C. Zhu, S. Luo, L. Jin, X. Gu, S. Chen, V. R. Feig, J. W. F. To, S. Rondeau-Gagné, J. Park, B. C. Schroeder, C. Lu, J. Y. Oh, Y. Wang, Y.-H. Kim, H. Yan, R. Sinclair, D. Zhou, G. Xue, B. Murmann, C. Linder, W. Cai, J. B. H. Tok, J. W. Chung and Z. Bao, *Science*, 2017, **355**, 59-64.

272. J. Mun, G.-J. N. Wang, J. Y. Oh, T. Katsumata, F. L. Lee, J. Kang, H.-C. Wu, F. Lissel, S. Rondeau-Gagné, J. B. H. Tok and Z. Bao, *Advanced Functional Materials*, 2018, **28**, 1804222.

273. J. Y. Oh, S. Rondeau-Gagné, Y.-C. Chiu, A. Chortos, F. Lissel, G.-J. N. Wang, B. C. Schroeder, T. Kurosawa, J. Lopez, T. Katsumata, J. Xu, C. Zhu, X. Gu, W.-G. Bae, Y. Kim, L. Jin, J. W. Chung, J. B. H. Tok and Z. Bao, *Nature*, 2016, **539**, 411-415.

274. G. Mabilleau and A. Sabokbar, in *Degradation Rate of Bioresorbable Materials*, ed. F. Buchanan, Woodhead Publishing, 2008, DOI: https://doi.org/10.1533/9781845695033.3.145, pp. 145-160.

275. A. Steude, M. Jahnel, M. Thomschke, M. Schober and M. C. Gather, *Advanced Materials*, 2015, **27**, 7657-7661.

276. A. Giovannitti, C. B. Nielsen, D.-T. Sbircea, S. Inal, M. Donahue, M. R. Niazi, D. A. Hanifi, A. Amassian, G. G. Malliaras, J. Rivnay and I. McCulloch, *Nature Communications*, 2016, **7**, 13066.

277. A. Giovannitti, K. J. Thorley, C. B. Nielsen, J. Li, M. J. Donahue, G. G. Malliaras, J. Rivnay and I. McCulloch, *Advanced Functional Materials*, 2018, **28**, 1706325.

278. T. Lei, M. Guan, J. Liu, H.-C. Lin, R. Pfattner, L. Shaw, A. F. McGuire, T.-C. Huang, L. Shao, K.-T. Cheng, J. B. H. Tok and Z. Bao, *Proc Natl Acad Sci USA*, 2017, **114**, 5107-5112.

279. Y. Kim, A. Chortos, W. Xu, Y. Liu, J. Y. Oh, D. Son, J. Kang, A. M. Foudeh, C. Zhu, Y. Lee, S. Niu, J. Liu, R. Pfattner, Z. Bao and T.-W. Lee, *Science*, 2018, **360**, 998-1003.

280. F. Molina-Lopez, T. Z. Gao, U. Kraft, C. Zhu, T. Öhlund, R. Pfattner, V. R. Feig, Y. Kim, S. Wang, Y. Yun and Z. Bao, *Nature Communications*, 2019, **10**, 2676.

281. B. C. Schroeder, Y.-C. Chiu, X. Gu, Y. Zhou, J. Xu, J. Lopez, C. Lu, M. F. Toney and Z. Bao, *Adv. Electron. Mater.*, 2016, **2**, 1600104.

282. A. Zen, J. Pflaum, S. Hirschmann, W. Zhuang, F. Jaiser, U. Asawapirom, J. P. Rabe, U. Scherf and D. Neher, *Advanced Functional Materials*, 2004, **14**, 757-764.

283. Y. Fu, N. Wang, A. Yang, H. K.-w. Law, L. Li and F. Yan, *Advanced Materials*, 2017, **29**, 1703787.

284. L. Bai, C. G. Elosegui, W. Li, P. Yu, J. Fei and L. Mao, *Front Chem*, 2019, **7**, 313.

285. R. Giridharagopal, L. Q. Flagg, J. S. Harrison, M. E. Ziffer, J. Onorato, C. K. Luscombe and D. S. Ginger, *Nat Mater*, 2017, **16**, 737-742.

286. M. Magliulo, A. Mallardi, M. Y. Mulla, S. Cotrone, B. R. Pistillo, P. Favia, I. Vikholm-Lundin, G. Palazzo and L. Torsi, *Adv Mater*, 2013, **25**, 2090-2094.

287. F. Buth, D. Kumar, M. Stutzmann and J. A. Garrido, *Applied Physics Letters*, 2011, **98**, 153302.

288. G. Palazzo, D. De Tullio, M. Magliulo, A. Mallardi, F. Intranuovo, M. Y. Mulla, P. Favia, I. Vikholm-Lundin and L. Torsi, *Advanced Materials*, 2015, **27**, 911-916.

289. S. Inal, J. Rivnay, A. O. Suiu, G. G. Malliaras and I. McCulloch, *Accounts of Chemical Research*, 2018, **51**, 1368-1376.

290. A.-M. Pappa, V. F. Curto, M. Braendlein, X. Strakosas, M. J. Donahue, M. Fiocchi, G. G. Malliaras and R. M. Owens, *Advanced Healthcare Materials*, 2016, **5**, 2295-2302.

291. M. Y. Mulla, E. Tuccori, M. Magliulo, G. Lattanzi, G. Palazzo, K. Persaud and L. Torsi, *Nature Communications*, 2015, **6**, 6010.

292. N. Wang, A. Yang, Y. Fu, Y. Li and F. Yan, *Accounts of Chemical Research*, 2019, **52**, 277-287.

293. M. Braendlein, A.-M. Pappa, M. Ferro, A. Lopresti, C. Acquaviva, E. Mamessier, G. G. Malliaras and R. M. Owens, *Advanced Materials*, 2017, **29**, 1605744.

294. A. M. Pappa, D. Ohayon, A. Giovannitti, I. P. Maria, A. Savva, I. Uguz, J. Rivnay, I. McCulloch, R. M. Owens and S. Inal, *Science Advances*, 2018, **4**, eaat0911.

295. A.-M. Pappa, S. Inal, K. Roy, Y. Zhang, C. Pitsalidis, A. Hama, J. Pas, G. G. Malliaras and R. M. Owens, *ACS Appl. Mater. Interfaces*, 2017, **9**, 10427-10434.

296. M. Rabe, D. Verdes and S. Seeger, *Advances in Colloid and Interface Science*, 2011, **162**, 87-106.

297. V. V. Hlady and J. Buijs, *Current Opinion in Biotechnology*, 1996, **7**, 72-77.

298. S. Guo, X. Zhu, M. Li, L. Shi, J. L. T. Ong, D. Jańczewski and K. G. Neoh, *ACS Appl. Mater. Interfaces*, 2016, **8**, 30552-30563.

299. M. Ozboyaci, D. B. Kokh, S. Corni and R. C. Wade, *Quarterly Reviews of Biophysics*, 2016, **49**, e4.

300. Y. Lyu, C. Xie, S. A. Chechetka, E. Miyako and K. Pu, *J. Am. Chem. Soc.*, 2016, **138**, 9049-9052.

301. A. V. Leopold, K. G. Chernov and V. V. Verkhusha, *Chemical Society Reviews*, 2018, **47**, 2454-2484.

302. S. Purohit, C. S. Deepak, N. Rajendran and K. S. Narayan, *Advanced Materials Technologies*, 2019, **4**, 1800564.

303. V. Gautam, M. Bag and K. S. Narayan, *Journal of the American Chemical Society*, 2011, **133**, 17942-17949.

304. V. Gautam, D. Rand, Y. Hanein and K. S. Narayan, *Advanced Materials*, 2014, **26**, 1751-1756.

305. M. Sytnyk, M. Jakešová, M. Litviňuková, O. Mashkov, D. Kriegner, J. Stangl, J. Nebesářová, F. W. Fecher, W. Schöfberger, N. S. Sariciftci, R. Schindl, W. Heiss and E. D. Głowacki, *Nature Communications*, 2017, **8**.

306. S. Park, Y. J. Kang and S. Majd, *Advanced Materials*, 2015, **27**, 7583-7619.

307. G. Lanzani, *Nat Mater*, 2014, **13**, 775-776.

308. J. F. Maya-Vetencourt, D. Ghezzi, M. R. Antognazza, E. Colombo, M. Mete, P. Feyen, A. Desii, A. Buschiazzo, M. Di Paolo, S. Di Marco, F. Ticconi, L. Emionite, D. Shmal, C. Marini, I. Donelli, G. Freddi, R. Maccarone, S. Bisti, G. Sambuceti, G. Pertile, G. Lanzani and F. Benfenati, *Nature Materials*, 2017, **16**, 681-689.

309. D. Ghezzi, M. R. Antognazza, M. Dal Maschio, E. Lanzarini, F. Benfenati and G. Lanzani, *Nature Communications*, 2011, **2**, 166.

310. T. D. Y. Kozai and A. L. Vazquez, *J. Mater. Chem. B*, 2015, **3**, 4965-4978.

311. S. Vaquero, C. Bossio, S. Bellani, N. Martino, E. Zucchetti, G. Lanzani and M. R. Antognazza, *J. Mater. Chem. B*, 2016, **4**, 5272-5283.

312. S. B. Srivastava, R. Melikov, M. M. Aria, U. M. Dikbas, I. H. Kavakli and S. Nizamoglu, *Phys. Rev. Applied*, 2019, **11**, 044012.

313. F. Lodola, V. Vurro, S. Crasto, E. Di Pasquale and G. Lanzani, *Advanced Healthcare Materials*, 2019, **8**, 1900198.

314. C. Bossio, I. Abdel Aziz, G. Tullii, E. Zucchetti, D. Debellis, M. Zangoli, F. Di Maria, G. Lanzani and M. R. Antognazza, *Front. Bioeng. Biotechnol.*, 2018, **6**, 114.

315. C. Tortiglione, M. R. Antognazza, A. Tino, C. Bossio, V. Marchesano, A. Bauduin, M. Zangoli, S. V. Morata and G. Lanzani, *Science Advances*, 2017, **3**, e1601699.

316. D. Rand, M. Jakešová, G. Lubin, I. Vėbraitė, M. David-Pur, V. Đerek, T. Cramer, N. S. Sariciftci, Y. Hanein and E. D. Głowacki, *Advanced Materials*, 2018, **30**, 1707292.

317. M. Jakešová, M. Silverå Ejneby, V. Đerek, T. Schmidt, M. Gryszel, J. Brask, R. Schindl, D. T. Simon, M. Berggren, F. Elinder and E. D. Głowacki, *Science Advances*, 2019, **5**, eaav5265.

318. O. S. Abdullaeva, F. Balzer, M. Schulz, J. Parisi, A. Lützen, K. Dedek and M. Schiek, *Advanced Functional Materials*, 2019, **29**, 1805177.

319. Z. Chen, S. N. Obaid and L. Lu, *Opt. Mater. Express*, 2019, **9**, 3843.

320. A. Sridharan, A. Shah, S. S. Kumar, J. Kyeh, J. Smith, J. Blain-Christen and J. Muthuswamy, *Biomed. Phys. Eng. Express*, 2020, **6**, 025003.

321. S. Park, S. W. Heo, W. Lee, D. Inoue, Z. Jiang, K. Yu, H. Jinno, D. Hashizume, M. Sekino and T. Yokota, *Nature*, 2018, **561**, 516.

322. S. Park, S. W. Heo, W. Lee, D. Inoue, Z. Jiang, K. Yu, H. Jinno, D. Hashizume, M. Sekino, T. Yokota, K. Fukuda, K. Tajima and T. Someya, *Nature*, 2018, **561**, 516-521.

323. H. Jinno, K. Fukuda, X. Xu, S. Park, Y. Suzuki, M. Koizumi, T. Yokota, I. Osaka, K. Takimiya and T. Someya, *Nat Energy*, 2017, **2**, 780-785.

324. A. Steude, E. C. Witts, G. B. Miles and M. C. Gather, *Science Advances*, 2016, **2**, e1600061.

325. H. Lee, E. Kim, Y. Lee, H. Kim, J. Lee, M. Kim, H.-J. Yoo and S. Yoo, *Science Advances*, 2018, **4**, eaas9530.

326. Y. Khan, D. Han, A. Pierre, J. Ting, X. Wang, C. M. Lochner, G. Bovo, N. Yaacobi-Gross, C. Newsome and R. Wilson, *Proc. Natl. Acad. Sci. U. S. A.*, 2018, **115**, E11015.

327. A. Morton, C. Murawski, S. R. Pulver and M. C. Gather, *Sci Rep*, 2016, **6**, 31117.

328. B. F. E. Matarèse, P. L. C. Feyen, J. C. de Mello and F. Benfenati, *Front. Bioeng. Biotechnol.*, 2019, **7**, 278.

329. M. D. Dickey, *Adv. Mater.*, 2017, **29**, 1606425.

330. J. Yang, W. Cheng and K. Kalantar-zadeh, *Proceedings of the IEEE*, 2019, **107**, 2168-2184.

331. S. Negi, R. Bhandari and F. Solzbacher, 2012.

332. R. M. Iost and F. N. Crespilho, *Biosensors and Bioelectronics*, 2012, **31**, 1-10.

333. G. Chen, M. Gatti and M. M. Cheng, 2019.

334.   M. Cai, H. Huang, X. Zuo, H. Ding and N. Stanford, *Materials Science and Technology*, 2020, **36**, 584-597.

335.   E. Guerrero, A. Polednik, M. Ecker, A. Joshi-Imre, W. Choi, G. Gutierrez-Heredia, W. E. Voit and J. Maeng, *Adv. Electron. Mater.*, 2020, **6**, 1901210.

336.   Y.-G. Park, H. Min, H. Kim, A. Zhexembekova, C. Y. Lee and J.-U. Park, *Nano Letters*, 2019, **19**, 4866-4872.

337.   I. R. Minev, P. Musienko, A. Hirsch, Q. Barraud, N. Wenger, E. M. Moraud, J. Gandar, M. Capogrosso, T. Milekovic, L. Asboth, R. F. Torres, N. Vachicouras, Q. Liu, N. Pavlova, S. Duis, A. Larmagnac, J. Voros, S. Micera, Z. Suo, G. Courtine and S. P. Lacour, *Science*, 2015, **347**, 159-163.

338.   T. N. H. Nguyen, J. K. Nolan, H. Park, S. Lam, M. Fattah, J. C. Page, H. E. Joe, M. B. G. Jun, H. Lee, S. J. Kim, R. Shi and H. Lee, *Biosens Bioelectron*, 2019, **131**, 257-266.

339.   L. Lipani, B. G. R. Dupont, F. Doungmene, F. Marken, R. M. Tyrrell, R. H. Guy and A. Ilie, *Nat Nanotechnol*, 2018, **13**, 504-511.

340.   B. Akkaya, B. Çakiroğlu and M. Özacar, *ACS Sustainable Chemistry & Engineering*, 2018, **6**, 3805-3814.

341.   T. L. Rose and L. S. Robblee, *IEEE Transactions on Biomedical Engineering*, 1990, **37**, 1118-1120.

342.   K. Wang, C. L. Frewin, D. Esrafilzadeh, C. Yu, C. Wang, J. J. Pancrazio, M. Romero-Ortega, R. Jalili and G. Wallace, *Adv Mater*, 2019, **31**, e1805867.

343.   J. Liu, T. M. Fu, Z. G. Cheng, G. S. Hong, T. Zhou, L. H. Jin, M. Duvvuri, Z. Jiang, P. Kruskal, C. Xie, Z. G. Suo, Y. Fang and C. M. Lieber, *Nature Nanotechnology*, 2015, **10**, 629-+.

344.   X. Yang, T. Zhou, T. J. Zwang, G. Hong, Y. Zhao, R. D. Viveros, T.-M. Fu, T. Gao and C. M. Lieber, *Nature Materials*, 2019, **18**, 510-517.

345.   C. Xie, Z. Lin, L. Hanson, Y. Cui and B. Cui, *Nature Nanotechnology*, 2012, **7**, 185-190.

346.   J. Abbott, T. Ye, K. Krenek, R. S. Gertner, S. Ban, Y. Kim, L. Qin, W. Wu, H. Park and D. Ham, *Nature Biomedical Engineering*, 2020, **4**, 232-241.

347.   S. G. Higgins, M. Becce, A. Belessiotis-Richards, H. Seong, J. E. Sero and M. M. Stevens, *Adv Mater*, 2020, **32**, e1903862.

348.   L. Liu, E. Pippel, R. Scholz and U. Gosele, *Nano Lett*, 2009, **9**, 4352-4358.

349.   C. Li, T. Sato and Y. Yamauchi, *Angew Chem Int Ed Engl*, 2013, **52**, 8050-8053.

350.   H. Li, A. Misra, J. K. Baldwin and S. T. Picraux, *Applied Physics Letters*, 2009, **95**, 201902.

351.   J.-L. Shui, J.-W. Zhang and J. C. M. Li, *Journal of Materials Chemistry*, 2011, **21**, 6225-6229.

352.   M. Ganji, A. C. Paulk, J. C. Yang, N. W. Vahidi, S. H. Lee, R. Liu, L. Hossain, E. M. Arneodo, M. Thunemann, M. Shigyo, A. Tanaka, S. B. Ryu, S. W. Lee, Y. Tchoe, M. Marsala, A. Devor, D. R. Cleary, J. R. Martin, H. Oh, V. Gilja, T. Q. Gentner, S. I. Fried, E. Halgren, S. S. Cash and S. A. Dayeh, *Nano Letters*, 2019, **19**, 6244-6254.

353.   A. Fendyur, N. Mazurski, J. Shappir and M. E. Spira, *Front Neuroeng*, 2011, **4**, 14.

354.   V. Gaillet, A. Cutrone, F. Artoni, P. Vagni, A. Mega Pratiwi, S. A. Romero, D. Lipucci Di Paola, S. Micera and D. Ghezzi, *Nature Biomedical Engineering*, 2020, **4**, 181-194.

355.   A. Miyamoto, S. Lee, N. F. Cooray, S. Lee, M. Mori, N. Matsuhisa, H. Jin, L. Yoda, T. Yokota, A. Itoh, M. Sekino, H. Kawasaki, T. Ebihara, M. Amagai and T. Someya, *Nat Nanotechnol*, 2017, **12**, 907-913.

356.   M. Dipalo, H. Amin, L. Lovato, F. Moia, V. Caprettini, G. C. Messina, F. Tantussi, L. Berdondini and F. De Angelis, *Nano Lett*, 2017, **17**, 3932-3939.

357. M. Kang, S. Jung, H. Zhang, T. Kang, H. Kang, Y. Yoo, J. P. Hong, J. P. Ahn, J. Kwak, D. Jeon, N. A. Kotov and B. Kim, *ACS Nano*, 2014, **8**, 8182-8189.

358. S. Choi, S. I. Han, D. Jung, H. J. Hwang, C. Lim, S. Bae, O. K. Park, C. M. Tschabrunn, M. Lee, S. Y. Bae, J. W. Yu, J. H. Ryu, S.-W. Lee, K. Park, P. M. Kang, W. B. Lee, R. Nezafat, T. Hyeon and D.-H. Kim, *Nature Nanotechnology*, 2018, **13**, 1048-1056.

359. W. H. Zimmermann, I. Melnychenko, G. Wasmeier, M. Didie, H. Naito, U. Nixdorff, A. Hess, L. Budinsky, K. Brune, B. Michaelis, S. Dhein, A. Schwoerer, H. Ehmke and T. Eschenhagen, *Nat Med*, 2006, **12**, 452-458.

360. J. Leor, S. Aboulafia-Etzion, A. Dar, L. Shapiro, M. Barbash Israel, A. Battler, Y. Granot and S. Cohen, *Circulation*, 2000, **102**, Iii-56-Iii-61.

361. T. Dvir, A. Kedem, E. Ruvinov, O. Levy, I. Freeman, N. Landa, R. Holbova, M. S. Feinberg, S. Dror, Y. Etzion, J. Leor and S. Cohen, *Proc Natl Acad Sci U S A*, 2009, **106**, 14990-14995.

362. S. Lee, D. Sasaki, D. Kim, M. Mori, T. Yokota, H. Lee, S. Park, K. Fukuda, M. Sekino, K. Matsuura, T. Shimizu and T. Someya, *Nature Nanotechnology*, 2019, **14**, 156-160.

363. G. Eng, B. W. Lee, L. Protas, M. Gagliardi, K. Brown, R. S. Kass, G. Keller, R. B. Robinson and G. Vunjak-Novakovic, *Nature Communications*, 2016, **7**, 10312.

364. T. Dvir, B. P. Timko, M. D. Brigham, S. R. Naik, S. S. Karajanagi, O. Levy, H. Jin, K. K. Parker, R. Langer and D. S. Kohane, *Nature Nanotechnology*, 2011, **6**, 720-725.

365. S. Yoo, R. Kim, J. H. Park and Y. Nam, *ACS Nano*, 2016, **10**, 4274-4281.

366. S. Yoo, J. H. Park and Y. Nam, *ACS Nano*, 2019, **13**, 544-551.

367. Y. C. Yeh, B. Creran and V. M. Rotello, *Nanoscale*, 2012, **4**, 1871-1880.

368. Y. Lu, J. Y. Huang, C. Wang, S. Sun and J. Lou, *Nature Nanotechnology*, 2010, **5**, 218-224.

369. M. E. Spira, D. Kamber, A. Dormann, A. Cohen, C. Bartic, G. Borghs, J. P. M. Langedijk, S. Yitzchaik, K. Shabthai and J. Shappir, 2007.

370. O. Staufer, S. Weber, C. P. Bengtson, H. Bading, A. Rustom and J. P. Spatz, *Nano Lett*, 2019, **19**, 3244-3255.

371. H. Amin, M. Dipalo, F. De Angelis and L. Berdondini, *ACS Appl Mater Interfaces*, 2018, **10**, 15207-15215.

372. J. Das, I. Ivanov, L. Montermini, J. Rak, E. H. Sargent and S. O. Kelley, *Nature Chemistry*, 2015, **7**, 569-575.

373. R. A. Sperling and W. J. Parak, *Philos Trans A Math Phys Eng Sci*, 2010, **368**, 1333-1383.

374. M. Khongkow, T. Yata, S. Boonrungsiman, U. R. Ruktanonchai, D. Graham and K. Namdee, *Sci Rep*, 2019, **9**, 8278.

375. B. P. Mugaka, Y. Hu, Y. Ma and Y. Ding, 2019, DOI: 10.1007/978-3-030-06115-9_20, pp. 391-403.

376. X. Wen, B. Wang, S. Huang, T. L. Liu, M. S. Lee, P. S. Chung, Y. T. Chow, I. W. Huang, H. G. Monbouquette, N. T. Maidment and P. Y. Chiou, *Biosens Bioelectron*, 2019, **131**, 37-45.

377. H. J. Koo, J. H. So, M. D. Dickey and O. D. Velev, *Adv Mater*, 2011, **23**, 3559-3564.

378. T. Kim, D. M. Kim, B. J. Lee and J. Lee, *Sensors (Basel)*, 2019, **19**.

379. J. H. Kim, S. Kim, J. H. So, K. Kim and H. J. Koo, *ACS Appl. Mater. Interfaces*, 2018, **10**, 17448.

380. J. Wang, K. Appusamy, S. Guruswamy and A. Nahata, *Sci Rep*, 2015, **5**, 8637.

381. M. R. Khan, J. Bell and M. D. Dickey, *Advanced Materials Interfaces*, 2016, **3**, 1600546.

382. R. C. Gough, J. H. Dang, M. R. Moorefield, G. B. Zhang, L. H. Hihara, W. A. Shiroma and A. T. Ohta, *ACS Appl Mater Interfaces*, 2016, **8**, 6-10.

383. I. D. Joshipura, H. R. Ayers, C. Majidi and M. D. Dickey, *J. Mater. Chem. C*, 2015, **3**, 3834-3841.

384. M. G. Kim, D. K. Brown and O. Brand, *Nat Commun*, 2020, **11**, 1002.

385. Y. Lin, Y. Liu, J. Genzer and M. D. Dickey, *Chemical Science*, 2017, **8**, 3832-3837.

386. M. Liao, H. Liao, J. Ye, P. Wan and L. Zhang, *ACS Appl Mater Interfaces*, 2019, **11**, 47358-47364.

387. E. J. Markvicka, M. D. Bartlett, X. Huang and C. Majidi, *Nature Materials*, 2018, **17**, 618-624.

388. T. Daeneke, K. Khoshmanesh, N. Mahmood, I. A. de Castro, D. Esrafilzadeh, S. J. Barrow, M. D. Dickey and K. Kalantar-Zadeh, *Chem Soc Rev*, 2018, **47**, 4073-4111.

389. Y. Yang, S. Ding, T. Araki, J. Jiu, T. Sugahara, J. Wang, J. Vanfleteren, T. Sekitani and K. Suganuma, *Nano Research*, 2016, **9**, 401-414.

390. H. J. Kim, K. Sim, A. Thukral and C. Yu, *Sci Adv*, 2017, **3**, e1701114.

391. N. Matsuhisa, M. Kaltenbrunner, T. Yokota, H. Jinno, K. Kuribara, T. Sekitani and T. Someya, *Nature Communications*, 2015, **6**, 7461.

392. N. Matsuhisa, D. Inoue, P. Zalar, H. Jin, Y. Matsuba, A. Itoh, T. Yokota, D. Hashizume and T. Someya, *Nature Materials*, 2017, **16**, 834-840.

393. D. A. Schwarz, M. A. Lebedev, T. L. Hanson, D. F. Dimitrov, G. Lehew, J. Meloy, S. Rajangam, V. Subramanian, P. J. Ifft, Z. Li, A. Ramakrishnan, A. Tate, K. Z. Zhuang and M. A. Nicolelis, *Nat Methods*, 2014, **11**, 670-676.

394. S. J. Chockattu, D. B. Suryakant and S. Thakur, *Restor Dent Endod*, 2018, **43**, e39.

395. S. Bussmann, R. Luechinger, J. M. Froehlich, C. von Weymarn, C. Reischauer, D. M. Koh and A. Gutzeit, *PLoS One*, 2018, **13**, e0204220.

396. J. Camakaris, I. Voskoboinik and J. F. Mercer, *Biochemical and Biophysical Research Communications*, 1999, **261**, 225-232.

397. P. B. Tchounwou, C. Newsome, J. Williams and K. Glass, *Met Ions Biol Med*, 2008, **10**, 285-290.

398. Z. Huang, Y. Hao, Y. Li, H. Hu, C. Wang, A. Nomoto, T. Pan, Y. Gu, Y. Chen, T. Zhang, W. Li, Y. Lei, N. Kim, C. Wang, L. Zhang, J. W. Ward, A. Maralani, X. Li, M. F. Durstock, A. Pisano, Y. Lin and S. Xu, *Nature Electronics*, 2018, **1**, 473-480.

399. C. Wang, X. Li, H. Hu, L. Zhang, Z. Huang, M. Lin, Z. Zhang, Z. Yin, B. Huang, H. Gong, S. Bhaskaran, Y. Gu, M. Makihata, Y. Guo, Y. Lei, Y. Chen, C. Wang, Y. Li, T. Zhang, Z. Chen, A. P. Pisano, L. Zhang, Q. Zhou and S. Xu, *Nat Biomed Eng*, 2018, **2**, 687-695.

400. S. K. Rastogi, A. Kalmykov, N. Johnson and T. Cohen-Karni, *J. Mater. Chem. B*, 2018, **6**, 7159-7178.

401. E. Masvidal-Codina, X. Illa, M. Dasilva, A. B. Calia, T. Dragojević, E. E. Vidal-Rosas, E. Prats-Alfonso, J. Martínez-Aguilar, J. M. De la Cruz, R. Garcia-Cortadella, P. Godignon, G. Rius, A. Camassa, E. Del Corro, J. Bousquet, C. Hébert, T. Durduran, R. Villa, M. V. Sanchez-Vives, J. A. Garrido and A. Guimerà-Brunet, *Nature Materials*, 2019, **18**, 280-288.

402. S. Zhao, X. Liu, Z. Xu, H. Ren, B. Deng, M. Tang, L. Lu, X. Fu, H. Peng, Z. Liu and X. Duan, *Nano Letters*, 2016, **16**, 7731-7738.

403. Z. Yang, J. Tian, Z. Yin, C. Cui, W. Qian and F. Wei, *Carbon*, 2019, **141**, 467-480.

404. H. Lee, T. K. Choi, Y. B. Lee, H. R. Cho, R. Ghaffari, L. Wang, H. J. Choi, T. D. Chung, N. Lu, T. Hyeon, S. H. Choi and D. H. Kim, *Nat Nanotechnol*, 2016, **11**, 566-572.

405. N. T. N. Phan, X. Li and A. G. Ewing, *Nature Reviews Chemistry*, 2017, **1**, 0048.

406.   L. Ren, M. D. Pour, S. Majdi, X. Li, P. Malmberg and A. G. Ewing, *Angew Chem Int Ed Engl*, 2017, **56**, 4970-4975.

407.   J. G. Roberts, E. C. Mitchell, L. E. Dunaway, G. S. McCarty and L. A. Sombers, *ACS Nano*, 2020, **14**, 2917-2926.

408.   X. Li, S. Majdi, J. Dunevall, H. Fathali and A. G. Ewing, *Angew Chem Int Ed Engl*, 2015, **54**, 11978-11982.

409.   S. Majdi, E. C. Berglund, J. Dunevall, A. I. Oleinick, C. Amatore, D. E. Krantz and A. G. Ewing, *Angew Chem Int Ed Engl*, 2015, **54**, 13609-13612.

410.   K. S. Novoselov, *Science*, 2004, **306**, 666-669.

411.   A. Bendali, L. H. Hess, M. Seifert, V. Forster, A.-F. Stephan, J. A. Garrido and S. Picaud, *Advanced Healthcare Materials*, 2013, **2**, 929-933.

412.   N. Li, X. Zhang, Q. Song, R. Su, Q. Zhang, T. Kong, L. Liu, G. Jin, M. Tang and G. Cheng, *Biomaterials*, 2011, **32**, 9374-9382.

413.   T. Bouzid, A. Sinitskii and J. Y. Lim, *Neural Regen Res*, 2016, **11**, 894-895.

414.   K. S. Novoselov, V. I. Fal'ko, L. Colombo, P. R. Gellert, M. G. Schwab and K. Kim, *Nature*, 2012, **490**, 192-200.

415.   N. Chen, L. Tian, A. C. Patil, S. Peng, I. H. Yang, N. V. Thakor and S. Ramakrishna, *Nano Today*, 2017, **14**, 59-83.

416.   A. Fabbro, D. Scaini, V. León, E. Vázquez, G. Cellot, G. Privitera, L. Lombardi, F. Torrisi, F. Tomarchio, F. Bonaccorso, S. Bosi, A. C. Ferrari, L. Ballerini and M. Prato, *ACS Nano*, 2016, **10**, 615-623.

417.   A. Bourrier, P. Shkorbatova, M. Bonizzato, E. Rey, Q. Barraud, G. Courtine, R. Othmen, V. Reita, V. Bouchiat and C. Delacour, *Adv Healthc Mater*, 2019, **8**, e1801331.

418.   H. P. Bei, Y. Yang, Q. Zhang, Y. Tian, X. Luo, M. Yang and X. Zhao, *Molecules*, 2019, **24**.

419.   C.-H. Chen, C.-T. Lin, W.-L. Hsu, Y.-C. Chang, S.-R. Yeh, L.-J. Li and D.-J. Yao, *Nanomedicine: Nanotechnology, Biology and Medicine*, 2013, **9**, 600-604.

420.   K. Zhou, G. A. Thouas, C. C. Bernard, D. R. Nisbet, D. I. Finkelstein, D. Li and J. S. Forsythe, *ACS Appl. Mater. Interfaces*, 2012, **4**, 4524-4531.

421.   N. Li, Q. Zhang, S. Gao, Q. Song, R. Huang, L. Wang, L. Liu, J. Dai, M. Tang and G. Cheng, *Sci Rep*, 2013, **3**.

422.   X. Liu, Y. Lu and D. Kuzum, *Sci Rep*, 2018, **8**.

423.   Y. Lu, H. Lyu, A. G. Richardson, T. H. Lucas and D. Kuzum, *Sci Rep*, 2016, **6**.

424.   D. Kuzum, H. Takano, E. Shim, J. C. Reed, H. Juul, A. G. Richardson, J. de Vries, H. Bink, M. A. Dichter, T. H. Lucas, D. A. Coulter, E. Cubukcu and B. Litt, *Nature Communications*, 2014, **5**.

425.   D.-W. Park, J. P. Ness, S. K. Brodnick, C. Esquibel, J. Novello, F. Atry, D.-H. Baek, H. Kim, J. Bong, K. I. Swanson, A. J. Suminski, K. J. Otto, R. Pashaie, J. C. Williams and Z. Ma, *ACS Nano*, 2018, **12**, 148-157.

426.   D. W. Park, A. A. Schendel, S. Mikael, S. K. Brodnick, T. J. Richner, J. P. Ness, M. R. Hayat, F. Atry, S. T. Frye, R. Pashaie, S. Thongpang, Z. Ma and J. C. Williams, *Nat Commun*, 2014, **5**, 5258.

427.   R. Yin, Z. Xu, M. Mei, Z. Chen, K. Wang, Y. Liu, T. Tang, M. K. Priydarshi, X. Meng, S. Zhao, B. Deng, H. Peng, Z. Liu and X. Duan, *Nature Communications*, 2018, **9**.

428.   S. Lee, I. Jo, S. Kang, B. Jang, J. Moon, J. B. Park, S. Lee, S. Rho, Y. Kim and B. H. Hong, *ACS Nano*, 2017, **11**, 5318-5324.

429.   J. Park, J. Kim, S.-Y. Kim, W. H. Cheong, J. Jang, Y.-G. Park, K. Na, Y.-T. Kim, J. H. Heo, C. Y. Lee, J. H. Lee, F. Bien and J.-U. Park, *Science Advances*, 2018, **4**, eaap9841.

430.   J. Kim, M. Kim, M.-S. Lee, K. Kim, S. Ji, Y.-T. Kim, J. Park, K. Na, K.-H. Bae, H. Kyun Kim, F. Bien, C. Young Lee and J.-U. Park, *Nature Communications*, 2017, **8**, 14997.

431.   A. Savchenko, V. Cherkas, C. Liu, G. B. Braun, A. Kleschevnikov, Y. I. Miller and E. Molokanova, *Science Advances*, 2018, **4**, eaat0351.

432.   V. Lovat, D. Pantarotto, L. Lagostena, B. Cacciari, M. Grandolfo, M. Righi, G. Spalluto, M. Prato and L. Ballerini, *Nano Letters*, 2005, **5**, 1107-1110.

433.   G. Cellot, E. Cilia, S. Cipollone, V. Rancic, A. Sucapane, S. Giordani, L. Gambazzi, H. Markram, M. Grandolfo, D. Scaini, F. Gelain, L. Casalis, M. Prato, M. Giugliano and L. Ballerini, *Nature Nanotechnology*, 2009, **4**, 126-133.

434.   M. Barrejón, R. Rauti, L. Ballerini and M. Prato, *ACS Nano*, 2019, **13**, 8879-8889.

435.   F. Vitale, S. R. Summerson, B. Aazhang, C. Kemere and M. Pasquali, *ACS Nano*, 2015, **9**, 4465-4474.

436.   C. Zhu, A. Chortos, Y. Wang, R. Pfattner, T. Lei, A. C. Hinckley, I. Pochorovski, X. Yan, J. W. F. To, J. Y. Oh, J. B. H. Tok, Z. Bao and B. Murmann, *Nature Electronics*, 2018, **1**, 183-190.

437.   K. Sim, Z. Rao, H. J. Kim, A. Thukral, H. Shim and C. Yu, *Sci Adv*, 2019, **5**, eaav5749.

438.   H. Wang, B. Zhu, W. Jiang, Y. Yang, W. R. Leow, H. Wang and X. Chen, *Adv Mater*, 2014, **26**, 3638-3643.

439.   D. Son, J. Kang, O. Vardoulis, Y. Kim, N. Matsuhisa, J. Y. Oh, J. W. To, J. Mun, T. Katsumata, Y. Liu, A. F. McGuire, M. Krason, F. Molina-Lopez, J. Ham, U. Kraft, Y. Lee, Y. Yun, J. B. Tok and Z. Bao, *Nat Nanotechnol*, 2018, **13**, 1057-1065.

440.   L. Lu, X. Fu, Y. Liew, Y. Zhang, S. Zhao, Z. Xu, J. Zhao, D. Li, Q. Li, G. B. Stanley and X. Duan, *Nano Letters*, 2019, **19**, 1577-1586.

441.   R. Rauti, M. Medelin, L. Newman, S. Vranic, G. Reina, A. Bianco, M. Prato, K. Kostarelos and L. Ballerini, *Nano Letters*, 2019, DOI: 10.1021/acs.nanolett.8b04903.

442.   Q. Zhang, J. Xu, Q. Song, N. Li, Z. Zhang, K. Li, Y. Du, L. Wu, M. Tang, L. Liu, G. Cheng and J. Liu, *J. Mater. Chem. B*, 2014, **2**, 4331-4337.

443.   N. I. Zaaba, K. L. Foo, U. Hashim, S. J. Tan, W.-W. Liu and C. H. Voon, *Procedia Engineering*, 2017, **184**, 469-477.

444.   J. Chen, B. Yao, C. Li and G. Shi, *Carbon*, 2013, **64**, 225-229.

445.   Z. C. Lin, C. Xie, Y. Osakada, Y. Cui and B. Cui, *Nat Commun*, 2014, **5**, 3206.

446.   B. Anasori, M. R. Lukatskaya and Y. Gogotsi, *Nature Reviews Materials*, 2017, **2**, 16098.

447.   N. Driscoll, A. G. Richardson, K. Maleski, B. Anasori, O. Adewole, P. Lelyukh, L. Escobedo, D. K. Cullen, T. H. Lucas, Y. Gogotsi and F. Vitale, *ACS Nano*, 2018, **12**, 10419-10429.

448.   K. Feron, R. Lim, C. Sherwood, A. Keynes, A. Brichta and P. C. Dastoor, *Int J Mol Sci*, 2018, **19**.

449.   C. Yang and Z. Suo, *Nature Reviews Materials*, 2018, **3**, 125-142.

450.   A. G. MacDiarmid and A. J. Epstein, *Makromolekulare Chemie. Macromolecular Symposia*, 1991, **51**, 11-28.

451.   K. Fidanovski and D. Mawad, *Advanced Healthcare Materials*, 2019, **8**, 1-9.

452.   Y. Wen and J. Xu, *Journal of Polymer Science, Part A: Polymer Chemistry*, 2017, **55**, 1121-1150.

453.   J. Huang, P. F. Miller, J. S. Wilson, A. J. de Mello, J. C. de Mello and D. D. C. Bradley, *Advanced Functional Materials*, 2005, **15**, 290-296.

454.   Y. Wang, C. Zhu, R. Pfattner, H. Yan, L. Jin, S. Chen, F. Molina-Lopez, F. Lissel, J. Liu, N. I. Rabiah, Z. Chen, J. W. Chung, C. Linder, M. F. Toney, B. Murmann and Z. Bao, *Science Advances*, 2017, **3**, e1602076.

455.   J. Goding, A. Gilmour, P. Martens, L. Poole-Warren and R. Green, *Advanced Healthcare Materials*, 2017, **6**.

456.   Y. Y. Lee, H. Y. Kang, S. H. Gwon, G. M. Choi, S. M. Lim, J. Y. Sun and Y. C. Joo, *Advanced Materials*, 2016, **28**, 1636-1643.

457.   V. R. Feig, H. Tran, M. Lee and Z. Bao, *Nature Communications*, 2018, **9**, 1-9.

458.   C. Yeon, G. Kim, J. W. Lim and S. J. Yun, *RSC Advances*, 2017, **7**, 5888-5897.

459.   L. Yin, Z. Zhao, F. Jiang, Z. Li, S. Xiong and Y. Zhou, *Organic Electronics*, 2014, **15**, 2593-2598.

460.   N. Kim, H. Kang, J. H. Lee, S. Kee, S. H. Lee and K. Lee, *Advanced Materials*, 2015, **27**, 2317-2323.

461.   X. Fan, B. Xu, S. Liu, C. Cui, J. Wang and F. Yan, *ACS Applied Materials and Interfaces*, 2016, **8**, 14029-14036.

462.   S. Zhang, H. Ling, Y. Chen, Q. Cui, J. Ni, X. Wang, M. C. Hartel, X. Meng, K. J. Lee, J. Lee, W. Sun, H. Lin, S. Emaminejad, S. Ahadian, N. Ashammakhi, M. R. Dokmeci and A. Khademhosseini, *Advanced Functional Materials*, 2020, **30**, 1-8.

463.   E. Cuttaz, J. Goding, C. Vallejo-Giraldo, U. Aregueta-Robles, N. Lovell, D. Ghezzi and R. A. Green, *Biomater Sci*, 2019, **7**, 1372-1385.

464.   D. Iandolo, A. Ravichandran, X. Liu, F. Wen, J. K. Y. Chan, M. Berggren, S.-H. Teoh and D. T. Simon, *Advanced Healthcare Materials*, 2016, **5**, 1505-1512.

465.   Y. Wang, C. Zhu, R. Pfattner, H. Yan, L. Jin, S. Chen, F. Molina-Lopez, F. Lissel, J. Liu, N. I. Rabiah, Z. Chen, J. W. Chung, C. Linder, M. F. Toney, B. Murmann and Z. Bao, *Sci Adv*, 2017, **3**, e1602076.

466.   H. He, L. Zhang, X. Guan, H. Cheng, X. Liu, S. Yu, J. Wei and J. Ouyang, *ACS Appl. Mater. Interfaces*, 2019, **11**, 26185-26193.

467.   B. Lu, H. Yuk, S. Lin, N. Jian, K. Qu, J. Xu and X. Zhao, *Nature Communications*, 2019, **10**.

468.   D. Gan, Z. Huang, X. Wang, L. Jiang, C. Wang, M. Zhu, F. Ren, L. Fang, K. Wang, C. Xie and X. Lu, *Advanced Functional Materials*, 2020, **30**, 1-10.

469.   C. Cea, G. D. Spyropoulos, P. Jastrzebska-Perfect, J. J. Ferrero, J. N. Gelinas and D. Khodagholy, *Nat Mater*, 2020, DOI: 10.1038/s41563-020-0638-3.

470.   S. Hara, T. Zama, W. Takashima and K. Kaneto, *Polymer Journal*, 2004, **36**, 151-161.

471.   A. T. Cullen and A. D. Price, *Synthetic Metals*, 2018, **235**, 34-41.

472.   M. Carlotti and V. Mattoli, *Small*, 2019, **15**, 1-22.

473.   J. Stejskal, M. Trchová, P. Bober, Z. Morávková, D. Kopecký, M. Vrňata, J. Prokeš, M. Varga and E. Watzlová, *RSC Advances*, 2016, **6**, 88382-88391.

474.   I. Sapurina, Y. Li, E. Alekseeva, P. Bober, M. Trchová, Z. Morávková and J. Stejskal, *Polymer*, 2017, **113**, 247-258.

475.   R. Texidó, A. Orgaz, V. Ramos-Pérez and S. Borrós, *Materials Science and Engineering C*, 2017, **76**, 295-300.

476.   S. Kim, Y. Jang, M. Jang, A. Lim, J. G. Hardy, H. S. Park and J. Y. Lee, *Acta Biomaterialia*, 2018, **80**, 258-268.

477.   C. W. Tsao, X. C. Guo and W. W. Hu, *RSC Advances*, 2016, **6**, 113344-113351.

478.   L. Han, L. Yan, M. Wang, K. Wang, L. Fang, J. Zhou, J. Fang, F. Ren and X. Lu, *Chemistry of Materials*, 2018, **30**, 5561-5572.

479.   L. K. Jang, S. Kim, J. Seo and J. Young Lee, *Biofabrication*, 2017, **9**.

480.   M. Golabi, L. Padiolleau, X. Chen, M. J. Jafari, E. Sheikhzadeh, A. P. F. Turner, E. W. H. Jager and V. Beni, *PLoS ONE*, 2016, **11**, 1-20.

481.   M. Golabi, A. P. F. Turner and E. W. H. Jager, *Sensors and Actuators, B: Chemical*, 2016, **222**, 839-848.

482.   Y. Wei, X. Mo, P. Zhang, Y. Li, J. Liao, Y. Li, J. Zhang, C. Ning, S. Wang, X. Deng and L. Jiang, *ACS Nano*, 2017, **11**, 5915-5924.

483.   L. Zhou, L. Fan, X. Yi, Z. Zhou, C. Liu, R. Fu, C. Dai, Z. Wang, X. Chen, P. Yu, D. Chen, G. Tan, Q. Wang and C. Ning, *ACS Nano*, 2018, **12**, 10957-10967.

484.   B. Zhang, P. J. Molino, A. R. Harris, Z. Yue, S. E. Moulton and G. G. Wallace, *J. Mater. Chem. B*, 2016, **4**, 2570-2577.

485.   M. B. González, L. I. Brugnoni and S. B. Saidman, *Materials Today Communications*, 2019, **18**, 119-123.

486.   M. Antensteiner, M. Khorrami, F. Fallahianbijan, A. Borhan and M. R. Abidian, *Advanced Materials*, 2017, **29**, 1-11.

487.   P. Humpolicek, V. Kasparkova, P. Saha and J. Stejskal, *Synthetic Metals*, 2012, **162**, 722-727.

488.   P. Humpolíček, K. A. Radaszkiewicz, V. Kašpárková, J. Stejskal, M. Trchová, Z. Kuceková, H. Vičarová, J. Pacherník, M. Lehocký and A. Minařík, *RSC Advances*, 2015, **5**, 68796-68805.

489.   R. L. Razalli, M. M. Abdi, P. M. Tahir, A. Moradbak, Y. Sulaiman and L. Y. Heng, *RSC Advances*, 2017, **7**, 25191-25198.

490.   D. Y. Liu, G. X. Sui and D. Bhattacharyya, *Composites Science and Technology*, 2014, **99**, 31-36.

491.   Y. Wu, Y. X. Chen, J. Yan, D. Quinn, P. Dong, S. W. Sawyer and P. Soman, *Acta Biomaterialia*, 2016, **33**, 122-130.

492.   D. Mawad, C. Mansfield, A. Lauto, F. Perbellini, G. W. Nelson, J. Tonkin, S. O. Bello, D. J. Carrad, A. P. Micolich, M. M. Mahat, J. Furman, D. J. Payne, A. R. Lyon, J. J. Gooding, S. E. Harding, C. M. Terracciano and M. M. Stevens, *Science Advances*, 2016, **2**.

493.   C. Cui, N. Faraji, A. Lauto, L. Travaglini, J. Tonkin, D. Mahns, E. Humphrey, C. Terracciano, J. J. Gooding, J. Seidel and D. Mawad, *Biomaterials Science*, 2018, **6**, 493-500.

494.   J. Liu, Y. S. Kim, C. E. Richardson, A. Tom, C. Ramakrishnan, F. Birey, T. Katsumata, S. Chen, C. Wang, X. Wang, L. M. Joubert, Y. Jiang, H. Wang, L. E. Fenno, J. B. Tok, S. P. Pasca, K. Shen, Z. Bao and K. Deisseroth, *Science*, 2020, **367**, 1372-1376.

495.   H. E. Kato, Y. S. Kim, J. M. Paggi, K. E. Evans, W. E. Allen, C. Richardson, K. Inoue, S. Ito, C. Ramakrishnan, L. E. Fenno, K. Yamashita, D. Hilger, S. Y. Lee, A. Berndt, K. Shen, H. Kandori, R. O. Dror, B. K. Kobilka and K. Deisseroth, *Nature*, 2018, **561**, 349-354.

496.   J. Eyckmans, T. Boudou, X. Yu and C. S. Chen, *Dev Cell*, 2011, **21**, 35-47.

497.   K. H. Vining and D. J. Mooney, *Nat Rev Mol Cell Biol*, 2017, **18**, 728-742.

498.   A. Brugues, E. Anon, V. Conte, J. H. Veldhuis, M. Gupta, J. Colombelli, J. J. Munoz, G. W. Brodland, B. Ladoux and X. Trepat, *Nat Phys*, 2014, **10**, 683-690.

499.   Y. Zhang, J. Li and G. S. Boutis, *J Phys D Appl Phys*, 2017, **50**.

500.   P. A. Janmey, D. A. Fletcher and C. A. Reinhart-King, *Physiol Rev*, 2020, **100**, 695-724.

501.   M. M. Pathak, J. L. Nourse, T. Tran, J. Hwe, J. Arulmoli, D. T. T. Le, E. Bernardis, L. A. Flanagan and F. Tombola, *Proc Natl Acad Sci USA*, 2014, **111**, 16148-16153.

502. D. E. Conway, B. G. Coon, M. Budatha, P. T. Arsenovic, F. Orsenigo, F. Wessel, J. Zhang, Z. Zhuang, E. Dejana, D. Vestweber and M. A. Schwartz, *Curr Biol*, 2017, **27**, 2727.

503. C. Wang, B. M. Baker, C. S. Chen and M. A. Schwartz, *Arterioscler Thromb Vasc Biol*, 2013, **33**, 2130-2136.

504. H.-Y. Lou, W. Zhao, X. Li, L. Duan, A. Powers, M. Akamatsu, F. Santoro, A. F. McGuire, Y. Cui, D. G. Drubin and B. Cui, *Proc Natl Acad Sci USA*, 2019, **116**, 23143-23151.

505. A. Veksler and N. S. Gov, *Biophys J*, 2009, **97**, 1558-1568.

506. K. Hayashi, T. S. Yamamoto and N. Ueno, *Sci Rep*, 2018, **8**, 2433.

507. J. M. Kim, M. Lee, N. Kim and W. D. Heo, *Proc Natl Acad Sci U S A*, 2016, **113**, 5952-5957.

508. A. Mogilner and G. Oster, *Biophysical Journal*, 2003, **84**, 1591-1605.

509. M. E. Arsenault, H. Zhao, P. K. Purohit, Y. E. Goldman and H. H. Bau, *Biophys J*, 2007, **93**, L42-44.

510. S. B. Asokan, L. Jawerth, R. L. Carroll, R. E. Cheney, S. Washburn and R. Superfine, *Nano Letters*, 2003, **3**, 431-437.

511. D. E. Chafai, V. Sulimenko, D. Havelka, L. Kubinova, P. Draber and M. Cifra, *Adv Mater*, 2019, **31**, e1903636.

512. D. Havelka, D. E. Chafai, O. Krivosudský, A. Klebanovych, F. Vostárek, L. Kubínová, P. Dráber and M. Cifra, *Adv. Mater. Technol.*, 2020, **5**, 1900669.

513. P. W. Oakes and M. L. Gardel, *Current Opinion in Cell Biology*, 2014, **30**, 68-73.

514. F. Martino, A. R. Perestrelo, V. Vinarský, S. Pagliari and G. Forte, *Front. Physiol.*, 2018, **9**, 824.

515. M. Aragona, T. Panciera, A. Manfrin, S. Giulitti, F. Michielin, N. Elvassore, S. Dupont and S. Piccolo, *Cell*, 2013, **154**, 1047-1059.

516. S. Dupont, L. Morsut, M. Aragona, E. Enzo, S. Giulitti, M. Cordenonsi, F. Zanconato, J. Le Digabel, M. Forcato, S. Bicciato, N. Elvassore and S. Piccolo, *Nature*, 2011, **474**, 179-183.

517. S. Piccolo, S. Dupont and M. Cordenonsi, *Physiological Reviews*, 2014, **94**, 1287-1312.

518. M. Fischer, P. Rikeit, P. Knaus and C. Coirault, *Front Physiol*, 2016, **7**, 41.

519. A. Elosegui-Artola, I. Andreu, A. E. M. Beedle, A. Lezamiz, M. Uroz, A. J. Kosmalska, R. Oria, J. Z. Kechagia, P. Rico-Lastres, A.-L. Le Roux, C. M. Shanahan, X. Trepat, D. Navajas, S. Garcia-Manyes and P. Roca-Cusachs, *Cell*, 2017, **171**, 1397-1410.e1314.

520. T. Bouzid, E. Kim, B. D. Riehl, A. M. Esfahani, J. Rosenbohm, R. Yang, B. Duan and J. Y. Lim, *J Biol Eng*, 2019, **13**, 68.

521. J. E. Van Lierop, D. P. Wilson, J. P. Davis, S. Tikunova, C. Sutherland, M. P. Walsh and J. D. Johnson, *J Biol Chem*, 2002, **277**, 6550-6558.

522. A. V. Gomes, J. D. Potter and D. Szczesna-Cordary, *IUBMB Life*, 2002, **54**, 323-333.

523. M. Zhao, B. Song, J. Pu, T. Wada, B. Reid, G. Tai, F. Wang, A. Guo, P. Walczysko, Y. Gu, T. Sasaki, A. Suzuki, J. V. Forrester, H. R. Bourne, P. N. Devreotes, C. D. McCaig and J. M. Penninger, *Nature*, 2006, **442**, 457-460.

524. M. Zhao, H. Bai, E. Wang, J. V. Forrester and C. D. McCaig, *J Cell Sci*, 2004, **117**, 397-405.

525. G. M. Allen, A. Mogilner and J. A. Theriot, *Curr Biol*, 2013, **23**, 560-568.

526. C. D. Cox, C. Bae, L. Ziegler, S. Hartley, V. Nikolova-Krstevski, P. R. Rohde, C.-A. Ng, F. Sachs, P. A. Gottlieb and B. Martinac, *Nature Communications*, 2016, **7**, 10366.

527. B. Coste, B. Xiao, J. S. Santos, R. Syeda, J. Grandl, K. S. Spencer, S. E. Kim, M. Schmidt, J. Mathur, A. E. Dubin, M. Montal and A. Patapoutian, *Nature*, 2012, **483**, 176-181.

528. M. Moroni, M. R. Servin-Vences, R. Fleischer, O. Sánchez-Carranza and G. R. Lewin, *Nature Communications*, 2018, **9**, 1096.

529. S. S. Ranade, Z. Qiu, S. H. Woo, S. S. Hur, S. E. Murthy, S. M. Cahalan, J. Xu, J. Mathur, M. Bandell, B. Coste, Y. S. J. Li, S. Chien and A. Patapoutian, *Proc Natl Acad Sci USA*, 2014, **111**, 10347-10352.

530. L. He, G. Si, J. Huang, A. D. T. Samuel and N. Perrimon, *Nature*, 2018, **555**, 103-106.

531. S.-H. Woo, S. Ranade, A. D. Weyer, A. E. Dubin, Y. Baba, Z. Qiu, M. Petrus, T. Miyamoto, K. Reddy, E. A. Lumpkin, C. L. Stucky and A. Patapoutian, *Nature*, 2014, **509**, 622-626.

532. P. W. Oakes, S. Banerjee, M. C. Marchetti and M. L. Gardel, *Biophys J*, 2014, **107**, 825-833.

533. C. M. Lo, H. B. Wang, M. Dembo and Y. L. Wang, *Biophysical journal*, 2000, **79**, 144-152.

534. J. Fu, Y. K. Wang, M. T. Yang, R. A. Desai, X. Yu, Z. Liu and C. S. Chen, *Nat Methods*, 2010, **7**, 733-736.

535. X. Li, L. Matino, W. Zhang, L. Klausen, A. F. McGuire, C. Lubrano, W. Zhao, F. Santoro and B. Cui, *Nature Protocols*, 2019, **14**, 1772-1802.

536. Y. Cho, M. Son, H. Jeong and J. H. Shin, *MBoC*, 2018, **29**, 2292-2302.

537. R. Kempaiah, A. Chung and V. Maheshwari, *ACS Nano*, 2011, **5**, 6025-6031.

538. B. Sabass, M. L. Gardel, C. M. Waterman and U. S. Schwarz, *Biophysical Journal*, 2008, **94**, 207-220.

539. E. N. Schaumann and B. Tian, *Small Methods*, 2020, DOI: 10.1002/smtd.201900868, 1900868.

540. J. I. Thornycroft and S. W. Barnaby, *Minutes of the Proceedings of the Institution of Civil Engineers*, 1895, **122**, 51-69.

541. K. S. Suslick, *Science*, 1990, **247**, 1439-1445.

542. T. G. McKenzie, F. Karimi, M. Ashokkumar and G. G. Qiao, *Chemistry*, 2019, **25**, 5372-5388.

543. B. Hidding, *Science*, 2018, **360**, 489-490.

544. M. Kumeta, D. Takahashi, K. Takeyasu and S. H. Yoshimura, *PLOS ONE*, 2018, **13**, e0188764.

545. E. Boni, A. C. H. Yu, S. Freear, J. A. Jensen and P. Tortoli, *IEEE Trans. Ultrason., Ferroelect., Freq. Contr.*, 2018, **65**, 1078-1092.

546. Y. I. Yoon, W. Tang and X. Chen, *Small Methods*, 2017, **1**, 1700173.

547. W. Tang, Z. Yang, S. Wang, Z. Wang, J. Song, G. Yu, W. Fan, Y. Dai, J. Wang, L. Shan, G. Niu, Q. Fan and X. Chen, *ACS Nano*, 2018, **12**, 2610-2622.

548. G.-Z. Yang, J. Bellingham, P. E. Dupont, P. Fischer, L. Floridi, R. Full, N. Jacobstein, V. Kumar, M. McNutt, R. Merrifield, B. J. Nelson, B. Scassellati, M. Taddeo, R. Taylor, M. Veloso, Z. L. Wang and R. Wood, *Sci. Robot.*, 2018, **3**, eaar7650.

549. C. Preston, W. S. Kasoff and R. S. Witte, *Ultrasound in Medicine & Biology*, 2018, **44**, 2345-2357.

550. J. Jossinet, B. Lavandier and D. Cathignol, *Annals of the New York Academy of Sciences*, 1999, **873**, 396-407.

551. R. Olafsson, R. S. Witte, S. W. Huang and M. O'Donnell, *IEEE Trans Biomed Eng*, 2008, **55**, 1840-1848.

552. C. Preston, A. M. Alvarez, A. Barragan, J. Becker, W. S. Kasoff and R. S. Witte, *Journal of Neural Engineering*, 2020, **17**, 016074.

553. X. Song, L. Feng, C. Liang, K. Yang and Z. Liu, *Nano Letters*, 2016, **16**, 6145-6153.

554. J.-M. Escoffre and A. Bouakaz, *Therapeutic Ultrasound*, Springer International Publishing, 2016.

555. J. B. Wang, M. Aryal, Q. Zhong, D. B. Vyas and R. D. Airan, *Neuron*, 2018, **100**, 728-738.e727.

556. G. Canavese, A. Ancona, L. Racca, M. Canta, B. Dumontel, F. Barbaresco, T. Limongi and V. Cauda, *Chemical Engineering Journal*, 2018, **340**, 155-172.

557. J. O. Szablowski, A. Lee-Gosselin, B. Lue, D. Malounda and M. G. Shapiro, *Nature Biomedical Engineering*, 2018, **2**, 475-484.

558. T. Sato, M. G. Shapiro and D. Y. Tsao, *Neuron*, 2018, **98**, 1031-1041 e1035.

559. A. Farhadi, G. H. Ho, D. P. Sawyer, R. W. Bourdeau and M. G. Shapiro, *Science*, 2019, **365**, 1469-1475.

560. J. Engels and E. J. Schlaeger, *J. Med. Chem.*, 1977, **20**, 907-911.

561. J. H. Kaplan, B. Forbush and J. F. Hoffman, *Biochemistry*, 1978, **17**, 1929-1935.

562. G. C. R. Ellis-Davies, *Nature Methods*, 2007, **4**, 619-628.

563. P. Gorostiza and E. Y. Isacoff, *Science*, 2008, **322**, 395-399.

564. M. L. DiFrancesco, F. Lodola, E. Colombo, L. Maragliano, M. Bramini, G. M. Paternò, P. Baldelli, M. D. Serra, L. Lunelli, M. Marchioretto, G. Grasselli, S. Cimò, L. Colella, D. Fazzi, F. Ortica, V. Vurro, C. G. Eleftheriou, D. Shmal, J. F. Maya-Vetencourt, C. Bertarelli, G. Lanzani and F. Benfenati, *Nature Nanotechnology*, 2020, DOI: 10.1038/s41565-019-0632-6.

565. V. Y. Chang, C. Fedele, A. Priimagi, A. Shishido and C. J. Barrett, *Adv. Optical Mater.*, 2019, **7**, 1900091.

566. T. Fehrentz, F. M. E. Huber, N. Hartrampf, T. Bruegmann, J. A. Frank, N. H. F. Fine, D. Malan, J. G. Danzl, D. B. Tikhonov, M. Sumser, P. Sasse, D. J. Hodson, B. S. Zhorov, N. Klöcker and D. Trauner, *Nature Chemical Biology*, 2018, **14**, 764-767.

567. M. Mansø, A. U. Petersen, Z. Wang, P. Erhart, M. B. Nielsen and K. Moth-Poulsen, *Nature Communications*, 2018, **9**, 1945.

568. K. Fukushima, A. J. Vandenbos and T. Fujiwara, *Chemistry of Materials*, 2007, **19**, 644-646.

569. M. Kathan, F. Eisenreich, C. Jurissek, A. Dallmann, J. Gurke and S. Hecht, *Nature Chemistry*, 2018, **10**, 1031-1036.

570. B. V. Zemelman, G. A. Lee, M. Ng and G. Miesenböck, *Neuron*, 2002, **33**, 15-22.

571. G. Nagel, T. Szellas, W. Huhn, S. Kateriya, N. Adeishvili, P. Berthold, D. Ollig, P. Hegemann and E. Bamberg, *Proc Natl Acad Sci USA*, 2003, **100**, 13940-13945.

572. B. V. Zemelman, N. Nesnas, G. A. Lee and G. Miesenbock, *Proc Natl Acad Sci USA*, 2003, **100**, 1352-1357.

573. D. Strickland, Y. Lin, E. Wagner, C. M. Hope, J. Zayner, C. Antoniou, T. R. Sosnick, E. L. Weiss and M. Glotzer, *Nature Methods*, 2012, **9**, 379-384.

574. O. J. Stone, N. Pankow, B. Liu, V. P. Sharma, R. J. Eddy, H. Wang, A. T. Putz, F. D. Teets, B. Kuhlman, J. S. Condeelis and K. M. Hahn, *Nature Chemical Biology*, 2019, **15**, 1183-1190.

575. R. P. Tas, C.-Y. Chen, E. A. Katrukha, M. Vleugel, M. Kok, M. Dogterom, A. Akhmanova and L. C. Kapitein, *Nano Letters*, 2018, **18**, 7524-7528.

576. J. Ricken, R. Medda and S. V. Wegner, *Adv. Biosys.*, 2019, **3**, 1800302.

577. P. W. Oakes, E. Wagner, C. A. Brand, D. Probst, M. Linke, U. S. Schwarz, M. Glotzer and M. L. Gardel, *Nature Communications*, 2017, **8**, 15817.

578. K. E. Cavanaugh, M. F. Staddon, E. Munro, S. Banerjee and M. L. Gardel, *Developmental Cell*, 2020, **52**, 152-166.e155.

579.   J. H. Yu, S.-H. Kwon, Z. Petrášek, O. K. Park, S. W. Jun, K. Shin, M. Choi, Y. I. Park, K. Park, H. B. Na, N. Lee, D. W. Lee, J. H. Kim, P. Schwille and T. Hyeon, *Nature Materials*, 2013, **12**, 359-366.

580.   S. I. Park, D. S. Brenner, G. Shin, C. D. Morgan, B. A. Copits, H. U. Chung, M. Y. Pullen, K. N. Noh, S. Davidson, S. J. Oh, J. Yoon, K.-I. Jang, V. K. Samineni, M. Norman, J. G. Grajales-Reyes, S. K. Vogt, S. S. Sundaram, K. M. Wilson, J. S. Ha, R. Xu, T. Pan, T.-i. Kim, Y. Huang, M. C. Montana, J. P. Golden, M. R. Bruchas, R. W. Gereau and J. A. Rogers, *Nature Biotechnology*, 2015, **33**, 1280-1286.

581.   P. Gutruf, V. Krishnamurthi, A. Vázquez-Guardado, Z. Xie, A. Banks, C.-J. Su, Y. Xu, C. R. Haney, E. A. Waters, I. Kandela, S. R. Krishnan, T. Ray, J. P. Leshock, Y. Huang, D. Chanda and J. A. Rogers, *Nature Electronics*, 2018, **1**, 652-660.

582.   J. F. Suyver, A. Aebischer, D. Biner, P. Gerner, J. Grimm, S. Heer, K. W. Krämer, C. Reinhard and H. U. Güdel, *Optical Materials*, 2005, **27**, 1111-1130.

583.   J. Zhao, D. Zhong and S. Zhou, *J. Mater. Chem. B*, 2018, **6**, 349-365.

584.   Y. Liu, Y. Lu, X. Yang, X. Zheng, S. Wen, F. Wang, X. Vidal, J. Zhao, D. Liu, Z. Zhou, C. Ma, J. Zhou, J. A. Piper, P. Xi and D. Jin, *Nature*, 2017, **543**, 229-233.

585.   S. Chen, A. Z. Weitemier, X. Zeng, L. He, X. Wang, Y. Tao, A. J. Y. Huang, Y. Hashimotodani, M. Kano, H. Iwasaki, L. K. Parajuli, S. Okabe, D. B. L. Teh, A. H. All, I. Tsutsui-Kimura, K. F. Tanaka, X. Liu and T. J. McHugh, 2018, 6.

586.   P. J. Hore, *Proc Natl Acad Sci USA*, 2012, **109**, 1357-1358.

587.   U. E. Steiner and T. Ulrich, *Chemical Reviews*, 1989, **89**, 51-147.

588.   A. L. Buchachenko, *Russ. Chem. Rev.*, 1976, **45**, 375-390.

589.   C. T. Rodgers, *Pure and Applied Chemistry*, 2009, **81**, 19-43.

590.   C. B. Grissom, *Chemical Reviews*, 1995, **95**, 3-24.

591.   A. L. Buchachenko and D. A. Kuznetsov, *J. Am. Chem. Soc.*, 2008, **130**, 12868-12869.

592.   D. Crotty, G. Silkstone, S. Poddar, R. Ranson, A. Prina-Mello, M. T. Wilson and J. M. D. Coey, *Proc Natl Acad Sci USA*, 2012, **109**, 1437-1442.

593.   G. Mohammadi Ziarani, M. Malmir, N. Lashgari and A. Badiei, *RSC Advances*, 2019, **9**, 25094-25106.

594.   C. P. Bean and J. D. Livingston, *Journal of Applied Physics*, 1959, **30**, S120-S129.

595.   I. V. Belyanina, T. N. Zamay, G. S. Zamay, S. S. Zamay, O. S. Kolovskaya, T. I. Ivanchenko, V. V. Denisenko, A. K. Kirichenko, Y. E. Glazyrin, I. V. Garanzha, V. V. Grigorieva, A. V. Shabanov, D. V. Veprintsev, A. E. Sokolov, V. M. Sadovskii, A. Gargaun, M. V. Berezovski and A. S. Kichkailo, *Theranostics*, 2017, **7**, 3326-3337.

596.   H. Huang, S. Delikanli, H. Zeng, D. M. Ferkey and A. Pralle, *Nature Nanotechnology*, 2010, **5**, 602-606.

597.   R. Munshi, S. M. Qadri, Q. Zhang, I. Castellanos Rubio, P. del Pino and A. Pralle, *eLife*, 2017, **6**, e27069.

598.   B.-Q. Lu, Y.-J. Zhu, G.-F. Cheng and Y.-J. Ruan, *Materials Letters*, 2013, **104**, 53-56.

599.   Q. Tseng, I. Wang, E. Duchemin-Pelletier, A. Azioune, N. Carpi, J. Gao, O. Filhol, M. Piel, M. Thery and M. Balland, *Lab Chip*, 2011, **11**, 2231-2240.

600.   J. Sun, X. Liao, A. M. Minor, N. P. Balsara and R. N. Zuckermann, *J. Am. Chem. Soc.*, 2014, **136**, 14990-14997.

601.   J. Sun, G. M. Stone, N. P. Balsara and R. N. Zuckermann, *Macromolecules*, 2012, **45**, 5151-5156.

602.   S. C. Hofferberth, M. Y. Saeed, L. Tomholt, M. C. Fernandes, C. J. Payne, K. Price, G. R. Marx, J. J. Esch, D. W. Brown, J. Brown, P. E. Hammer, R. W. Bianco, J. C. Weaver, E. R. Edelman and P. J. del Nido, *Sci. Transl. Med.*, 2020, **12**, eaay4006.

603.   M. Faraday, *Notice of the character and direction of the electric force of the Gymnotus*, The Royal Society, [London, 1839.

604. G. Xie, L. Wen and L. Jiang, *Nano Research*, 2016, **9**, 59-71.

605. T. B. H. Schroeder, A. Guha, A. Lamoureux, G. VanRenterghem, D. Sept, M. Shtein, J. Yang and M. Mayer, *Nature*, 2017, **552**, 214-218.

606. K. C. Catania, *Proc Natl Acad Sci USA*, 2016, **113**, 6979-6984.

607. E. Stavrinidou, R. Gabrielsson, E. Gomez, X. Crispin, O. Nilsson, D. T. Simon and M. Berggren, *Sci Adv*, 2015, **1**, e1501136.

608. E. Stavrinidou, R. Gabrielsson, K. P. Nilsson, S. K. Singh, J. F. Franco-Gonzalez, A. V. Volkov, M. P. Jonsson, A. Grimoldi, M. Elgland, I. V. Zozoulenko, D. T. Simon and M. Berggren, *Proc Natl Acad Sci U S A*, 2017, **114**, 2807-2812.

609. S. Ye, C. Ding, R. Chen, F. Fan, P. Fu, H. Yin, X. Wang, Z. Wang, P. Du and C. Li, *J. Am. Chem. Soc.*, 2018, **140**, 3250-3256.

610. L. Altamura, C. Horvath, S. Rengaraj, A. Rongier, K. Elouarzaki, C. Gondran, A. L. B. Maçon, C. Vendrely, V. Bouchiat, M. Fontecave, D. Mariolle, P. Rannou, A. Le Goff, N. Duraffourg, M. Holzinger and V. Forge, *Nature Chemistry*, 2017, **9**, 157-163.

611. K. Guo, A. Prévoteau, S. A. Patil and K. Rabaey, *Current Opinion in Biotechnology*, 2015, **33**, 149-156.

612. C. M. Ding, M. L. Lv, Y. Zhu, L. Jiang and H. Liu, *Angew Chem Int Ed Engl*, 2015, **54**, 1446-1451.

613. A. Kumar, L. H.-H. Hsu, P. Kavanagh, F. Barrière, P. N. L. Lens, L. Lapinsonnière, J. H. Lienhard V, U. Schröder, X. Jiang and D. Leech, *Nature Reviews Chemistry*, 2017, **1**, 0024.

614. W. Chen, H. Yu, S.-Y. Lee, T. Wei, J. Li and Z. Fan, *Chemical Society Reviews*, 2018, **47**, 2837-2872.

615. Y. Liu, J. Zhou, E. Zhu, J. Tang, X. Liu and W. Tang, *J. Mater. Chem. C*, 2015, **3**, 1011-1017.

616. Q. Niu, K. Gao and Z. Shao, *Nanoscale*, 2014, **6**, 4083.

617. K. Gao, Z. Shao, J. Li, X. Wang, X. Peng, W. Wang and F. Wang, *J. Mater. Chem. A*, 2013, **1**, 63-67.

618. R. Liu, L. Ma, S. Huang, J. Mei, J. Xu and G. Yuan, *RSC Advances*, 2016, **6**, 107426-107432.

619. S. Li, D. Huang, J. Yang, B. Zhang, X. Zhang, G. Yang, M. Wang and Y. Shen, *Nano Energy*, 2014, **9**, 309-317.

620. Z. Wang, P. Tammela, J. Huo, P. Zhang, M. Strømme and L. Nyholm, *Journal of Materials Chemistry A*, 2016, **4**, 1714-1722.

621. Z. Wang, D. O. Carlsson, P. Tammela, K. Hua, P. Zhang, L. Nyholm and M. Stromme, *ACS Nano*, 2015, **9**, 7563-7571.

622. I. M. Mosa, A. Pattammattel, K. Kadimisetty, P. Pande, M. F. El-Kady, G. W. Bishop, M. Novak, R. B. Kaner, A. K. Basu, C. V. Kumar and J. F. Rusling, *Adv Energy Mater*, 2017, **7**.

623. X. Chen, N. S. Villa, Y. Zhuang, L. Chen, T. Wang, Z. Li and T. Kong, *Advanced Energy Materials*, 2020, **10**, 1902769.

624. A. Khan, V. Nair, J. C. Colmenares and R. Gläser, *Topics in Current Chemistry*, 2018, **376**, 20.

625. Y. Wu, J. Wang, X. Qiu, R. Yang, H. Lou, X. Bao and Y. Li, *ACS Appl. Mater. Interfaces*, 2016, **8**, 12377-12383.

626. H.-C. Hu, H. Xu, J. Wu, L. Li, F. Yue, L. Huang, L. Chen, X. Zhang and X. Ouyang, *Advanced Functional Materials*, 2020, **30**, 2001494.

627. K. Zhang, M. Liu, T. Zhang, X. Min, Z. Wang, L. Chai and Y. Shi, *Journal of Materials Chemistry A*, 2019, **7**, 26838-26848.

628.   P. Schlee, S. Herou, R. Jervis, P. R. Shearing, D. J. L. Brett, D. Baker, O. Hosseinaei, P. Tomani, M. M. Murshed, Y. Li, M. J. Mostazo-López, D. Cazorla-Amorós, A. B. Jorge Sobrido and M.-M. Titirici, *Chemical Science*, 2019, **10**, 2980-2988.

629.   R. Kautz, D. D. Ordinario, V. Tyagi, P. Patel, T. N. Nguyen and A. A. Gorodetsky, *Advanced Materials*, 2018, **30**, 1704917.

630.   C. Zhong, A. Cooper, A. Kapetanovic, Z. Fang, M. Zhang and M. Rolandi, *Soft Matter*, 2010, **6**, 5298-5301.

631.   Y. Wan, K. A. M. Creber, B. Peppley and V. T. Bui, *Polymer*, 2003, **44**, 1057-1065.

632.   J. T. Robinson, J. J. Pietron, B. Blue, F. K. Perkins, E. Josberger, Y. Deng and M. Rolandi, *Journal of Materials Chemistry C*, 2017, **5**, 11083-11091.

633.   S. A. Fischer, B. I. Dunlap and D. Gunlycke, *Journal of Polymer Science Part B: Polymer Physics*, 2017, **55**, 1103-1109.

634.   C. Zhong, Y. Deng, A. F. Roudsari, A. Kapetanovic, M. P. Anantram and M. Rolandi, *Nature Communications*, 2011, **2**, 476.

635.   E. M. Leung, M. Colorado Escobar, G. T. Stiubianu, S. R. Jim, A. L. Vyatskikh, Z. Feng, N. Garner, P. Patel, K. L. Naughton, M. Follador, E. Karshalev, M. D. Trexler and A. A. Gorodetsky, *Nature Communications*, 2019, **10**, 1947.

636.   T. J. Wardill, P. T. Gonzalez-Bellido, R. J. Crook and R. T. Hanlon, *Proceedings of the Royal Society B: Biological Sciences*, 2012, **279**, 4243-4252.

637.   W. J. Crookes, L.-L. Ding, Q. L. Huang, J. R. Kimbell, J. Horwitz and M. J. McFall-Ngai, *Science*, 2004, **303**, 235.

638.   R. Levenson, C. Bracken, N. Bush and D. E. Morse, *J Biol Chem*, 2016, **291**, 4058-4068.

639.   K. L. Naughton, L. Phan, E. M. Leung, R. Kautz, Q. Lin, Y. Van Dyke, B. Marmiroli, B. Sartori, A. Arvai, S. Li, M. E. Pique, M. Naeim, J. P. Kerr, M. J. Aquino, V. A. Roberts, E. D. Getzoff, C. Zhu, S. Bernstorff and A. A. Gorodetsky, *Advanced Materials*, 2016, **28**, 8405-8412.

640.   D. D. Ordinario, L. Phan, W. G. Walkup Iv, J.-M. Jocson, E. Karshalev, N. Hüsken and A. A. Gorodetsky, *Nature Chemistry*, 2014, **6**, 596-602.

641.   D. D. Ordinario, E. M. Leung, L. Phan, R. Kautz, W. K. Lee, M. Naeim, J. P. Kerr, M. J. Aquino, P. E. Sheehan and A. A. Gorodetsky, *Advanced Optical Materials*, 2017, **5**, 1600751.

642.   D. D. Ordinario, L. Phan, J.-M. Jocson, T. Nguyen and A. A. Gorodetsky, *APL Materials*, 2014, **3**, 014907.

643.   J. Wünsche, Y. Deng, P. Kumar, E. Di Mauro, E. Josberger, J. Sayago, A. Pezzella, F. Soavi, F. Cicoira, M. Rolandi and C. Santato, *Chemistry of Materials*, 2015, **27**, 436-442.

644.   M. Sheliakina, A. B. Mostert and P. Meredith, *Advanced Functional Materials*, 2018, **28**, 1805514.

645.   P. Ertl and T. Schuhmann, *J. Nat. Prod.*, 2019, **82**, 1258-1263.

646.   S. Basith, M. Cui, S. J. Y. Macalino, J. Park, N. A. B. Clavio, S. Kang and S. Choi, *Front. Pharmacol.*, 2018, **9**, 128.

647.   E. A. Pfeif and K. Kroenlein, *APL Mater.*, 2016, **4**, 053203.

648.   P. J. McGinn, *ACS Comb. Sci.*, 2019, **21**, 501-515.

649.   K. Alberi, M. B. Nardelli, A. Zakutayev, L. Mitas, S. Curtarolo, A. Jain, M. Fornari, N. Marzari, I. Takeuchi, M. L. Green, M. Kanatzidis, M. F. Toney, S. Butenko, B. Meredig, S. Lany, U. Kattner, A. Davydov, E. S. Toberer, V. Stevanovic, A. Walsh, N.-G. Park, A. Aspuru-Guzik, D. P. Tabor, J. Nelson, J. Murphy, A. Setlur, J. Gregoire, H. Li, R. Xiao, A. Ludwig, L. W. Martin, A. M. Rappe, S.-H. Wei and J. Perkins, *Journal of Physics D: Applied Physics*, 2019, **52**, 013001.

650. H. Bronstein, C. B. Nielsen, B. C. Schroeder and I. McCulloch, *Nature Reviews Chemistry*, 2020, **4**, 66-77.

651. A. L. Samuel, *IBM Journal of Research and Development*, 1959, **3**, 210-229.

652. J. Ngiam, A. Khosla, M. Kim, J. Nam, H. Lee and A. Y. Ng, 8.

653. G. Carleo, I. Cirac, K. Cranmer, L. Daudet, M. Schuld, N. Tishby, L. Vogt-Maranto and L. Zdeborová, *Rev. Mod. Phys.*, 2019, **91**, 045002.

654. J. Vamathevan, D. Clark, P. Czodrowski, I. Dunham, E. Ferran, G. Lee, B. Li, A. Madabhushi, P. Shah, M. Spitzer and S. Zhao, *Nat Rev Drug Discov*, 2019, **18**, 463-477.

655. T. Olsen, B. Jackson, T. Feeser, M. Kent, J. Moad, S. Krishnamurthy, D. Lunsford and R. Soans, *J Pathol Inform*, 2018, **9**, 32.

656. C. Bouton, *Bioelectronic Medicine*, 2015, **2**, 20-24.

657. J. B. Ritchie, D. M. Kaplan and C. Klein, *The British Journal for the Philosophy of Science*, 2019, **70**, 581-607.

658. G. K. Anumanchipalli, J. Chartier and E. F. Chang, *Nature*, 2019, **568**, 493-498.

659. L. R. Hochberg, D. Bacher, B. Jarosiewicz, N. Y. Masse, J. D. Simeral, J. Vogel, S. Haddadin, J. Liu, S. S. Cash, P. van der Smagt and J. P. Donoghue, *Nature*, 2012, **485**, 372-375.

660. J. A. George, D. T. Kluger, T. S. Davis, S. M. Wendelken, E. V. Okorokova, Q. He, C. C. Duncan, D. T. Hutchinson, Z. C. Thumser, D. T. Beckler, P. D. Marasco, S. J. Bensmaia and G. A. Clark, *Sci. Robot.*, 2019, **4**, eaax2352.

661. V. L. Deringer, N. Bernstein, A. P. Bartók, M. J. Cliffe, R. N. Kerber, L. E. Marbella, C. P. Grey, S. R. Elliott and G. Csányi, *J. Phys. Chem. Lett.*, 2018, **9**, 2879-2885.

662. A. P. Bartók, J. Kermode, N. Bernstein and G. Csányi, *Phys. Rev. X*, 2018, **8**, 041048.

663. A. Anelli, E. A. Engel, C. J. Pickard and M. Ceriotti, *Phys. Rev. Materials*, 2018, **2**, 103804.

664. Y. Morimoto, H. Onoe and S. Takeuchi, *Sci. Robot.*, 2018, **3**, eaat4440.

665. L. Ricotti, B. Trimmer, A. W. Feinberg, R. Raman, K. K. Parker, R. Bashir, M. Sitti, S. Martel, P. Dario and A. Menciassi, *Sci. Robot.*, 2017, **2**, eaaq0495.

666. Y. Zhang, L. H.-H. Hsu and X. Jiang, *Nano Research*, 2019, DOI: 10.1007/s12274-019-2570-x.

667. D. K.-C. Liu, J. Friend and L. Yeo, *Acoust. Sci. & Tech.*, 2010, **31**, 115-123.

668. S. Rosset and H. R. Shea, *Appl. Phys. A*, 2013, **110**, 281-307.

669. H. A. Sonar and J. Paik, *Frontiers in Robotics and AI*, 2016, **2**, 38.

670. D. S. Kuchin, P. V. Lega, A. P. Orlov, V. V. Koledov and A. V. Irzhak, 2017 International Conference on Manipulation, Automation and Robotics at Small Scales (MARSS), 2017.

671. P. Boyraz, G. Runge and A. Raatz, *Actuators*, 2018, **7**.

672. Y. Chen, H. Zhao, J. Mao, P. Chirarattananon, E. F. Helbling, N.-s. P. Hyun, D. R. Clarke and R. J. Wood, *Nature*, 2019, **575**, 324-329.

673. J. A. Goding, A. D. Gilmour, U. A. Aregueta-Robles, E. A. Hasan and R. A. Green, *Advanced Functional Materials*, 2018, **28**, 1702969.

674. S. J. Park, M. Gazzola, K. S. Park, S. Park, V. Di Santo, E. L. Blevins, J. U. Lind, P. H. Campbell, S. Dauth, A. K. Capulli, F. S. Pasqualini, S. Ahn, A. Cho, H. Yuan, B. M. Maoz, R. Vijaykumar, J. W. Choi, K. Deisseroth, G. V. Lauder, L. Mahadevan and K. K. Parker, *Science*, 2016, **353**, 158-162.

675. G. Vizsnyiczai, G. Frangipane, C. Maggi, F. Saglimbeni, S. Bianchi and R. Di Leonardo, *Nature Communications*, 2017, **8**, 15974.

676. B. A. Trimmer, *Sci. Robot.*, 2020, **5**, eaba6149.

677.   C. Appiah, C. Arndt, K. Siemsen, A. Heitmann, A. Staubitz and C. Selhuber-Unkel, *Advanced Materials*, 2019, **31**, 1807747.
678.   L. Cabrera, C. Sadle and E. Purcell, *Nat Biomed Eng*, 2019, **3**, 586-589.
679.   N. Bostrom and E. Yudkowsky, in *The Cambridge Handbook of Artificial Intelligence*, eds. K. Frankish and W. M. Ramsey, Cambridge University Press, Cambridge, 2014, pp. 316-334.
680.   L. Floridi, *The Blackwell guide to the philosophy of computing and information*, John Wiley & Sons, 2008.
681.   J. A. Lockwood, *Annu. Rev. Entomol.*, 2012, **57**, 205-227.
682.   B. L. Docherty, *Making the case: the dangers of killer robots and the need for a preemptive ban*, Human Rights Watch ; IHRC, International Human Rights Clinic, New York, N.Y.] : [Cambridge, MA, 2016.
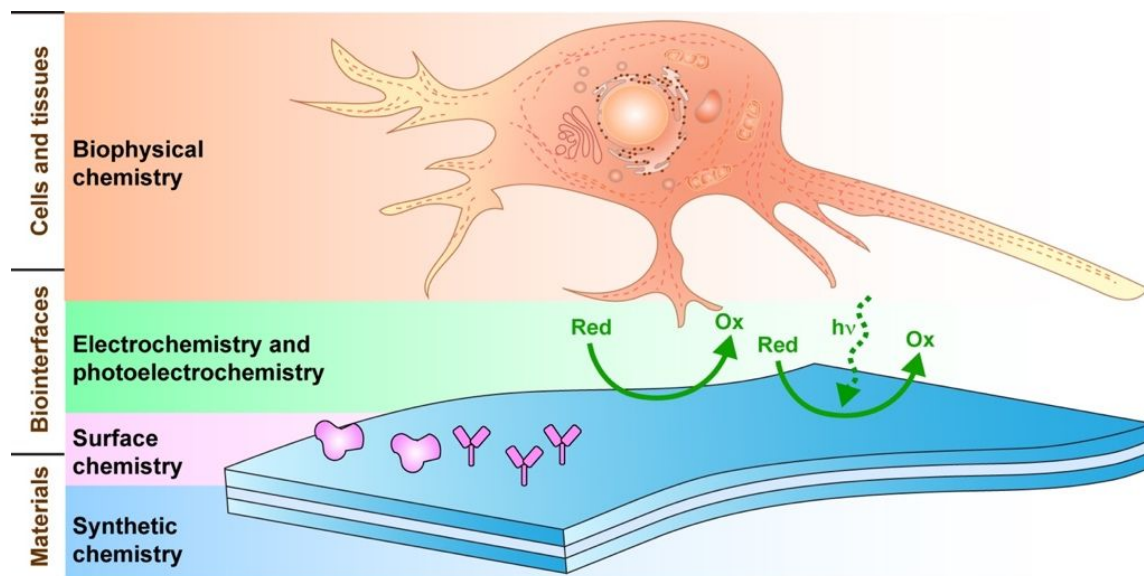
In this Review, we focus on the contributions made to the bioelectronic field from various aspects of chemistry.